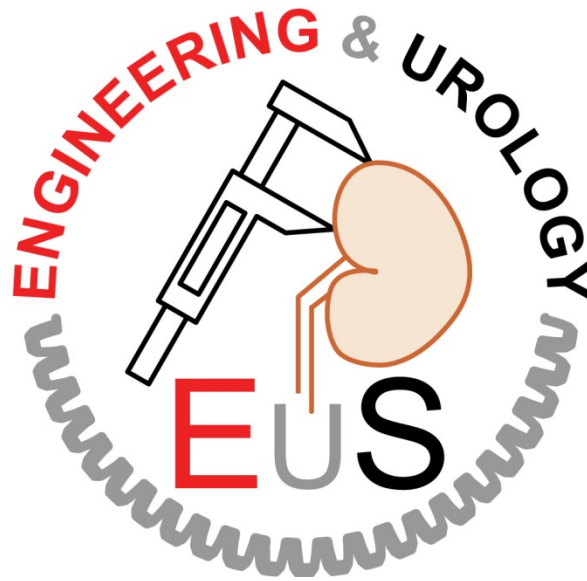


# Engineering and Urology Society

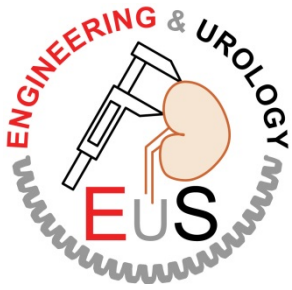


**29<sup>th</sup> Annual Meeting**

Saturday May 17<sup>th</sup>, 2014

Orlando, FL

<http://engineering-urology.org/>



The Engineering and Urology Society offers a unique opportunity for collaboration where engineering innovation meets clinical demand. This leads to an unparalleled exchange of ideas and routes to address clinical problems with engineering solutions. The ultimate forum where these interchanges occur is at the Annual Meeting of the Engineering and Urology Society held in conjunction with the Annual American Urological Association Meeting. The EUS meeting is also the only dedicated section of the Endourology Society at the AUA. The Annual Meeting of the Engineering and Urology Society offers the delegates an opportunity

to present and learn about the latest research developments in urologic technology. The morning session consists of state of the art lectures and discussions in cutting-edge areas of technology. The afternoon poster sessions and ever-growing subgroup meetings allow members to present their work, discuss, and obtain further feedback and ideas from fellow technophiles.

This year's 29th Annual Meeting will take place on May 17th, and has been organized by program chairmen Stavros Gravas, Bodo Knudsen, and M. Pilar Laguna. The morning sessions will begin with a thought-provoking discussion on the intersection of lab training and new imaging technology and urology. Following that, the spotlight is turned to advances in evidence making in uro-technology. Next, colleagues from the European Association of Urology (EAU), Uro-Technology section (ESUT) will present developments for new endoscopic instrumentation. After the lunch break, a brand-new session on "Innovations in Urology" will be held at the Science & Technology Hall, highlighting the grant and patent application processes which are an integral part of engineering and urology. Current updates on LESS and NOTES returns this year. The Stent Working Group will discuss about new designs with challenging case scenarios. The final session will review image-guided interventions, focusing on the management of diagnosis and treatment of renal masses and upper tract urothelial carcinoma.

Two poster session during the afternoon will provide a forum for uro-technology researchers to present and discuss their latest findings. The review of the abstracts for the poster sessions was performed online by a group of 87 reviewers from around the world. Each paper received between 30 and 35 reviews. We would like to thank the reviewers, listed at the end of this program book, for their essential contribution to the quality of the meeting and their constructive comments that they made for the research.

Based on the peers review, two equally ranked abstracts have been selected. Top 10 abstracts have also been selected and are listed at the end of this program book. Their authors are invited to submit full articles to the Journal of Endourology on the respective topics.

We gratefully thank all reviewers for their hard work, objective scoring, and contribution to the success of the meeting. The society also presents Best Reviewer Awards based on the grading performance and the number of reviews performed. The Best Reviewer Awards are presented to Drs. Jeffrey Cadeddu, Mohamed Elkoushy, Petrisor Geavlete, Kamol Panumatrassamee, Govindarajan Srimathveeravalli, Chong Xue, and Hessel Wijkstra.

We congratulate all award winners and welcome all urologists, engineers, and scientists to join us for this unique multi and interdisciplinary experience. As always, we are grateful to Dr. George Nagamatsu, the founder and first president of the society for setting the foundations based upon which we meet.

Please visit the website <http://engineering-urology.org> for a complete version of this program including the abstracts presented.

Thank you for your continued scientific support,

Jeffrey Cadeddu  
Koon Ho Rha  
Dan Stoianovici

# CONTINUING MEDICAL EDUCATION

## AUA ACCREDITATION INFORMATION

**Accreditation:** The American Urological Association (AUA) is accredited by the Accreditation Council for Continuing Medical Education (ACCME) to provide continuing medical education for physicians.

**Credit Designation:** The American Urological Association designates this live activity for a maximum of 8.0 *AMA PRA Category 1 Credits*<sup>™</sup>. Physicians should claim only the credit commensurate with the extent of their participation in the activity.

**Evidence Based Content:** It is the policy of the AUA to ensure that the content contained in this CME activity is valid, fair, balanced, scientifically rigorous, and free of commercial bias.

**AUA Disclosure Policy:** All persons in a position to control the content of an educational activity (i.e., activity planners, presenters, authors) participating in an educational activity provided by the AUA are required to disclose to the provider any relevant financial relationships with any commercial interest. The AUA must determine if the individual's relationships may influence the educational content and resolve any conflicts of interest prior to the commencement of the educational activity. The intent of this disclosure is not to prevent individuals with relevant financial relationships from participating, but rather to provide learners information with which they can make their own judgments.

**Resolution of Identified Conflict of Interest:** All disclosures will be reviewed by the program/course directors or editors for identification of conflicts of interest. Peer reviewers, working with the program directors and/or editors, will document the mechanism(s) for management and resolution of the conflict of interest and final approval of the activity will be documented prior to implementation. Any of the mechanisms below can/will be used to resolve conflict of interest:

- Peer review for valid, evidence-based content of all materials associated with an educational activity by the course/program director, editor, and/or Education Content Review Committee or its subgroup.
- Limit content to evidence with no recommendations
- Introduction of a debate format with an unbiased moderator (point-counterpoint)
- Inclusion of moderated panel discussion
- Publication of a parallel or rebuttal article for an article that is felt to be biased
- Limit equipment representatives to providing logistics and operation support only in procedural demonstrations
- Divestiture of the relationship by faculty

**Off-label or Unapproved Use of Drugs or Devices:** It is the policy of the AUA to require the disclosure of all references to off-label or unapproved uses of drugs or devices prior to the presentation of educational content. The audience is advised that this continuing medical education activity may contain reference(s) to off-label or unapproved uses of drugs or devices. Please consult the prescribing information for full disclosure of approved uses.

**Disclaimer:** The opinions and recommendations expressed by faculty, authors and other experts whose input is included in this program are their own and do not necessarily represent the viewpoint of the AUA.

**Audio, Video and Photographic Equipment:** The use of audio, video and other photographic recording equipment by attendees is prohibited inside AUA meeting rooms.

**Reproduction Permission:** Reproduction of written materials developed for this AUA course is prohibited without the written permission from individual authors and the American Urological Association.

**Special Assistance/Dietary Needs:** The American Urological Association complies with the Americans with Disabilities Act §12112(a). If any participant is in need of special assistance or has any dietary restrictions, please see the registration desk.

# CONTINUING MEDICAL EDUCATION

## FACULTY DISCLOSURES:

Best, Sara: American Urological Association: Meeting participant or lecturer

Bianchi, Giampaolo: Nothing to disclose

Borin, James: Cook Medical: Consultant or Advisor, Journal of Endourology, Videourology Part B: Health publishing, J. Laparoendoscopic & Advanced Surgical Techniques, Part B: Videoscopy: Health publishing

Castle, Erik P: Dendreon: Consultant or Advisor

Clayman, Ralph V: Applied Urology: Investment interest, Greenwald, Inc: Other, Orthopedic Services, Inc. (OSI): Other, Boston Scientific: Other, Cook Urological: Other

Cookson, Michael: Nothing to disclose

Cristancho, Sayra: Nothing to disclose

Dahm, Philipp: Medtronic: Consultant or Advisor

De Bruin, Daniel Martin: Nothing to disclose

Derweesh, Ithaar: GlaxoSmithKline, Inc: Scientific study or trial

Gravas, Stavros: GSK: Consultant or Advisor, meeting participant or lecturer, Pierre Fabre Medicament: Consultant or Advisor, meeting participant or lecturer

Irwin, Brian: Nothing to disclose

Janetschek, Gunter: Storz: Scientific study or trial

Jichlinski, Patrice: Nothing to disclose

Joshi, Hrishi: Nothing to disclose

Knoll, Thomas: Scholly: Consultant or advisor, Richard Wolf: Meeting participant or lecturer, Cook Medical: Scientific study or trial, Boston Scientific: Consultant or advisor, meeting participant or lecturer, Karl Storz: Consultant or Advisor, meeting participant or lecturer

Knudsen, Bodo: Boston Scientific: Consultant or Advisor, Cook Urological: Meeting participant or lecturer, Olympus Surgical: Consultant or Advisor

Kulkarni, Ravindra: Nothing to disclose

Laguna Pes, Pilar M.: Nothing to disclose

Landman, Jaime: Cook Urological: Consultant or Advisor, Owner, Product Development, Galil Medical: Consultant or Advisor, Owner, Product Development

Lange, Dirk: Boston Scientific: Consultant or Advisor, Scientific Study or Trial, PercSys: Consultant or Advisor, Scientific Study or Trial, Urotech, GmbH: Consultant or Advisor, Scientific Study or Trial, Bard Medical: Consultant or Advisor

Lee, Benjamin: Porges: Consultant or Advisor

Lendvay, Thomas S.: Spi Surgical, Inc: Consultant or Advisor, owner, product development, MIMIC Technologies, Inc.: Other

Leveillee, Raymond: Medwaves: Other

Liao, Joseph C.: Nothing to disclose

McDougall, Elspeth M: Nothing to disclose

N'Dow, James: Nothing to disclose

Nakada, Stephen: Endourology Society: Leadership position, ACGME/Urology RRC: Leadership position, American College of Surgeons, Governor: Leadership position, Urology Times: Health publishing, American Board of Urology: Leadership position

# CONTINUING MEDICAL EDUCATION

Pace, Kenneth: Cook Urological, Inc: Other, Baxter, Inc.: Consultant or Advisor, Amgen: Consultant or Advisor, Janssen: Consultant or Advisor

Pinto, Peter: Nothing to disclose

Preminger, Glenn: Boston Scientific: Consultant or Advisor, Mission Pharmacal: Consultant or Advisor, Olympus: Meeting Participant or Lecturer, Endourological Society: Leadership position, UptoDate: Health publishing

Rane, Abhay: Nothing to disclose

Rao, P.P.: Nothing to disclose

Rassweiler, Jens: Karl Storz, Germany: Other

Rassweiler, Marie-Claire: Nothing to disclose

Roberts, William W. III, HistoSonics, Inc.: Consultant or Advisor, Scientific Study or Trial, Investment Interest, Owner, Product Development

Sommer, Kai-Jong: Health Care Management Institute of the European Business School in Oestrich-Winkel: Meeting participant or lecturer

Sotelo, Rene: Intuitive Surgical Systems: Other

Stoianovici, Dan: Samsung: Other

Sundaram, Chandru: Cook Medical Inc.: Scientific Study or Trial, North Central Section of the AUA: Leadership position, Journal of Endourology & Videourology: Leadership position, Society of Urological Robotic Surgeons: Leadership positions

Sweet, Robert: American Medical Systems Holding, Inc: Scientific Study or Trial, Coruthers Health Consulting: Consultant or Advisor, Medtronic: Scientific Study or Trial, Olympus: Other, Department of Defense: Scientific Study or Trial

Teber, Dogu: Nothing to disclose

Tihon, Claude: Nothing to disclose

Tolley, David A.: Nothing to disclose

Traxer Olivier: Cook Medical: Meeting participant or lecturer, Boston Scientific: Meeting participant or lecturer, Coloplast: Consultant or advisor, meeting participant or lecturer, scientific study or trial, Rocamed-Socomed: Consultant or advisor, Karl Storz Endoscopy: Meeting participant or lecturer, Olympus: Meeting participant or lecturer

Van Poelgeest, Auguste : Nothing to disclose

Verhoest, Gregory: Nothing to disclose

Vitenson, Jack H.: Nothing to disclose

Wijkstra, Hessel: Nothing to disclose

Yamamoto, Takunori: Nothing to disclose

## EXHIBITORS

### **Boston Scientific – Urology**

Boston Scientific is a leading developer of less-invasive medical technologies. Products for the Urology/Women's Health division include devices for the diagnosis and treatment of kidney stones, BPH, female urinary incontinence, and pelvic floor reconstruction. Please visit our exhibit to learn about our newest technologies and our commitment to physician education.

### **Cook Medical**

Cook Medical has been a leading supplier of medical devices for urologists for over 35 years. Offering interventional and Biodesign® technologies that support diagnostic and therapeutic procedures in adult and pediatric urology, Cook has placed particular emphasis on stone management as well as both male and female pelvic health.

# PROGRAM



29<sup>th</sup> Annual Meeting

Saturday, May 17, 2014

Hyatt Regency, Plaza Intl Ballroom C-F

Orlando, FL

**Program Chairmen:** Stavros Gravas, Bodo Knudsen, M. Pilar Laguna

**7:15am – 4:00pm Registration Open**

**7:25 - 7:30am Welcome – Program Chairmen**

Stavros Gravas  
Bodo Knudsen  
M. Pilar Laguna

**7:30 - 8.20am SESSION 1: Current Status of Lab Training in Urology**

Bodo Knudsen  
Elspeth McDougal  
Sayra Cristancho  
Tom Lendvay  
Robert Sweet

7:30 - 7:45am Surgical Expertise: Walking through Streetlights & Shadows

7:45 - 8.00am RAVEN as a Tool for da Vinci Curriculum

8.00 - 8.15am Tissue Engineering and Simulation

8:15 - 8.20am The Two “Hottest” Questions

**8:20 – 9:00am SESSION 2: New Imaging Techniques at the Service of Urology**

Stavros Gravas  
Hessel Wijkstra  
Gregory Verhoest  
Martijn de Bruijn  
Joseph C. Liao

8.20 - 8.35am Spectroscopy

8.35 - 8.50am Optical Coherence Tomography

8.50 - 9.05am In Vivo Microscopy in Urology

9.05 - 9.10am The Two “Hottest” Questions

**9:10 - 10:00am SESSION 3: Evidence in Uro-Technology**

M. Pilar Laguna  
Ralph Clayman  
Philipe Dahm  
Ralph Clayman  
James N’Dow

9:10 - 9.25am Stages of Surgical Innovations: The IDEAL

9:25 - 9.40am From Laboratory to Human: The Challenge of Transfer?

9.40 - 9.55am RCTs and Alternative Studies (Real Life Global Studies?)

9.55 - 10.00am The Two “Hottest” Questions

**10:00 – 10:30 AWARDS PRESENTATIONS**

Dan Stoianovici

10:00 – 10:10am Awards

10:10 – 10:15am In Memoriam, Dr. George Nagamatsu

Jack Vitenson

10:15 – 10:22am Human Urethra Engineered with Human Mesenchymal Stem Cell by

Tokunori Yamamoto

Newly Developed Scaffold-Free Three-Dimensional Cell Printer

10:23 – 10:30am Direct MRI-Guided Transperineal Prostate Biopsy with MR-Safe

Dan Stoianovici

Robot. First FDA-Approved Robot for the MR Environment

**10:30 - 12:00pm SESSION 4: ESUT Session**

Thomas Knoll

David Tolley

Jens Rassweiler

10:30 – 10:45am Error Management in Aviation – What Can Surgeons Learn From It?

Kai J. Sommer

10:45 – 11:00am Error Management in Urology – Where are We Actually?

Marie-Claire Rassweiler

11:00 – 11:15am The Wire-Less Cystoscope

Auguste van Poelgeest

11:15 – 11:30am Ultra-Micro PCNL – European Experience

Giannpaolo Bianchi

11:30 – 11:45am Microscopic Cystoscopy – Where is the End

Patrice Jichlinski

11:45 - 12:00pm Targeted Pelvic Lymph Node Dissection

Gunter Janetschek

**12:00 – 1:00pm LUNCH BREAK**



# PROGRAM

## POSTER SESSION 1

1:00 PM – 2:30 PM

### Moderators

Jeffrey Cadeddu  
Kevin Zorn  
Govindarajan Srimathveeravalli  
Marie-Claire Rassweiler

### Presenting Author

Doyoung Chang

No.	Title	
1	THE NUMBER OF SYSTEMATIC BIOPSY CORES RAISES PREDOMINANTLY THE DETECTION OF INSIGNIFICANT CANCER <b>TOP 10 ABSTRACT</b>	
2	IS THE AMOUNT OF RADIATION EXPOSURE DURING FOLLOW-UP IMAGING SAFE IN PATIENTS UNDERGOING ABLATION OF T1 RENAL MASSES?	Necole M. Streeper
3	ACCURACY OF TRANS-RECTAL ULTRASONOGRAPHY TO EVALUATE PATHOLOGICAL PROSTATE WEIGHT: THE IMPACT OF PROSTATE SIZE AND THE PRESENCE OF A MEDIAN	Roger Valdivieso
4	CORRELATION OF MULTI-PARAMETRIC MRI WITH ROBOT-ASSISTED TRANSPERINEAL PROSTATE MAPPING IN DIAGNOSIS OF PROSTATE CANCER	J. Yek
5	TROCAR-SHARPENED NEEDLES IMPROVE IMAGE-GUIDED BIOPSY	Tobias Simpfendörfer
6	CYSTOSCOPIC IMPLANTATION OF A WIRELESS IMPLANTABLE PRESSURE SENSOR IN A LARGE ANIMAL MODEL	Elizabeth Ferry
7	DEVELOPMENT AND INITIAL PORCINE AND CADAVER EXPERIENCE WITH THREE-DIMENSIONAL PRINTING OF ENDOSCOPIC AND LAPAROSCOPIC EQUIPMENT	Michael Del Junco
8	INCORPORATION OF THE GREENLIGHT-SIM™ SIMULATOR AT THE ANNUAL QUEBEC UROLOGY OBJECTIVE STRUCTURED CLINICAL EXAMINATIONS	Yasser Noureldin
9	PRECISION OF URETEROSCOPIC VISUAL ESTIMATION OF STONE FRAGMENT SIZE	Leone, Andrew
10	EXAMINING THE BENEFITS OF ROBOTIC TECHNOLOGY FOR EXPERIENCED UROLOGICAL SURGEONS	Lee J. Moore
11	WILL THE INCREASED APPLICATION OF ROBOTIC TECHNOLOGY HELP ADDRESS THE LEARNING CURVE FOR SURGICAL TRAINEES?	Lee J. Moore

# PROGRAM

- 12 DIRECT MRI-GUIDED TRANSPERINEAL PROSTATE BIOPSY WITH MR-SAFE ROBOT. FIRST FDA-APPROVED ROBOT FOR THE MR ENVIRONMENT  
**BEST PAPER AWARD** Chunwoo Kim
- 13 SONOELASTOGRAPHY OF INTRATESTICULAR LESIONS: HISTOLOGIC CORRELATION Gideon Richards
- 14 IMPACT OF IRRIGANT VISCOSITY ON STONE DUST DURING LASER LITHOTRIPSY—*IN VITRO* ANALYSIS Ashish Patil
- 15 THREE-DIMENSIONAL VOLUME EVALUATION OF PERIRENAL ADIPOSE TISSUE VOLUME USING NOVEL VITREA SOFTWARE AS A PREDICTOR RENAL CORTICAL NEOPLASM HISTOPATHOLOGY Zhamshid Okhunov
- 16 LOWER AND UPPER URINARY SYSTEM EVALUATION WITH HIGH RESOLUTION MANOMETRY: INITIAL ANIMAL STUDY Guy Hidas
- 17 FIBROSIS AND COLLAGEN CONTENT AFTER HISTOTRIPSY IN THE CANNINE PROSTATE Sarah E. Darnell
- 18 COMPARISON OF CATHETER-DIRECTED WST11-VASCULAR TARGETED PHOTOTHERAPY (WST11-VTP) AND IRREVERSIBLE ELECTROPORATION (IRE) FOR INTRALUMINAL ABLATION IN THE PORCINE URETER  
**TOP 10 ABSTRACT** Govindarajan Srimathveeravalli
- 19 NOVEL NEEDLE-PROTECTED TROCAR PORT FASCIAL CLOSURE SYSTEM EMPLOYING A STYLET MECHANISM AND APPLICATOR FOR TRANSVERSUS ABDOMINIS PLANE (TAP) ANALGESIC BLOCK Philip T. Zhao
- 20 ACE RENORRHAPHY: A NOVEL TECHNIQUE FOR CLOSURE OF RENAL DEFECT DURING ROBOT-ASSISTED PARTIAL NEPHRECTOMY USING ALTERNATING COLORED SUTURES AND EVICEL<sup>®</sup> Bennett Y. Hong
- 21 COGNITIVE-AUGMENTED ROBOTIC SYSTEM FOR ENDOSCOPIC NAVIGATION (CARSEN): A PROOF OF CONCEPT FOR MIND-CONTROL ENDOSURGERY USING LEGO<sup>®</sup>  
**TOP 10 ABSTRACT** Neal Patel
- 22 INITIAL CLINICAL EXPERIENCE WITH PERCUTANEOUS IRREVERSIBLE ELECTROPORATION OF KIDNEY TUMORS Monica S.C. Morgan
- 23 PILOT EVALUATION OF A NON-INVASIVE, ULTRASOUND-BASED LIQUID MOLECULAR BIOPSY: INDUCED RELEASE OF PROSTATE CANCER ASSOCIATED MIRNAS IN A RAT MODEL USING BOILING HISTOTRIPSY George R. Schade

# PROGRAM

- 24 RE-DEFINING BLADDER INNERVATION WITH 3D IMAGE RECONSTRUCTION Garen Abedi
- 25 MORPHOMETRIC ANALYSIS OF PROSTATE ZONAL ANATOMY USING MRI IN 307 MEN BY COOPERATIVE STUDY IN JAPAN AND USA T Matsugasumi
- 26 PILOT EVALUATION OF BOILING HISTOTRIPTY OF THE KIDNEY: ASSESSMENT IN HUMAN *EX VIVO* KIDNEYS AND VALIDATION OF THE PORCINE MODEL George R. Schade  
**TOP 10 ABSTRACT**
- 27 A NEW MULTI-DOF DEXTEROUS MANUAL INSTRUMENT FOR LAPAROSCOPIC SURGERY C. Mitchell
- 28 ELASTIC REGISTRATION OF ULTRASOUND IMAGES P. Zogal
- 29 *IN VITRO* FRAGMENTATION OF RENAL CALCULI BY BURST WAVE LITHOTRIPTY: EFFECT OF STONE COMPOSITION Adam D. Maxwell
- 30 PCA SCORE: A SIMPLE MR IMAGING-BASED SYSTEM TO IDENTIFY MEN AT RISK FOR PROSTATE CANCER Jason T. Rothwax
- 31 IMPACT OF SPATIAL DISTRIBUTION OF SAMPLES ON TARGETING ACCURACY IN MR-US FUSION GUIDED BIOPSY James Garritano
- 32 COMPARISON OF *IN VIVO* TEMPERATURE CHANGES INDUCED BY A 902-928 MHZ AND A 2450 MHZ MICROWAVE SYSTEM Karli Pease

# PROGRAM

## POSTER SESSION 2

3:00 PM – 4:30 PM

### Moderators

Thomas Polascik  
Mathew Sorensen  
Martijn de Bruin  
Jessica Kreshover

No.	Title	Presenting Author
33	A LONG TERM SOLUTION IN SECONDARY BLADDER NECK SCLEROSIS CASES – BIPOLAR PLASMA VAPORIZATION OVERCOMING STANDARD TUR IN A PROSPECTIVE, RANDOMIZED COMPARISON	Bogdan Geavlete
34	WHEN IS AN OPERATION LEARNED? HOW TO MONITOR PATIENT SAFETY? PROSPECTIVE EVALUATION OF PERFORMANCE UTILIZING TECHNIQUES OF STATISTICAL PROCESS CONTROL DURING ADOPTION OF ROBOTIC KIDNEY TRANSPLANTATION	Akshay Sood
35	INNOVATION, CONSTRUCTION AND ASSESSMENT OF A NOVEL SEAMLESS LAPAROSCOPIC PORT PLACEMENT SYSTEM	Ashish Rawandale-Patil
36	WITHDRAWN	
37	COMPARISON OF RADIATION DOSE MEASUREMENTS FROM CONVENTIONAL AND TRIPLE BOLUS CT UROGRAPHY PROTOCOLS IN THE DIAGNOSIS AND MANAGEMENT OF RENAL CORTICAL NEOPLASMS	Garen Abedi
38	EFFECT OF OUTPUT POWER ON THERMAL LESION ZONE DURING RADIOFREQUENCY ABLATION	Matthew Ishahak
39	PROSTATE CANCER LOCALIZATION BY MAGNETIC RESONANCE DISPERSION IMAGING	M. Mischi
40	EVALUATION OF A DISPOSABLE FLEXIBLE DIVERTING 17FR CYSTOSCOPE IN EVERYDAY UROLOGICAL PRACTICE	Joseph V. DiTrolio
41	<i>IN VITRO</i> RESULTS OF ROBOTIC CYSTOSCOPE AND 3D PANORAMA FOR AUTOMATED BLADDER SURVEILLANCE SYSTEM (ABSS) <b>TOP 10 ABSTRACT</b>	Xianming Ye
42	MRI-GUIDED PROSTATE CANCER FOCAL LASER ABLATION THERAPY USING A MECHATRONIC NEEDLE GUIDANCE SYSTEM: INITIAL EXPERIENCE AND FUTURE DIRECTIONS <b>TOP 10 ABSTRACT</b>	Jeremy Cepek
43	<i>IN VITRO</i> EVALUATION OF LithAsisst: A NOVEL COMBINED HOLMIUM LASER AND SUCTION DEVICE	Zhamshid Okhunov

# PROGRAM

- |    |  |                     |
|----|--|---------------------|
| 44 | FAT EMULSIFICATION BENEFIT OF SURFACTANT COMPARED TO WATER FOR LAPAROSCOPIC DEFOGGING AND CLEANING   | Peter Stuhldreher   |
| 45 | COMPARISON OF TWO HIGH FIDELITY WITH ONE LOW FIDELITY ENDOUROLOGICAL SIMULATOR   | Andreas J. Gross    |
| 46 | COMPARISON OF NITINOL STONE RETRIEVAL BASKETS IN AN URETEROSCOPY SIMULATOR   | Andreas J. Gross    |
| 47 | TRANS-PERITONEAL ROBOT-ASSISTED LAPAROSCOPIC HIGH INTENSITY FOCUSED ULTRASOUND FOR TARGETED THERAPY OF THE PROSTATE AND BLADDER: NOVEL APPROACH      | T. Matsugasumi      |
| 48 | BODY WALL FORCES AT PORT SITES IN LAPAROSCOPIC AND ROBOTIC SURGERY<br><b>TOP 10 ABSTRACT</b>   | Smita De            |
| 49 | DESIGN AND EVALUATION OF 3D PRINTED MOLDS AND SLICING DEVICE FOR WHOLE MOUNT PROSTATE SECTIONING   | Alan Priester       |
| 50 | EXPLORATION OF AN AMPLITUDE-MODULATED PULSE SEQUENCE USING THE VORTX R <sub>x</sub> <sup>®</sup> SYSTEM FOR PROSTATE HISTOTRIPSY IN A CANINE MODEL   | Jonathan M. Cannata |
| 51 | THE INTRODUCTION OF ADVANCED BIOMATERIALS FOR USE IN UROLOGIC PROCEDURES   | Robert Grubb III    |
| 52 | THEORETICAL AND EX VIVO THERMAL MAPPING FOR RENAL TUMOR RADIOFREQUENCY ABLATION WITH PYELOPERFUSION  | M. Glamore          |
| 53 | HUMAN URETHRA ENGINEERED WITH HUMAN MESENCHYMAL STEM CELL BY NEWLY DEVELOPED SCAFFOLD-FREE THREE-DIMENSIONAL CELL PRINTER<br><b>BEST PAPER AWARD</b> | Tokunori Yamamoto   |
| 54 | DEVELOPMENT OF A SYNTHETIC HUMAN MODEL FOR TRAINING IN UROLOGY OF PERCUTANEOUS NEPHROLITHOTRIPSY SURGERY   | Enrico Andrade      |
| 55 | INITIAL EVALUATION OF A THIRD GENERATION HIGH INTENSITY FOCUSED ULTRASOUND CLAMP FOR LAPAROSCOPIC PARTIAL NEPHRECTOMY                                | George R. Schade    |

# PROGRAM

56	WRINKLE CELLOMICS: SCREENING BLADDER CANCER CELLS WITH ULTRA-THIN SILICONE MEMBRANE WRINKLE PATTERNS	Jennie H. Appel
57	CONSTANT COAGULATION DEPTH WITH NANOSECOND GREEN LASER-BASED PHOTOSELECTIVE WARM VAPORIZATION (PWV)	Hui Wang
58	INTEGRATED IMAGING AND HISTOTRIPSY THERAPY RAT MODEL PLATFORM FOR UROLOGIC APPLICATIONS	Timothy L Hall
59	ULTRASONIC PROPULSION OF KIDNEY STONES: PRELIMINARY RESULTS OF THE INITIAL CLINICAL TRIAL	Jonathan Harper
60	SETUP USING UNIVERSAL SMARTPHONE ADAPTERS TO TELESCOPES DURING VIDEO CYSTOURETHROSCOPY WITH SCREEN MIRRORING	Ernesto V. Arada III
61	LAPAROSCOPIC WIRELESS PALPATION PROBE: FEASIBILITY OF SIMULATED TUMOR DETECTION IN A HUMAN PROSTATE <b>TOP 10 ABSTRACT</b>	Christopher Mitchell
62	USING CROWD-ASSESSMENT TO SUPPORT SURGICAL TRAINING IN THE DEVELOPING WORLD	Lee W. White
63	CYSTOSCOPIC TELECONFERENCING OF IMAGES FROM INTRAOPERATIVE REFERRALS SHARED ONLINE USING SMARTPHONES	Ernesto V. Arada III
64	DIFFERENTIATING SURGICAL SKILL THROUGH THE WISDOM OF CROWDS	Daniel Holst

## THE NUMBER OF SYSTEMATIC BIOPSY CORES RAISES PREDOMINANTLY THE DETECTION OF INSIGNIFICANT CANCER

Doyoung Chang, Chong Xue, Chunwoo Kim, Changhan Jun, Doru Petrisor,  
Misop Han, Dan Stoianovici

*Robotics Laboratory, Department of Urology, Johns Hopkins University, Baltimore, MD*

**Purpose:** To evaluate and compare the best probability of detection (PoD) of significant and insignificant prostate cancer (PCa) for three systematic (untargeted) biopsy approaches (transrectal, parallel needle transperineal, and angled needle transperineal) using different number of cores.

**Methods:** To simulate transrectal ultrasound (TRUS) guided prostate-biopsy and evaluate the PoD, we re-constructed the human anatomy from the Visible Human Project (National Library of Medicine). Manual segmentation of the whole pelvic structures including the prostate, bladder, urethra, rectum, and pubic bone with the perineal wall was done by an experienced urologist using the Amira Visualization platform (Visage Imaging Inc., San Diego, CA). The volume of the prostate was 21.4 cc.

We assumed that tumors are spherical, the significant tumor size is  $\geq 0.5 \text{ cm}^3$ , and insignificant tumor size  $\leq 0.2 \text{ cm}^3$ . A capsule model that we have previously defined in our previous work (PMCID: 23088974) was used. We considered that the tumor was sampled if its center was within a capsule with a radius equal to that of the tumor. Sampled volume was defined as the volume of the intersection between the capsule and the prostate. The PoD for multiple cores was defined as the ratio of the combined volume of individual sampled volumes to the total prostate volume. We applied our model to maximize the PoD, and compared the maximum PoD for

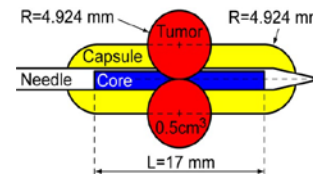


Figure 1. Capsule Model

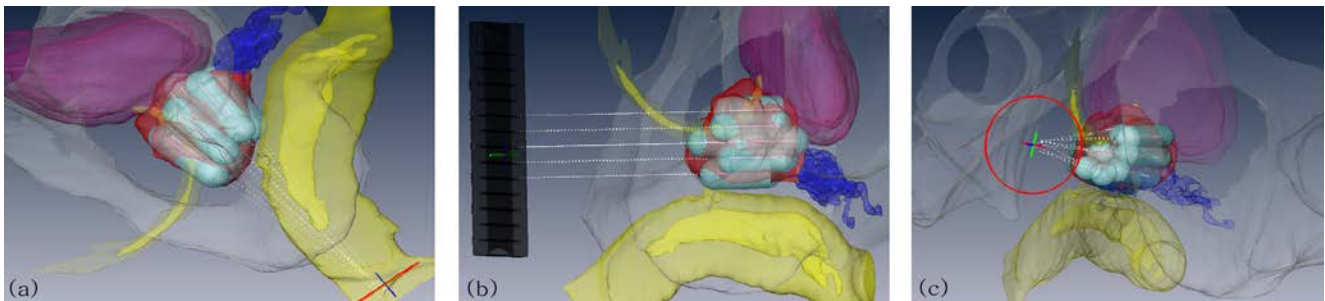


Figure 2. Biopsy simulation: (a) Transrectal, (b) Parallel needle transperineal, and (c) Angled needle transperineal biopsy

different core numbers (6 to 28 cores) and for the mentioned 3 biopsy approaches.

**Results:** If more cores were sampled, the PoD for significant tumors increased. For the same numbers of cores, PoD was higher using transrectal or angled needle transperineal biopsy, as shown in Figure 3a. However, when more cores were used, the PoD of insignificant tumor also increased, so that the ratio of significant to insignificant PoDs decreased, for all 3 biopsy approaches (Figure 3b). For 12-core extended sextant biopsy, significant and insignificant PoD was 79% and 48% respectively, and the ratio was 1.6.

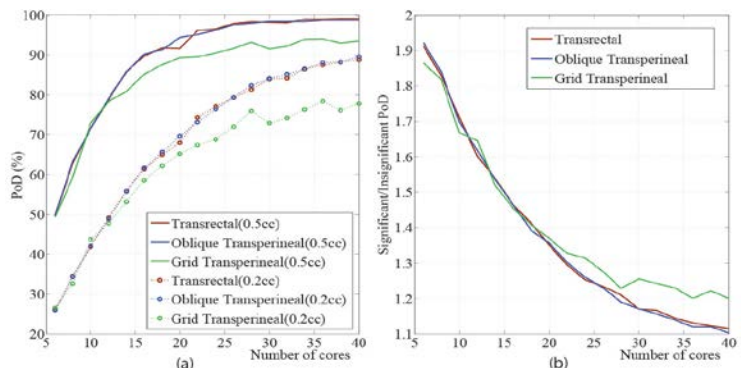


Figure 3. (a) Significant / Insignificant PoD (b) their ratio: VS core number

**Conclusion:** As expected, cancer PoD increases with the number of biopsy cores for both the significant (larger) and insignificant (smaller) lesions. However, as the number of cores is increased, the insignificant PoD increases more than the significant one. This controlled environment experiment demonstrates that increasing the number of cores in systematic biopsy may contribute to PCa overdiagnosis. The study also underscores the limitation of systematic, untargeted (not guided by PCa imaging) biopsy approaches to avoid sampling insignificant lesions.

**Acknowledgement:** This work was supported by the Patrick C. Walsh Prostate Cancer Research Foundation at Johns Hopkins.

## ABSTRACT 2

### IS THE AMOUNT OF RADIATION EXPOSURE DURING FOLLOW-UP IMAGING SAFE IN PATIENTS UNDERGOING ABLATION OF T1 RENAL MASSES?

Necole M Streeper<sup>1</sup>, Timothy J Ziemlewicz<sup>2</sup>, Sara L Best<sup>1</sup>

<sup>1</sup>University of Wisconsin, Department of Urology, Madison, WI

<sup>2</sup>University of Wisconsin, Department of Radiology, Madison, WI

**Introduction:** Percutaneous thermal ablation is an accepted minimally invasive treatment option for small renal masses, proven to be a safe and effective alternative for patients felt to be high-risk for surgery. Serial follow-up imaging is recommended for surveillance in order to identify recurrence. The aim of this study was to quantify the amount of radiation exposure per year for follow-up imaging after ablation procedures for stage T1 renal masses.

**Methods:** After obtaining institutional review board approval, a retrospective review of 71 patients with biopsy-proven, stage T1 primary renal cell carcinoma who underwent CT-guided cryoablation (N=49) or microwave ablation (N=22) from 2009-2013 were identified. The effective radiation dose in milli-sieverts (mSv) was calculated using the reported dose-length product (DLP) multiplied by the adult abdomen conversion factor (0.015) suggested by the American Association of Physicists in Medicine. Follow-up imaging was performed with either CT scans or MRI per preference of the individual urologist. Patient characteristics, tumor size, ablation radiation dose, type of follow-up imaging, radiation exposure of follow-up imaging and length of follow-up were measured.

**Results:** Of the 71 patients (mean age 66±8, 70.4% male) the average follow-up was 16.7±12.4 months. Mean maximum diameter of the renal mass was 2.64cm ±1.00, with 90.1% of the patients classified as stage T1a disease. Surveillance imaging was performed with MRI (66.2%) and/or CT scans (26.8%). Between the cryoablation and microwave ablation groups there was no difference in age, tumor size, ablation radiation dose or total radiation exposure. The average radiation during the ablation procedure was 40.69±28.18mSv. The radiation dose exposure per year was extrapolated from the length of follow-up for patients with available dose reports (N=67). On average, the radiation dose per year during follow-up was 17.30mSv (range 0-148.48mSv).

**Conclusion:** With the acceptable occupational radiation exposure limit of 50 mSv per year set by the nuclear regulatory commission, radiation for patients undergoing surveillance imaging after ablation for T1 primary renal cell cancer is at an acceptable level. Therefore, concern for harmful levels of radiation should not deter urologists from using renal tumor ablation in appropriate patients. Variation in surveillance regimens among urologists suggests a role for a standardized protocol that takes into account both cost and radiation exposure

## ABSTRACT 3

### ACCURACY OF TRANS-RECTAL ULTRASONOGRAPHY TO EVALUATE PATHOLOGICAL PROSTATE WEIGHT: THE IMPACT OF PROSTATE SIZE AND THE PRESENCE OF A MEDIAN

Marc Bienz<sup>1</sup>, Roger Valdivieso<sup>1</sup>, Simon Fortin-Deschenes<sup>3</sup>, Pierre-Alain Hueber MD-PhD<sup>1</sup>, Naif Al-Hathal MD<sup>1</sup>, Michael McCormack MD<sup>1</sup>, Naeem Bhojani MD<sup>1</sup>, Quoc-Dien Trinh MD<sup>2</sup>, Kevin C. Zorn MD<sup>1</sup>

<sup>1</sup>Department of Surgery, Division of Urology, Montreal University Hospital Center, Montreal, PQ, Canada, <sup>2</sup>Division of Urologic Surgery and Center for Surgery and Public Health, Brigham and Women's Hospital / Dana-Farber Cancer Institute, Harvard Medical School, Boston, MA, USA

<sup>3</sup>Polytechnique Montréal, PQ, Canada

**Introduction:** Accurate prostate size estimation is determinant for selecting treatment modalities for prostate cancer and BPH treatment, as well as assessing surgical risk. The aim of this study is to examine the accuracy and the strength of the correlation of trans-rectal ultrasonography (TRUS) for measuring prostate size using the prolate ellipsoid formula ( $H \cdot W \cdot L \cdot \pi / 6$ ) according to prostate size strata.

**Methods:** Preoperative prostate size estimated by TRUS and the weight of post-operative prostate specimens was compared from 440 men that underwent robotic-assisted radical prostatectomy for localized prostate cancer. Patients were stratified according to preoperative prostate size: < 30 g, 30-60 g, 60-80 g, and > 80 g. To evaluate accuracy, the mean absolute percentage of error (MAPE) was used. A percentage of error <15% was considered accurate. The mean percentage of error (MPE) was also used to indicate whether the estimation of TRUS had a tendency to overestimate or underestimate prostate size. Lastly, a bivariate Pearson correlation between TRUS size and prostate weight was performed for each group.

**Results:** Accuracy of TRUS estimation was associated with increased prostate size. TRUS estimation was more accurate for larger prostates. The MAPE associated with each size group was 38.64% (<30 g), 21.33% (30-60 g), 13.23% (60-80 g) and 14.96% (>80 g). Correlation followed a similar size-dependent trend, with a stronger "r" coefficient for larger prostates: 0.174 (<30 g), 0.327 (30-60 g), 0.457 (60-80 g) and 0.839 (>80 g). Interestingly, smaller prostates were underestimated, while larger glands (>80 g) had a tendency to be overestimated by TRUS. Also, the presence of a median lobe did not have a significant impact on accuracy (figure1).

**Conclusion:** This study demonstrates that the accuracy of the prolate ellipsoid formula for TRUS varies according to prostate size. While this formula is fairly accurate for assessing larger prostates, it shows some limitations for smaller prostates. This must be taken into account when evaluating treatment modalities such as transurethral incision of the prostate and brachytherapy.

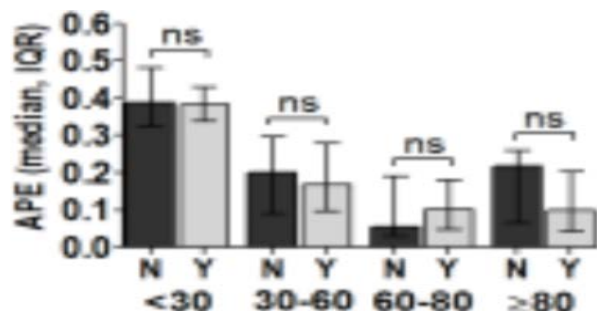


Figure1. Absolute percentage of error (APE) of TRUS function of prostate size and the presence (Y) or absence (N) of a median lobe

### CORRELATION OF MULTI-PARAMETRIC MRI WITH ROBOT-ASSISTED TRANSPERINEAL PROSTATE MAPPING IN DIAGNOSIS OF PROSTATE CANCER

J Yek<sup>1</sup>, K Chen<sup>1</sup>, KJ Tay<sup>1</sup>, H Ho<sup>1</sup>, J Yuen<sup>1</sup>, EC Tan<sup>2</sup>, C Cheng<sup>1</sup>

<sup>1</sup> Department of Urology, Singapore General Hospital, Singapore

<sup>2</sup> Mount Elizabeth Hospital, Singapore

**Introduction:** To correlate findings detected on multi-parametric Magnetic Resonance Imaging (mp-MRI) with positive prostate biopsy in template trans-perineal prostate-mapping (TTPM) biopsy, in diagnosis of prostate cancer (PCa).

**Methods:** A consecutive cohort of patients in a tertiary institution, from May 2011 to December 2013, with rising PSA and between 0 - 2 negative TRUS biopsies underwent mp-MRI and TTPM biopsy. mp-MRI protocol included T1-weighted, T2-weighted, apparent diffusion coefficient maps of diffusion-weighted images and dynamic contrast-enhanced imaging. Images were read independently in routine clinical setting by experienced radiologists. Suspicious lesions, defined as any lesions seen on 1 – 3 sequences, were categorized into an 8-region subdivision of the prostatic gland, according to the anatomical (anterior fibromuscular stroma, central, transitional and peripheral) zones of each prostatic lobe. Systematic biopsy cores were grouped into identical anatomical subdivisions and Gleason score of each region was taken as the highest score observed amongst all positive biopsies.

14 patients with mpMRI-detected lesions were included, and their histology findings were compared with mpMRI-detected lesions to determine the detection rate of PCa in each region.

**Results:** Mean patient age was 60 years with mean prostate volume of 31.8 mls; mean PSA 9.10ng/ml; mean PSA density of 0.25; mean number of cores 31. Prostate cancer was detected in 11 of the 14 patients. Seven of these patients had corresponding mpMRI-detected lesions, of which four had Gleason  $\geq 7$ .

Seven patients had positive biopsy in regions undetected by mp-MRI - of which, three had Gleason  $\geq 7$ . Six of these patients had undetected lesions in TZ, four in AFS, three in CZ and only one in PZ.

The mpMRI has a positive predictive value of 47.0% and negative predictive value of 76.8 % for PCa.

**Conclusion:** MpMRI and TTPM are useful in detection of prostate cancer in men with previous negative TRUS biopsies. Mp-MRI aids detection of clinically significant cancer particularly in the peripheral zone and can guide targeted prostatic biopsy but cannot replace it altogether.

## ABSTRACT 5

### TROCAR-SHARPENED NEEDLES IMPROVE IMAGE-GUIDED BIOPSY

Tobias Simpfindörfer<sup>1</sup>, Timur H. Kuru<sup>1,2</sup>, Sarah Steinemann<sup>1</sup>, Claudia Bergsträsser<sup>1</sup>, Jan P. Radtke<sup>1</sup>, Wilfried Roth<sup>3</sup>, Matthias Roethke<sup>2</sup>, Markus Hohenfellner<sup>1</sup>, Boris A. Hadaschik<sup>1</sup>

<sup>1</sup> Department of Urology, University Hospital Heidelberg, Germany

<sup>2</sup> Department of Radiology, German Cancer Research Center (DKFZ), Heidelberg, Germany

<sup>3</sup> Department of Pathology, University Hospital Heidelberg, Germany

**Introduction:** Hitting target lesions reliably during image-guided prostate biopsy requires accurate needle driving. However, standard needles tend to deviate away from the planned trajectory because of their beveled tip. To improve target errors of MRI-targeted prostate biopsy we introduced trocar-sharpened needles and compared them to standard beveled needles (Figure 1).

**Methods:** 22 men underwent MRI-targeted fusion guided transperineal saturation prostate biopsy, each with half standard beveled and half trocar-sharpened needles. All taken biopsies were scored (1= worse to 5= best) by one urologist for the following criteria: - Accuracy of matching between planned and performed biopsy. - Histologic quality of the sample. - Elegance, which is the easiness to take the biopsy in proper time, planned position and best histologic quality. Afterwards the histologic sample quality was evaluated by a blinded pathologist. The target error in the transversal plane was calculated as the distance between the planned and performed biopsy trajectory (Figure 2). To show a possible training effect a blinded untrained junior resident performed additional biopsies in two men (55 cores).

**Results:** Overall, 552 single biopsies were analyzed. The trocar-sharpened needles had a significantly ( $p<0.05$ ) better scoring for accuracy and elegance rated by the urologist. Moreover histologic quality scored by the pathologist was superior ( $p<0.05$ ). Significantly lower target errors with trocar-sharpened needles were achieved by the untrained resident but not by the experienced user.

**Conclusion:** Using trocar-sharpened needles allows performing targeted prostate biopsy more elegantly and accurately. Better histopathologic sample quality may directly improve the diagnostic certainty. There is a training effect in image-guided biopsy and unexperienced users can significantly reduce target errors.

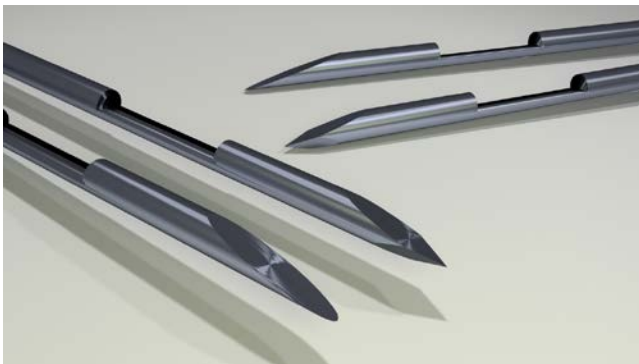


Figure 1: Standard beveled needle (upper and lower) and trocar-sharpened needle

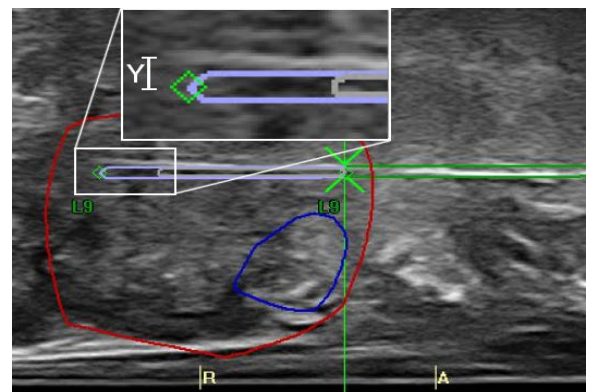


Figure 2: Sagittal live image during biopsy procedure. Deviation of standard beveled biopsy needle in transversal plane between the planned trajectory and the biopsy can be recognized immediately (Y).

## ABSTRACT 6

### CYSTOSCOPIC IMPLANTATION OF A WIRELESS IMPLANTABLE PRESSURE SENSOR IN A LARGE ANIMAL MODEL

Elizabeth Ferry,<sup>1,2</sup> Steve Majerus,<sup>1,3</sup> Hui Zhu,<sup>1,5</sup> Steven Garverick,<sup>1,3</sup>  
Margot S. Damaser<sup>1,4,5</sup>

<sup>1</sup>Advanced Platform Technology Center of Excellence, Louis Stokes Cleveland Veterans Affairs Medical Center, Cleveland, OH; <sup>2</sup>Urology Institute, University Hospitals Case Medical Center, Cleveland, OH; <sup>3</sup>Department of Electrical Engineering and Computer Science, Case Western Reserve University, Cleveland, OH; <sup>4</sup>Department of Biomedical Engineering, Cleveland Clinic, Cleveland, OH; <sup>5</sup>Glickman Urological and Kidney Institute, Cleveland Clinic, Cleveland, OH

**Introduction:** Current methods of determining intravesical pressure are limited in their snap-shot nature and artificial environment, in addition to not being amenable to chronic or ambulatory settings. Chronic bladder pressure monitoring could enable conditional neuromodulation, increasing effectiveness and efficiency. An ideal chronic pressure sensor must be wireless, fully internalized, non-irritative, out of contact with the urine, and placed in a minimally-invasive manner. We have developed a wireless implantable micro-manometer (WIMM) that consists of a micro-battery, pressure transducer, and custom integrated circuit with instrumentation, telemetry, and power management circuitry. An external radio frequency receiver/recharger receives pressure telemetry and intermittently recharges the implanted micro-battery, enabling chronic implantation. The device was sized to be compatible with conventional urological instruments, and the form factor permits cystoscopic implantation in a suburothelial location in the bladder. This study aims to evaluate the safety and feasibility of cystoscopic implantation of WIMM devices in a large animal model.

**Methods:** A 59.2 kg female Jersey calf was anesthetized following an IACUC-approved protocol. Cystourethroscopy was performed and a suburothelial pocket was made using an electrode and cystoscopic scissors. The device was placed into the suburothelial pocket by placing the sheath in the pocket mouth, removing the lens, and advancing the device through the sheath. Placement adjustments were performed using the rigid graspers. This process was repeated to test insertion feasibility in several pockets. Fluoroscopic CT-rendered cystograms were obtained to assess bladder integrity and device location. Necropsy was subsequently performed after euthanasia.

**Results:** Pocket placement was subjectively more straightforward immediately cephalad to, but not involving, the trigone. Cystograms before and after initial pocket creation were identical and confirmed bladder integrity. Visually, the device was placed completely within the suburothelial pocket in two peri-trigone areas, without urothelium interposition. Adequate placement closer to the dome was subjectively more difficult. Necropsy did not reveal perforation grossly, or on filling with Toluidine blue.

**Conclusions:** WIMM devices may be successfully placed in a suburothelial position using minimally invasive, standard equipment and techniques. Posterior wall locations immediately cephalad to the trigone appear to be optimal. Further survival studies are needed to determine long-term outcomes.

**Funding:** Dept of Veterans Affairs RR&D Merit Review 1I01RX000443-01

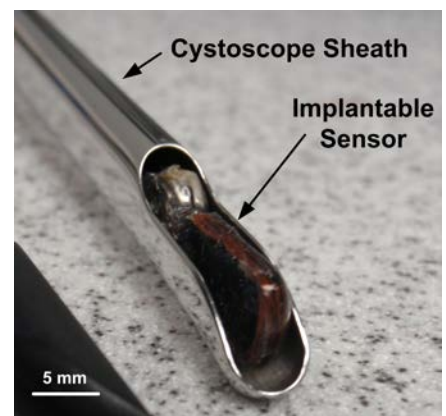


Figure 1. The implantable pressure sensor prototype inside the sheath of a 24 French rigid cystoscope.

### DEVELOPMENT AND INITIAL PORCINE AND CADAVER EXPERIENCE WITH THREE-DIMENSIONAL PRINTING OF ENDOSCOPIC AND LAPAROSCOPIC EQUIPMENT

Michael del Junco, Renai Yoon, Zhamshid Okhunov, Ramtin Khanipour,  
Samuel Juncal, Garen Abedi, Achim Lusch and Jaime Landman

*Department of Urology, University of California, Irvine*

**Introduction:** Recent advances in three-dimensional (3D) printing technology have made it feasible to print surgical devices in the operating theater. We report our initial experience with the printing and deployment of endoscopic and laparoscopic surgical equipment.

**Methods:** We created computer-aided designs for ureteral stents and laparoscopic trocars using SolidWorks. Three generations of stents (7Fr, 9Fr and 12Fr, respectively) were printed with an Objet500 Connex printer (Stratasys Ltd., Minneapolis, MN, USA) using a rubber-like PolyJet photopolymer (Tango Black Plus FLX980; 70-shore value). Fourth generation stents (9Fr) were printed with an EOSINT P 395 (EOS e-Manufacturing Solutions, Krailing, Germany) printer using a nylon polyether block amide (Elasto Plastic, Shapeways, Eindhoven, Netherlands). Laparoscopic trocars were printed with an Objet30 Connex printer using a rigid opaque photopolymer (Vero White Plus RDG835). We deployed the printed stents and trocars in an *in vivo* porcine model and in a cadaver models. We compared the printed trocars to two standard trocars for defect size and wound area using a digital caliper.

**Results:** Using contemporary printing technology, the first three generations of stents were functional failures as they possessed a diminutive inner lumen required to allow the passage of a 0.035 guide-wire. With technological advances, we printed a fourth generation (9Fr) stent with a functional lumen and improved wall thickness. We successfully deployed the fourth generation stent in a porcine model over a 0.035 guide-wire using standard Seldinger technique. We successfully deployed the first generation 3D printed trocars without difficulty in an *in-vivo* porcine model (n=4). The trocars demonstrated no significant difference for the creation and maintenance of pneumoperitoneum and instrument passage when compared to the contemporary trocars examined. The printed trocar had a larger superficial trocar defect area ( $p<0.001$ ) and superficial defect length ( $p<0.001$ ) compared to Karl Storz, and Ethicon trocars (29.41mm<sup>2</sup>, 18.06mm<sup>2</sup>, and 17.22mm<sup>2</sup> respectively and 14.29mm, 11.39mm, and 12.15mm, respectively).

**Conclusions:** 3D printing of ureteral stents and trocars is feasible, and these devices can be deployed in a porcine and cadaver models. 3D printing technology is rapidly advancing and may be clinically viable in the future.

### INCORPORATION OF THE GREENLIGHT-SIM™ SIMULATOR AT THE ANNUAL QUEBEC UROLOGY OBJECTIVE STRUCTURED CLINICAL EXAMINATIONS

Yasser Noureldin<sup>1,2</sup>, Mohamed A. Elkoushy<sup>1</sup>, Nader Fahmy<sup>1</sup>, Serge Carrier<sup>1</sup>, Mostafa M. Elhilali<sup>1</sup>, Sero Andonian<sup>1</sup>

<sup>1</sup> McGill University Health Centre, Montreal, QC, Canada

<sup>2</sup> Urology Department, Benha University, Egypt

**Introduction:** To assess laser prostatectomy skills of postgraduate trainees (PGTs) during the annual Quebec Urology Objective Structured Clinical Examinations (OSCEs).

**Methods:** After obtaining Institutional Review Board (IRB) approval and written informed consent, urology PGTs in Post-Graduate Years (PGY-3 to PGY-5) from all five urology training programs in Quebec were recruited to participate in assessment of their laser Photoselective Vaporization of the Prostate (PVP) skills using the GreenLight-SIM™ (GL-SIM) during two annual OSCEs on Dec 1<sup>st</sup> 2012 and Dec 7<sup>th</sup> 2013. PGTs were asked to perform two exercises: anatomical identification and PVP of a 30 g normal prostate within a 20-minute station. Grams vaporized, global scores and number of correct anatomical landmarks were recorded and correlated with PGY level, training on the GL-SIM and previous PVP experience.

**Results:** 25 PGTs were recruited at each OSCE with 13 PGTs participating in both OSCEs. PGTs had performed on average 2.8 and 4.5 PVP cases ( $p > 0.05$ ) prior to the 1<sup>st</sup> and 2<sup>nd</sup> OSCEs, respectively. When comparing scores from the 1<sup>st</sup> to the 2<sup>nd</sup> OSCE, there was a significant increase in the number of grams vaporised ( $2.9 \pm 0.2$  vs.  $4.3 \pm 0.4$ g;  $p = 0.003$ ) and global score ( $100 \pm 15$  vs.  $165 \pm 26$ ;  $p = 0.03$ ). There was good correlation between the number of previously performed PVP cases and the global score ( $r = 0.4$ ,  $p = 0.04$ ). PGTs with previous practice on the GL-SIM (27/50) showed significantly increased global score ( $100.6 \pm 19.6$  vs.  $162.6 \pm 22.4$ ;  $p = 0.04$ ) and grams vaporised ( $3.1 \pm 0.27$  vs  $4.1 \pm 0.36$ ;  $p = 0.04$ ) compared with those who did not practice on GL-SIM before. PGY level did not significantly affect grams vaporised and global score ( $p > 0.05$ ). For the 13 PGTs who participated at both OSCEs, there was significant improvement in the global score ( $107 \pm 21$  vs.  $219 \pm 31$ ;  $p = 0.003$ ) and grams vaporised ( $2.9 \pm 0.3$  vs.  $5.2 \pm 0.5$ ;  $p = 0.001$ ) from the 1st to the 2nd OSCE.

**Conclusion:** Performance on the GreenLight-SIM at OSCEs significantly correlated with previous practice on the GL-SIM simulator and number of previous PVP cases performed rather than PGY level.

## PRECISION OF URETEROSCOPIC VISUAL ESTIMATION OF STONE FRAGMENT SIZE

Leone, Andrew<sup>1</sup>, Tran, Timothy<sup>1</sup>, Afiadata, Achankeng<sup>2</sup>, Thavaseelan, Simone<sup>1</sup>, Pareek, Gyan,<sup>1</sup> Yates, Jennifer<sup>2</sup>

<sup>1</sup> Brown University/ Kidney Stone Center, Providence, RI

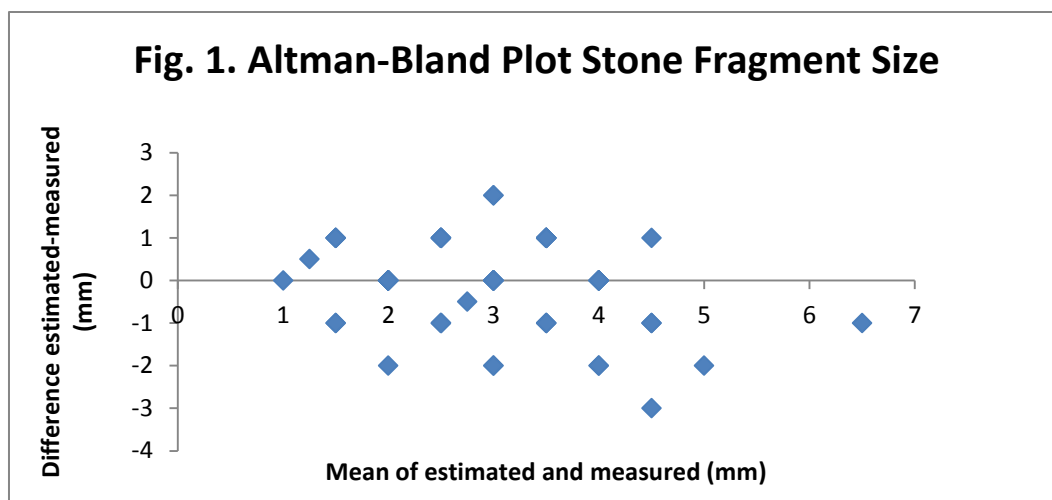
<sup>2</sup> UMass Medical Center, Worcester, MA

**Introduction:** We sought to establish the accuracy of fellowship trained endourologists in estimating *in vivo* stone fragment size during flexible ureterorenoscopy by comparing visual estimated size to measured size. Previously other literature has investigated endourologists accuracy at predicting *ex vivo* stone fragment size.

**Methods:** An IRB approved prospective study was conducted with all patients undergoing laser lithotripsy for renal and ureteral stones by three fellowship trained endourologists from November 2013 to February 2014. In all patients ureteral access sheaths were successfully placed and there was no deviation from standard management of surgeons' clinical practice. The size of 61 stone fragments in 15 patients was initially visually estimated by the surgeon from estimation based on the size of the laser fiber (in all cases a 200 micron laser fiber) and a 0 tip nitinol basket (all cases 1.9 Fr) . The stone fragment was then basket extracted using a standard 0 tip nitinol stone basket and the largest dimension of the stone was measured by the surgeon using a ruler. Accuracy of measurement was performed by creation of correlation coefficients and creation of Altman-Brand plots.

**Results:** Fellowship trained endourologists overall underestimated stone size by 0.11 mm. The correlation coefficient was  $r=0.61$  with  $p$  value  $<0.00001$ . Stones smaller than 4mm were overestimated by 0.25 mm ( $R=0.49$ ,  $p=<0.0001$ ) and stones larger than 4 mm were underestimated by 0.94 mm ( $R=0.39$ ,  $P=0.09$ ). Altman-Brand plots demonstrated that the endourologists estimated stone size within a range of -0.11 to 1.42 mm (Figure 1). There were no complications encountered in any of the patients.

**Conclusion:** Endourologists overall underestimated stone fragment size during ureterorenoscopy. However when subdivided based upon stone fragment size, stone fragments smaller than 4 mm were overestimated and those larger than 4 mm were underestimated. Further research is needed to determine if technology or surgeon training can improve measurement accuracy of *in vivo* stone fragments. Future research will look at improvement over time with repeated estimations and if varying the size of laser fiber/basket utilized can improve precision. Because of slight underestimation of fragment size we recommend performing basket stone extraction at the conclusion of ureterorenoscopy as a final check in order to improve stone fee rates.



### EXAMINING THE BENEFITS OF ROBOTIC TECHNOLOGY FOR EXPERIENCED UROLOGICAL SURGEONS

Lee J. Moore<sup>1</sup>, Elizabeth Waine<sup>2</sup>, John S. McGrath<sup>2</sup>, Mark R. Wilson<sup>1</sup>, Samuel J. Vine<sup>1</sup>

<sup>1</sup> College of Life and Environmental Sciences, University of Exeter

<sup>2</sup> Exeter Surgical Health Services Research Unit, Royal Devon and Exeter NHS Trust

**Introduction:** Robotic surgery represents an engineered solution to some of the physical constraints placed upon laparoscopic surgeons (e.g., reduced visual acuity and dexterity). However, limited research has examined how this technology benefits the surgeon. In collaboration with urologists from the Royal Devon and Exeter NHS Trust and with funding from Intuitive Surgical (CA, USA) the present study had two aims; (1) to compare the performance, mental effort, and workload of experienced surgeons performing a surgical task on both robotic and laparoscopic systems, and (2) to compare surgeons' cardiovascular response and performance when executing stressful surgical tasks on these two systems.

**Methods:** Thirty-two qualified and trainee surgeons (Mean age = 39.91, *SD* = 8.96) attended two sessions. In session one, the surgeons were fitted with a heart rate monitor before performing a two-instrument rope threading task on both the robotic (da Vinci) and laparoscopic (3dmed Lapbox) systems in a counterbalanced order. Measures of performance (completion time), mental effort (subjective: Rating Scale for Mental Effort [RSME] and objective: root mean square of successive R-R intervals [r-MSSD]), and workload (The Surgery Task Load Index [SURG-TLX]) were recorded. This data was subject to a series of dependent *t*-tests.

In session two, the surgeons were assigned to perform a ball pick-and-drop task under 3 stress conditions (time pressure, multi-tasking, and evaluative pressure) on either the robotic or laparoscopic system. The surgeons' cardiovascular response (challenge and threat index), performance (number of errors), and multi-tasking performance (tone counting error calculated by subtracting the actual number of target tones, from the surgeons' estimate) were assessed. A series of 2 (Group: Robotic vs. Laparoscopic) x 3 (Condition: Time Pressure, Multi-tasking, Evaluative Pressure) mixed design ANOVAs with follow-up LSD *t*-tests were conducted on the cardiovascular and performance data, while a one-way ANOVA was run on the multi-tasking performance data.

**Results:** In relation to the first aim, results indicated that the surgeons completed the task quicker on the robotic system than the laparoscopic system (72.91 *s* vs. 99.68 *s*; *p* < .001). Further, the surgeons reported that the task required less mental effort on the robotic system (43.78 vs. 57.44; *p* < .001). The surgeons also exhibited higher r-MSSD (reflecting lower mental effort) when performing the task on the robotic system (33.59 *ms* vs. 27.69 *ms*; *p* = .013). Finally, the surgeons reported lower workload when completing the task on the robotic system (92.66 vs. 120.84; *p* = .001).

In terms of the second aim, the results showed that the robotic group exhibited a higher index value (reflecting a more favorable cardiovascular response) than the laparoscopic group across the stress conditions (0.59 vs. -0.59; *p* = .001). The robotic group also made fewer errors across these conditions (0.44 vs. 0.88; *p* = 0.26). Finally, although the robotic group made fewer tone counting errors in the multi-tasking condition, this difference was not statistically significant (0.19 vs. 0.50; *p* = .180).

**Conclusion:** The results highlight the benefits of robotic technology for experienced surgeons. The results suggest that surgical tasks can be performed quicker and more accurately with a robotic system. Further, these tasks can be performed with the investment of less mental effort and at a lower workload, potentially allowing surgeons greater cognitive resources for dealing with other demands (e.g., decision-making). Finally, surgeons' cardiovascular responses are more favorable when asked to perform stressful tasks on a robotic system (i.e., a challenge state consisting of higher cardiac output and lower total peripheral resistance has been associated with more positive performance and health outcomes).

### WILL THE INCREASED APPLICATION OF ROBOTIC TECHNOLOGY HELP ADDRESS THE LEARNING CURVE FOR SURGICAL TRAINEES?

Lee J. Moore<sup>1</sup>, Elizabeth Waine<sup>2</sup>, John S. McGrath<sup>2</sup>, Mark R. Wilson<sup>1</sup>, Samuel J. Vine<sup>1</sup>

<sup>1</sup> College of Life and Environmental Sciences, University of Exeter

<sup>2</sup> Exeter Surgical Health Services Research Unit, Royal Devon and Exeter NHS Trust

**Introduction:** Robotic technology has revolutionized surgery in the UK and USA, particularly in the area of urology. However, although clinical studies have demonstrated the benefits of robotic versus laparoscopic surgery for the patient, little is known about the benefits of using robotic technology for the learning curves of trainee urologists. Therefore, the present study, a collaborative study between researchers at the University of Exeter and urologists from the Royal Devon and Exeter NHS Trust, aimed to compare how novice surgeons acquired surgical skills using a robotic device or a basic laparoscopic system.

**Methods:** Forty novice participants (Mean age = 25.27;  $SD = 3.23$ ) were assigned to one of two groups (robotic or laparoscopic trained). After 1 baseline trial on a simple ball pick-and-drop task, participants performed 50 learning trials. Following the learning trials, participants completed a retention trial and a transfer trial (rope threading task). One month later, participants performed a delayed retention trial and a multi-tasking trial (secondary tone counting task; designed to load cognitive resources). Measures of performance (completion time) and multi-tasking performance (tone counting error calculated by subtracting the actual number of target tones, from the surgeons' estimate) were recorded. A series of 2 (System: Robotic vs. Laparoscopic) x 3 (Time: Baseline, Immediate Retention, Delayed Retention) mixed design ANOVAs with follow-up LSD  $t$ -tests were conducted on the performance data, while independent  $t$ -tests were conducted on the transfer trial and multi-tasking trial performance data.

**Results:** Results showed that the robotic trained group completed the ball pick-and-drop task quicker than the laparoscopic trained group across baseline, immediate retention, and delayed retention trials (26.03  $s$  vs. 36.38  $s$ ;  $p = .006$ ). Moreover, the robotic trained group also performed the transfer rope threading trial (90.95  $s$  vs. 205.18  $s$ ;  $p = .001$ ) and the multi-tasking tone counting trial (21.23  $s$  vs. 27.88  $s$ ;  $p = .004$ ) quicker than the laparoscopic trained group. Finally, in the multi-tasking trial, the robotic trained group made fewer tone counting errors than the laparoscopic group (0.00 vs. 1.05;  $p = .036$ ).

**Conclusion:** The results highlight the benefits of using robotic technology for the acquisition of technical surgical skills. Trainees were able to perform the surgical tasks more quickly using the robotic platform under all conditions as well as showing transferability of surgical skills to a more complex task. This advantage was also maintained over an extended period of time (delayed retention) and while performing a surgical task under distracting multi-tasking conditions (secondary tone counting).

## DIRECT MRI-GUIDED TRANSPERINEAL PROSTATE BIOPSY WITH MR-SAFE ROBOT. FIRST FDA-APPROVED ROBOT FOR THE MR ENVIRONMENT

Dan Stoianovici<sup>1</sup>, Chunwoo Kim<sup>1</sup>, Changhan Jun<sup>1</sup>, Doru Petrisor<sup>1</sup>, Katarzyna J. Macura<sup>2</sup>,

Ashley Ross<sup>1</sup>, Mohamad Allaf<sup>1</sup>

*Robotics Laboratory, Urology<sup>1</sup> and Radiology<sup>2</sup> Departments, Johns Hopkins University, Baltimore, MD*

**Introduction:** MRI has emerged as the gold standard for imaging localized prostate cancer (PCa). Targeted biopsy of cancer suspicious lesions (CSR) depicted in the MRI is being investigated clinically. Most current methods use image “fusion” (registration) between pre-acquired MRI and interventional transrectal ultrasound (TRUS) (PMCID:23938941). But temporal, patient position, gland deformation and motion, and registration errors between the MRI and TRUS are difficult to account for and result in biopsy targeting errors that are difficult to quantify. Direct MRI-Guidance circumvents these problems by using MRI to identify the CSR and also guide the procedure. However, the biopsy must be performed in the MRI gantry and requires special devices.

**Methods:** A robotic device was developed to assist in-gantry MRI targeted biopsy. This mounts on the MRI table alongside the patient placed in the lateral decubitus position and is registered to the MRI space. The physician selects a CSR depicted on MRI and the robot automatically orients a needle-guide to the target and presets the depth of insertion allowing targeted biopsy to be performed. The procedure then cycles to the next biopsy target.

The robot presents 6 degrees of freedom, is entirely constructed of non-magnetic and non-conducting materials (plastic, ceramic, glass, and rubber), is pneumatically actuated, and uses optical sensor feedback. No electricity is used in the MRI scanner room (ACR Zone 4). The robot is covered with a sterile bag and the needle-guide is a biocompatible (ISO-10993) and sterilized component.

A clinical protocol and Risk Hazard Analysis were developed. The FDA determined that the use of the device according to the clinical protocol presents a significant risk (21CFR812.3(m)). Accordingly, an investigational device exemption (IDE) application was filed and subsequently approved by the FDA. The IRB approval of the study followed. Formal monitoring of the clinical study has been instituted. The first biopsy case was performed.

**Results:** Based on experimental data and scientific rationale the FDA agreed that the robotic device is MRI-Safe according to ASTM F2503 (safe to use in any MR environment) and allowed it to be labeled accordingly. This is an item that poses no known hazards in all MR environments.

The first biopsy case has been performed. Biopsy samples were acquired in the MRI scanner under direct MRI guidance assisted by the device. The figure shows the patient in the MRI scanner and the robot placed on position next to the patient to access the perineal site for biopsy. The patient tolerated the procedure well with no complications and no subsequent adverse events.

**Conclusion:** Only four devices have been used clinically for direct MRI-guided prostate biopsy: two manually operated for transrectal biopsy (PMCID:16406885, 18791410), an actuated remote controlled transrectal device (PMCID:21406625), and a robotic device for transperineal biopsy (ISI:000325974500005). Novel to our robot is its MRI-Safe technology, which enabled its FDA clearance for clinical trials. To the best of our knowledge this is the only robot approved by the FDA to operate in the MR Environment, in general, not only for the prostate. The first clinical case suggests that robotic biopsy may be safe and feasible. Fundamentally, unlike MRI fusion methods, direct MRI-guided biopsy is capable to verify biopsy targeting by imaging the inserted needle with MR and observing its location relative to the CSR. This objective mean of quality control may help raise urologists’ confidence in the results of biopsy, and then help validating PCa imaging. Next cases are being scheduled.

**Acknowledgement:** The project described was supported by Award RC1EB010936 from the National Institute of Biomedical Imaging and Bioengineering. **Disclosure:** Under a licensing agreement between Samsung and the Johns Hopkins University, Dr. Stoianovici has received income on an invention described in this article. This arrangement has been reviewed and approved by the JHU in accordance with its conflict of interest policies.



Figure: Patient and robot in the MRI scanner

# ABSTRACTS

## ABSTRACT 13

### SONOELASTOGRAPHY OF INTRATESTICULAR LESIONS: HISTOLOGIC CORRELATION

Gideon Richards<sup>1</sup> MD, Amin Herati MD<sup>1</sup>, Henry Pek<sup>2</sup> MD, Bruce Gilbert<sup>1</sup> MD, PhD

<sup>1</sup>The Smith Institute for Urology, Hofstra University-North Shore/LIJ School of Medicine

<sup>2</sup>North Shore/Long Island Jewish Health System, Department of Radiology

**Introduction:** Intratesticular masses have classically been treated as malignant until proven otherwise by histology. Smaller masses have been associated with benign histology. Testis sparing approaches with partial orchiectomy and ultrasound surveillance protocols have been used to decrease the number of orchiectomies for benign lesions. Sonoelastography has emerged as an imaging modality with a high specificity for predicting benign lesions. Shear-wave sonoelastography employs ultrasound measurements of the propagation of shear waves in tissues to calculate the elastic moduli of those tissues. Increased moduli of elasticity are reflective of firmer tissues. The purpose of this study is to correlate testicular sonoelastography findings with pathology.

**Methods:** We retrospectively reviewed the charts of all patients undergoing scrotal sonoelastography and subsequent biopsy with intraoperative ultrasound guidance or orchiectomy for intratesticular lesions. Sonoelastography was performed by a single Radiologist using an ultrasound equipped with shear wave sonoelastography technology (Aixplorer®, SuperSonic Imagine, Aix-en-Provence, France). The pathologic findings were correlated with elastography findings. One patient had resolution of his lesions on imaging and did not undergo biopsy.

**Results:** Five patients had subcentimeter lesions all with no increase to minimal increase in lesion firmness on sonoelastography. Four out of five had benign pathology and the fifth had resolution of his lesions. Four patients had lesions with markedly increased firmness, two had germ cell tumors and two had benign pathologies (Table1).

**Conclusions:** Lesions that do not demonstrate an increased elastic modulus with sonoelastography in this series have benign pathology. Our experience and the findings in the existing literature suggest that subcentimeter lesions that are soft on sonoelstography are more appropriate for surveillance than operative management. Sonoelastography is an evolving technology the holds great promise for being a non-invasive diagnostic modality to identify which subcentimeter testis lesions are benign.

Table 1. Sonoelastographic findings associated with ultrasonically demonstrated testicular lesions with their corresponding pathologic or clinical (in the case of lesions that resolved) findings.

Patient	Right lesion(s) elastic modulus	Left lesion(s) elastic modulus	Histologic/Clinical Diagnosis
1	no increase	no increase	benign, right Sertoli nodule with hypospermatogenic tubules, bilaterally
2	-	no increase	benign, Leydig cell hyperplasia with hypospermatogenic tubules
3	no increase	no increase	benign, left Leydig cell lesion with Sertoli cell-only pattern and maturation arrest in tubules bilaterally
4	no increase	no increase	benign, interstitial fibrosis with hyalinization of tubules rare Sertoli cell-only pattern and Leydig cell nodule, bilaterally.
5	minimal increase	minimal increase	probable sarcoid, lesions resolved after steroid treatment
6	marked increase	marked increase	benign, necrosis, hyalinization and Sertoli cell only patterns, fibrosis
7	-	marked increase	malignant, Mixed GCT (embryonal and seminoma)
8	marked increase	-	benign, epidermoid cyst
9	marked increase	-	malignant, NSGCT (embryonal, yolk sac and teratoma)

## IMPACT OF IRRIGANT VISCOSITY ON STONE DUST DURING LASER LITHOTRIPSY—*IN VITRO* ANALYSIS

Dr Ashish Patil, Dr Lokesh Patni, Dr Preeti Patil

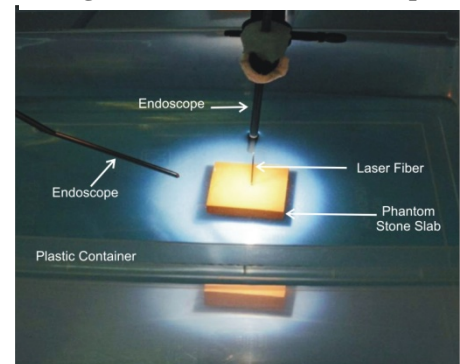
*Institute of Urology, Dhule.*

**Introduction:** Stone dust generated during stone pulverisation with laser impairs endoscopic vision. We studied the impact of irrigant viscosity on the same.

**Methods:** An invitro hands free bench was constructed using a fish tank, phantom stone slab, two endoscopes and an 800 μ laser fiber (Figure 1). The fish tank was successively filled with distilled water (Viscosity =1.002 mPa.s), normal saline (viscosity = 1.018 mPa.s) and glycine (viscosity = 1.07 mPa.s). Single impulses of 800, 2000 and 3000 mJ of Holmium laser were delivered to the phantom in each media. The volume of dust cloud formed was measured using a vertical and horizontal, calibrated visual scales and two endocamera systems (Figures 2 and 3). SPSS analysis for different energy cohorts was carried out.

**Results:** Volume of stone dust observed showed linear correlation with the laser energy used and inversely proportional to the viscosity of irrigant used across all the energy cohorts.

**Figure 4: Invitro fish tank setup**



Quantum of Holmium energy	Irrigant	Volume of stone dust (cm <sup>3</sup> ) (Median (IQR))	p value (compared with water)
800 mj	Water	12.60 (10.14-14.57)	NA
	Saline	4.50 (2.93-5.11)	<0.001*
	Glycine	2.53 (2.00-3.79)	0.007**
2000 mj	Water	30.29 (18.74-39.57)	NA
	Saline	13.77 (10.34-13.77)	<0.001*
	Glycine	3.80 (3.62-5.22)	<0.001**
3000 mj	Water	36.99 (34.11-39.57)	NA
	Saline	17.21 (12.93-21.36)	<0.001*
	Glycine	14.17 (11.09-16.41)	0.09**

\*compared with water \*\*compared with saline

**Conclusion:** Viscosity of the irrigant fluid is a determinant of the volume of stone dust formed at all energy levels. Using an optimally higher viscosity irrigant along with low laser power may help curb stone dust formation

**Figure 2: Visual calibrated scale – vertical**

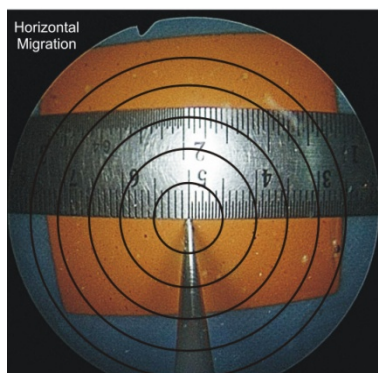
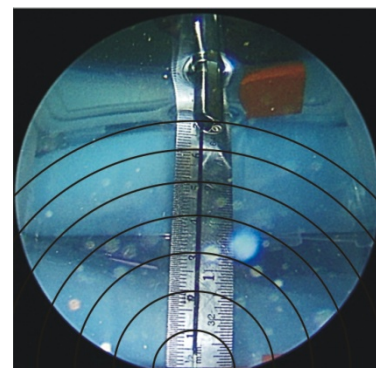


**Figure 3: Visual calibrated scale - horizontal**



### THREE-DIMENSIONAL VOLUME EVALUATION OF PERIRENAL ADIPOSE TISSUE VOLUME USING NOVEL VITREA SOFTWARE AS A PREDICTOR RENAL CORTICAL NEOPLASM HISTOPATHOLOGY

Zhamshid Okhunov<sup>1</sup>, Mari Bozoghlanian<sup>1</sup>, Kevin Labadie<sup>1</sup>, Martin R. Hofmann<sup>1</sup>, Michael del Junco<sup>1</sup>, Allen Jeon<sup>2</sup>, Mohammad Helmy<sup>2</sup>, and Jaime Landman<sup>1</sup>

<sup>1</sup>*Department of Urology, University of California, Irvine*

<sup>2</sup>*Department of Radiology, University of California, Irvine*

**Introduction:** Contemporary axial imaging technology allows for advanced three-dimensional (3D) visualization of human anatomy from computerized tomography (CT) or magnetic resonance imaging (MRI). Axial imaging allows for accurate volumetric measurement of different organs for accurate clinical volume estimation. Visceral and perirenal adipose tissue (PAT) have been shown to be metabolically active. Previously we have demonstrated that two-dimensional PAT measurements are associated with more aggressive renal cell carcinoma (RCC) subtypes. In this study, we evaluated total PAT volume as a predictor of renal tumor histopathology using novel 3D imaging software Vitrea LT (Vital Images, Inc., Minnetonka, MN).

**Methods:** We retrospectively evaluated patients who underwent laparoscopic radical or partial nephrectomy for RCN. PAT volume was measured by post-processing of preoperative computed tomography images using Vitrea software (Vital Images, Inc., Minnetonka, MN). We measured total perirenal space volume by manual contouring. We subtracted out structures with densities greater than adipose tissue (e.g. kidney, adrenal gland, vessels), thereby yielding only a total PAT volume (Figure 1). We evaluated demographic, clinical and operative parameters, PAT volume, and final tumor histopathology.

**Results:** In this pilot analysis, a total of 18 patients were included. There were 7 (39%) men and 11 (61%) women with a median body mass index (BMI) of 26 kg/m<sup>2</sup>. Median tumor size was 2.5 cm (1.3-6.0 cm), and the median PAT volume was 205.8 cm<sup>3</sup>. Mean PAT for RCC and benign histopathology was 345.50 cm<sup>3</sup> and 92.67 cm<sup>3</sup> respectively (p=0.026).

**Conclusions:** With improvement in rapid 3D volumetric assessment of radiological data, PAT volume may be more accurate measurement of adipose tissue. In our preliminary analysis, increased PAT volume is a significant predictor of RCC histopathology over a benign RCN. Further analysis with more patients is in progress to confirm our initial findings.

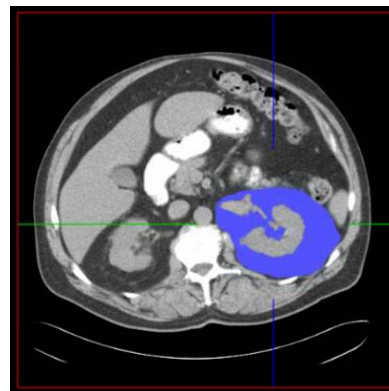


Figure 1. Vitrea LT 3D PAT measurement on axial CT image.

### LOWER AND UPPER URINARY SYSTEM EVALUATION WITH HIGH RESOLUTION MANOMETRY: INITIAL ANIMAL STUDY

Guy Hidas, Hak J. Lee and Antoine E. Khoury,

*Department of Urology, University of California Irvine, Children Hospital Orange County, Orange, CA*

**Propose:** Major drawbacks of Urodynamic study are that the critical components of continence, the bladder neck, urethral and sphincter muscle functions are only indirectly measured. ManoScan™ (Sierra Scientific, CA USA) is a high resolution Manometry (HRM), catheter used in the gastrointestinal system for the diagnosis of esophageal and anorectal sphincters disorders. Along this catheter there are 36 miniature intraluminal pressure sensors that provide real time dynamic pressure measurements and are able to localize precisely the exact anatomical point of obstruction. The aim of this study is to test the feasibility and efficacy of this technology to measure intraluminal pressures along the lower and upper urinary system.

**Methods:** Two farm female pigs were used in this study. After administration of general anesthesia, 8.2 French HRM catheter was inserted into the bladder. A few cycles of bladder filling and emptying were performed on each pig. HRM pressures were captured simultaneously along the bladder and urethra. Pressure topography as well as traditional pressures tracing were plotted. In the HRM was inserted to the lower part of the ureter to measure ureteral pressures during peristaltic waves.

**Results:** We observed gradually increase in sphincter and intravesicle pressures during natural bladder filling (Figure 1). Toward the end of the filling phase bladder pressures and sphincter pressures equalize and leak occurred. After installing the HRM in the lower ureter, Peristaltic waves were observed and recorded (Figure 2).

**Conclusion:** HRM precisely measures simultaneously and continuously the intraluminal vesicle, and urethral pressures and activity. This technology accurately correlates bladder events with the outlet in patients with incontinence. HRM could be applied for the diagnosis of numerous storage and voiding disorders in the office or as a natural fill ambulatory Urodynamic procedure. HRM may also have a potential role in the diagnosis of renal and ureteral obstruction.

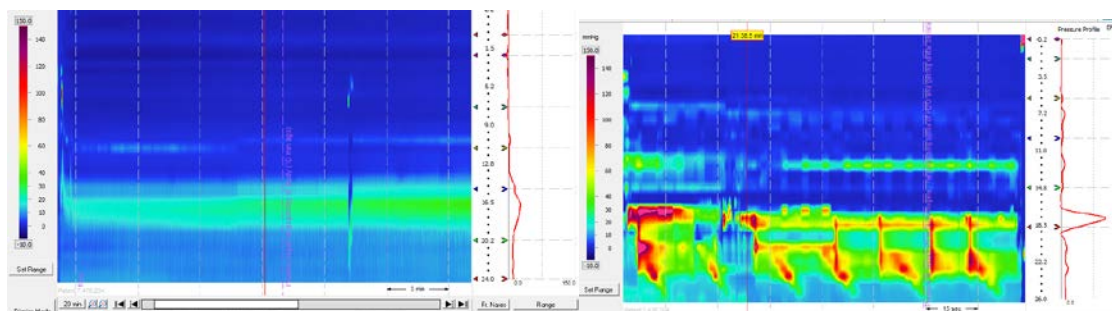


Figure 1

Figure 2

Pressure topography plotted during HRM catheter insertion into the bladder (Figure 1), and ureter (Figure2). Time is on the X-axis and length along the Lower urinary system on the Y-axis, where the most proximal part is on the bottom. Pressure magnitude is encoded in color corresponding to the scale shown at the side. High-pressure regions are denoted by the red end of the spectrum while the low-pressure regions by the blue end of the spectrum. Figure 1 showed increased sphincter pressures during bladder filling. Figure 2 shows peristaltic wave in the lower ureter.

### FIBROSIS AND COLLAGEN CONTENT AFTER HISTOTRIPSY IN THE CANINE PROSTATE

Sarah E. Darnell<sup>1</sup>, Timothy L. Hall<sup>1</sup>, Xu Cheng<sup>2</sup>, Kimberly A. Ives<sup>1</sup>, William W. Roberts<sup>1,2</sup>

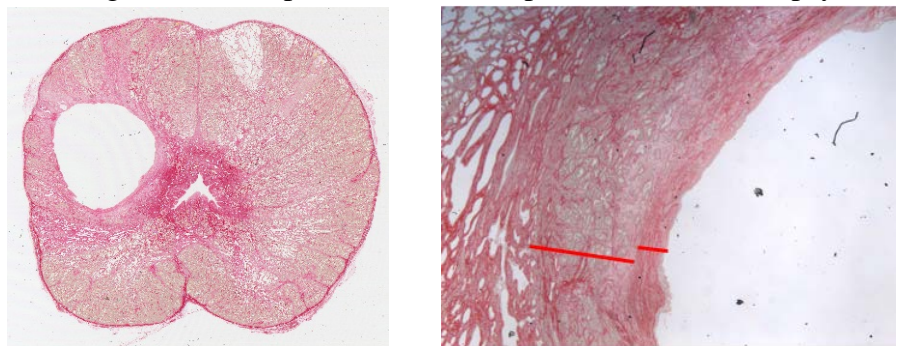
*Departments of Biomedical Engineering<sup>1</sup> and Urology<sup>2</sup> University of Michigan*

**Introduction:** Histotripsy is a noninvasive, pulsed ultrasound technology in which short bursts of intense acoustic energy are applied at low duty cycle (< 1%) to achieve tissue homogenization within a targeted tissue volume. As with any ablative modality, histotripsy induces an inflammatory response. However, in examining tissue samples from previous experiments, it appeared that the resultant fibrotic response from histotripsy was limited compared to the typical tissue response seen after thermoablation. The objective of this study was to describe the fibrotic response and quantify collagen density immediately adjacent to the histotripsy ablation zone and throughout the prostate in a canine model 6 weeks after histotripsy treatment.

**Methods:** Histotripsy was applied in standard fashion (750 kHz, 5 cycle burst, pulse repetition frequency 500 Hz) to the left half of 8 canine prostates to produce an intraparenchymal zone of tissue homogenization. Six weeks after treatment, prostates were harvested and Picrosirius red microscope slides created. The width of the fibrotic bands was recorded. Average collagen density in the treated and untreated half of each canine prostate was measured from 2400 dpi scans of whole mount specimens using a computerized colorimetric algorithm (Matlab) which quantifies the red stained collagen. Additionally, eight regions in the treated area with the most extensive visual fibrosis (20x magnification) were assessed for collagen density.

**Results:** Visual microscopic analysis of Picrosirius red slides generally revealed a band of dense collagen (~ 0.5mm wide) immediately adjacent to the cavity produced by histotripsy. This was surrounded by a second band (~ 1mm wide) of mildly increased collagen interspersed among glandular architecture. The percent of collagen in the untreated portion of the prostate averaged 35% though exhibited a broad range (18-73%). In the treated half of each prostate, collagen density was found to have increased by 4% compared to the untreated half of the prostate.

**Conclusion:** Histotripsy mechanically homogenizes tissue by mechanical means, frequently producing a treatment “cavity” within the prostate. The subsequent fibrotic response to histotripsy appears limited and likely reflects the sharp margin between homogenized and preserved tissue (precision of histotripsy). Potentially, in markedly fibrotic prostates, histotripsy may provide a method to achieve a net reduction in collagen content (*i.e.* homogenization and removal of fibrous tissue with deposition of less collagen during recovery). Future work is aimed at understanding the relationship between histotripsy tissue effects and prostate stiffness.



*Left: Whole prostate section showing histotripsy treatment in the left lobe. Right: 20x magnification of the histotripsy treatment lesion with the inner and outer fibrotic bands shown in red.*

Funding: R01 DK087871  
TLH & WWR have royalty, equity, and consulting interests with HistoSonics, Inc.

## COMPARISON OF CATHETER-DIRECTED WST11-VASCULAR TARGETED PHOTOTHERAPY (WST11-VTP) AND IRREVERSIBLE ELECTROPORATION (IRE) FOR INTRALUMINAL ABLATION IN THE PORCINE URETER

Govindarajan Srimathveeravalli<sup>1</sup>, Ashley Winter<sup>2</sup>, Haruyuki Takaki<sup>1</sup>, Simon Kimm<sup>2</sup>, Tatum V Tarin<sup>3</sup>, Sebastien Monette<sup>3</sup>, Stephen B Solomon<sup>1</sup>, Jeremy C Durack<sup>1</sup> and Jonathan Coleman<sup>2</sup>.

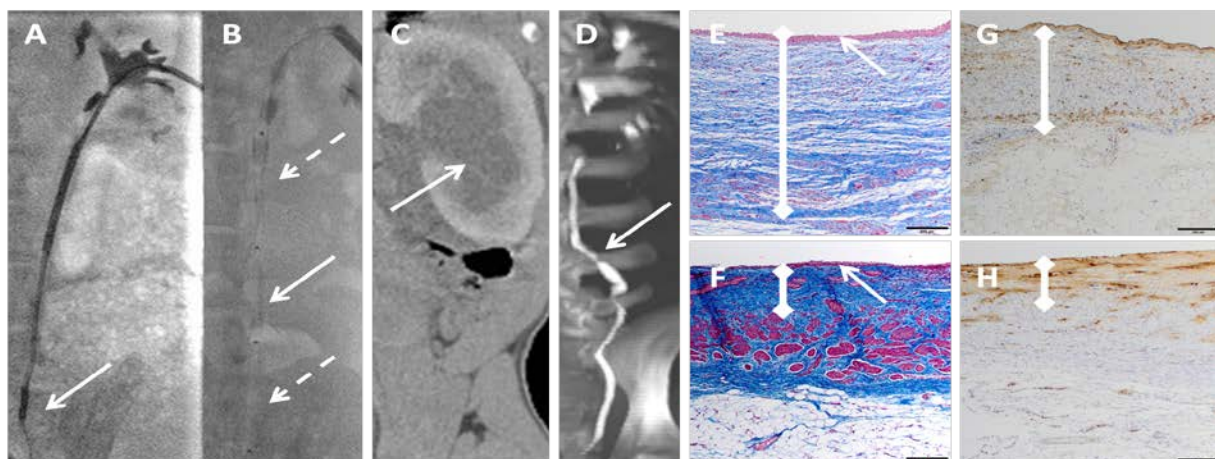
<sup>1</sup>Dept. of Radiology, <sup>2</sup>Dept. of Surgery, <sup>3</sup>Laboratory of Comparative Pathology, Memorial Sloan Kettering Cancer Center, New York, NY. <sup>3</sup>Dept. of Urology, Univ. of Pittsburg Medical Center, PA.

**Introduction:** The purpose of the study was to evaluate feasibility and to study the long-term outcomes of catheter directed focal intraluminal ablation using WST11-VTP and IRE in the ureter.

**Methods:** Fluoroscopy guided nephrostomy was performed on 5 healthy swine for unilateral ureteral ablation at one location with WST11-VTP (n=3) or two locations with IRE (n=2). A custom designed electrode catheter (A) was used to perform IRE (settings: 2000V, 100µs, 90pulses). A custom designed balloon catheter (B) was used to position a 20µm laser fiber and a photosensitizing agent (WST-11) was infused intravenously before illumination (settings: 50, 100 or 200mW/cm, 753nm, 10min). Immediate post-treatment ureteral patency was assessed by fluoroscopic antegrade nephrostograms. Nephrographic and delayed phase contrast-enhanced CT imaging was obtained 1, 7, 14, 21 and 28 days after ablation. All animals were sacrificed at 28 days and treated ureters underwent histopathologic evaluation.

**Results:** Fluoroscopic imaging immediately following treatment indicated ureteral patency in both treatment cohorts. Both animals treated with IRE demonstrated focal ureteral stricture formation after 7 days on CT imaging, developing moderate hydronephrosis (C). CT imaging of animals treated with WST11-VTP appeared normal (D). Mason-Trichome stain of ureters treated with IRE showed regeneration of urothelium with extensive transmural fibrosis (E). Ureters treated with WST11-VTP demonstrated regeneration of urothelium with mild fibrosis of the lamina propria (F). Representative depth of cell death expected following IRE (G) and WST11-VTP (H) treatment at early time point is shown using TUNEL stain of ureters treated at same settings in a different set of animals.

**Conclusion:** It is feasible to use WST11-VTP or IRE to perform catheter directed intraluminal ablation of the ureter with varying depths of penetration.



*A: IRE catheter in the distal ureter (arrow shows IRE coil). B: VTP device in mid-ureter (arrow), flanked by balloons (dashed arrows) C: Hydronephrosis following IRE (arrow). D: Normal urine flow 4 weeks after VTP (arrow) E: IRE treated ureter with regenerated urothelium (arrow) and fibrosis (line). F: VTP treated ureter with regenerated urothelium (arrow) and fibrosis (line). G: Depth of cell death within 24 hours following IRE (line). G: Depth of cell death within 24 hours following VTP (line).*

**Acknowledgement:** This work was supported by a philanthropic grant from the Thompson Foundation.

### NOVEL NEEDLE-PROTECTED TROCAR PORT FASCIAL CLOSURE SYSTEM EMPLOYING A STYLET MECHANISM AND APPLICATOR FOR TRANSVERSUS ABDOMINIS PLANE (TAP) ANALGESIC BLOCK

Philip T. Zhao<sup>1</sup>, Neal Patel<sup>1</sup>, David M. Albala<sup>2</sup>, Manoj B. Patel<sup>3</sup>

<sup>1</sup>Rutgers–Robert Wood Johnson Medical School, New Brunswick, NJ

<sup>2</sup>Crouse Hospital, Syracuse, NY; <sup>3</sup>Cooper Medical School of Rowan University, Camden, NJ

**Introduction:** The adoption of minimally invasive surgery (MIS) is increasing with over 4 million procedures done in the USA annually. At completion of MIS cases, trocar sites must be properly closed to prevent complications including wound dehiscence, bowel herniation, infection, obstruction, evisceration, etc. The rate of port site hernias in MIS is 5%-14% in multiple series, contributing to over \$2.5 billion annually in rehospitalization, reoperation, and malpractice costs to the healthcare industry. There are several existing commercial trocar fascial closure devices but they all have significant limitations. We tested a novel fascial closure system (FCS) developed by Endolutions LLC (Dover, DE) to evaluate its feasibility, success rate, and overall time to closure in a porcine model.

**Methods:** The Endolutions FCS (Figure A) can be introduced into a 12 mm trocar with and without the need for pneumoperitoneum. We tested the FCS to measure closure times and margin distance with 1-0 Vicryl ties in live porcine models. The device was also designed to inject analgesic agents for a transversus abdominis plane (TAP) block through the needle-protected (hollow-bore) guides that sequentially deploy immediately above the transversus abdominis muscle (for TAP block); then through the transversalis fascia (for suture placement). We injected lidocaine/methylene blue (LMB) solution through the TAP port to determine the analgesic distribution pattern (Fig F) prior to suture placement.

**Results:** With and without establishing pneumoperitoneum, twenty 12 mm trocar insertions were made in the abdomen (ten in each of two Yorkshire pigs). The fascia was closed properly (Fig E, mean 1.1 cm margin from incisional edge) in all twenty (100%) trials based on intra-abdominal exam with laparoscope and autopsy inspection. No bowel/viscera injury was noted. Average duration of closure from FCS introduction to complete knot tying was 54 seconds (range 41-70 seconds). LMB injection (10cc) via the TAP port yielded a radial distribution range of 3-5 cm around the trocar incision on tissue cut-down inspection (G). The highest concentration of staining was above the transverse fascial layer.

**Conclusion:** The Endolutions FCS was able to successfully close 12 mm trocar port fascia in under a minute with adequate fascial margins and a wide distribution of the injected lidocaine/methylene blue analgesic solution in the appropriate fascial plane. As demonstrated, the device consistently adheres to the Jonsen-Israelsson principles of wound closure; does not require pneumoperitoneum; employs a needle-protected mechanism that poses no harm to

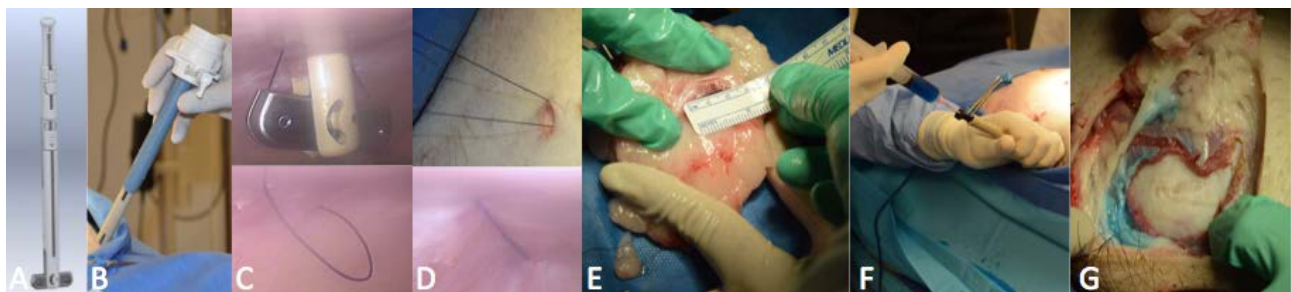


**Figure:** A. EndoFCS rendering. B. Device introduced through trocar to maintain access. C. After suture deployment. D. Knot tied above fascia. E. 1.1-cm margin from incisional edge. F. Injection of LMB. G. Interfascial distribution.

visceral structures. The device is appealing in that any suture can be used and it can be introduced through the trocar itself to maintain access to the port site. The FCS is unique in that it not only allows for quick suture placement and closure but also application of TAP analgesia at the correct level within the abdominal wall. Further data in human trials is needed to demonstrate its efficacy as a clinical tool.

### ACE RENORRHAPHY: A NOVEL TECHNIQUE FOR CLOSURE OF RENAL DEFECT DURING ROBOT-ASSISTED PARTIAL NEPHRECTOMY USING ALTERNATING COLORED SUTURES AND EVICEL®

Bennett Y. Hong<sup>1</sup>, Kevin Gioia<sup>1</sup>, Brian Caldwell<sup>1</sup>, David Gershbaum<sup>2</sup>

<sup>1</sup> Department of Urology, Stony Brook University School of Medicine, Stony Brook, NY

<sup>2</sup> Department of Urology, Winthrop University Hospital, Mineola, NY

**Introduction:** Within the past decade, rapid advances in robot technology and surgical technique has allowed for robot-assisted partial nephrectomy (RAPN) to become the standard of care for nephron sparing surgery. Recently, much attention has been placed on procedural refinements to decrease warm ischemia time and attenuate ischemic damage to the affected kidney. For example, sliding-clip renorrhaphy and assistant-placed Lapra-Ty closures have replaced the use of tied-suture closures in many institutions. We propose a unique technique to further simplify renorrhaphy for renal reconstruction. We will also describe a method that will accelerate the closure of Gerota's fascia during RAPN.

**Methods:** At our center, renorrhaphy employs the usage of a rolled bolster of oxidized cellulose sheets (Surgicel®, Ethicon Inc., Somerville, NJ, USA), followed by insertion of interrupted sutures and assistant-placed Lapra-Ty® clips (Ethicon Inc., Somerville, NJ, USA). We propose the usage of alternating colored sutures during renal reconstruction to enhance the surgeon's visualization of sutures and facilitate parenchymal closure (Figure 1). The closure of Gerota's fascia after partial nephrectomy and kidney reconstruction is generally recommended and techniques vary from tied sutures to Lapra-Ty® clips. We propose the application of Evicel® Fibrin Sealant (Ethicon Inc., Somerville, NJ, USA) as an alternative method of closure (Figure 2). While Evicel® is commonly used as a hemostatic agent, we believe that its usage in lieu of sutures and clips will expedite the closure of Gerota's fascia, and thusly decrease ischemia time.

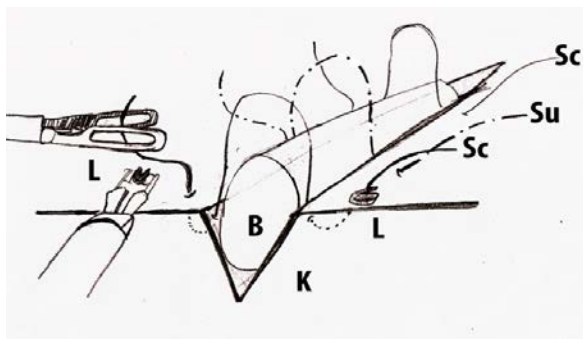


**Figure 1:** Sc: Colored Suture, Su: Uncolored Suture, L: Lapra-Ty®, B: Surgicel® Bolster, K: Kidney

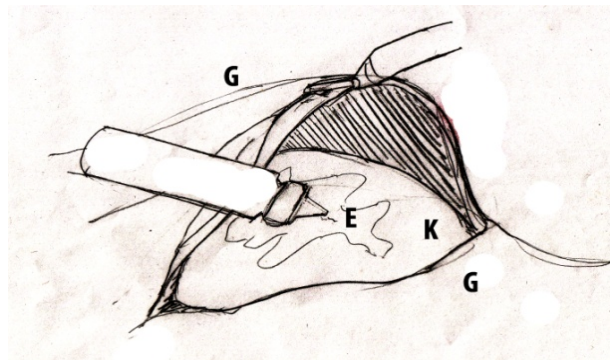


**Figure 2:** G: Gerota's Fascia, E: Evicel®, K: Kidney

**Results:** When these two techniques were incorporated into our surgical practice, we found that they simplified the processes of parenchymal reconstruction and Gerota's fascia closure. It was also our impression that warm ischemia time and operation time were decreased.

**Conclusion:** We believe that the use of alternating colored sutures in renorrhaphy and Evicel® assisted closure of Gerota's fascia (ACE technique) is a valid and reproducible method that accelerates the closing process and reduces the challenges posed by post-RAPN closure by enhancing the surgeon's visualization of sutures and simplifying the closure process. We believe that these two refinements in technique warrant further research to formally analyze their efficacy and cost-effectiveness in comparison with commonly practice methods.

## COGNITIVE-AUGMENTED ROBOTIC SYSTEM FOR ENDOSCOPIC NAVIGATION (CARSEN): A PROOF OF CONCEPT FOR MIND-CONTROL ENDOSURGERY USING LEGO®

Neal Patel<sup>1</sup>, Philip T. Zhao<sup>1</sup>, Manoj B. Patel<sup>2</sup>

<sup>1</sup> Rutgers–Robert Wood Johnson Medical School, New Brunswick, NJ

<sup>2</sup> Cooper Medical School of Rowan University, Camden, NJ

**Introduction:** Significant advancements in neuro-technology have made it easier to perform more complex tasks using human-computer interaction. We applied this interface to endoscopic surgery by designing a robotic mechanism that manipulates a cystoscope using a neuro-headset. Through the development of this Cognitive-Augmented Robotic System for Endoscopic Navigation (CARSEN), we identified some of the essential components and strategies to make mind-control maneuvering of an endoscope plausible and accurate.

**Methods:** Using a set of LEGO® Mindstorm NXT 2.0 (Billund, Denmark), we built a robot that harnesses an Olympus CYF5 flexible cystoscope (Tokyo, Japan). The Mindstorm robot has three motors, which can move the cystoscope forward and back, rotate it 180 degrees along its main axis, and push its control arm level to flex and deflex the tip of the scope – essentially all of the functions necessary to utilize a cystoscope in the clinical environment. After confirming the Mindstorm robot-cystoscope harness works using native NXT software, we then integrated the EPOC neuro-headset (Emotiv, Eveleigh, Australia) and its access applications to control the system. EPOC works using a set of 14 sensors and 2 references to tune multi-channel electroencephalogram (EEG) signals into electrical signals in real-time. These signals are then translated by Emotiv software to control our device wirelessly from a computer. We used a third-party soft application MonoBrick Remote (Hillerod, Denmark) to control all three motors/axes spontaneously. We used a dice to randomly determine the decision of movement for CARSEN (1: move forward; 2: move backwards; 3: rotate clockwise; 4: rotate counter-clockwise; 5: flex upwards; 6: flex downwards). We carried out 200 movements and trended the accuracy in quartiles (50 movements each). The two-tailed z-test was used for statistical analysis.

**Results:** The EPOC neuro-headset required significant initial calibration and testing. There is a 0.5 to 1.2 second-delay in transmission of the EEG signals to the computer and then to the NXT unit in CARSEN to facilitate movement. After 50 movements of the robot determined by dice, our initial accuracy was 34%; followed by 42% (p=0.41), 48% (p=0.15), and 44% (p=0.30) for the next three quartiles.

**Conclusion:** Using a neuro-headset to control basic movements of an endoscopic instrument can be feasibly and economically achieved. Our total cost to build the system was under \$600 (excluding cystoscope) using commercially accessible parts. Although there is a slight delay in transmitting the EEG signals to movement, CARSEN is able to translate thought to real-time maneuvering with limited accuracy and reproducibility. We are the first to apply cognitive augmentation to a robotic system for endoscopic navigation, indicating that mind-control endosurgery is a possibility.

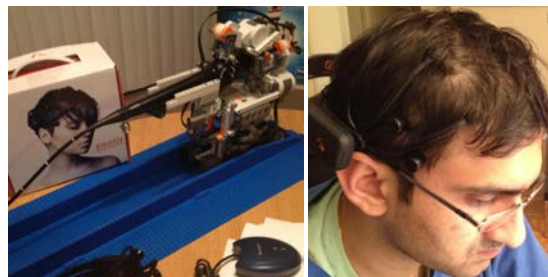


Figure. CARSEN built using LEGO® Mindstorm NXT 2.0; controlled using EPOC neuro-headset.

### INITIAL CLINICAL EXPERIENCE WITH PERCUTANEOUS IRREVERSIBLE ELECTROPORATION OF KIDNEY TUMORS

Monica S.C. Morgan MD<sup>1</sup>, Jeffrey C. Gahan MD<sup>1</sup>, Asim Ozayar MD<sup>1</sup>, Clayton Trimmer DO<sup>2</sup>,  
Jeffrey A. Cadeddu MD<sup>1</sup>

<sup>1</sup>*Department of Urology, University of Texas Southwestern Medical Center, Dallas, Texas*

<sup>2</sup>*Department of Radiology, University of Texas Southwestern Medical Center, Dallas, Texas*

**Purpose:** Irreversible electroporation (IRE) is a nonthermal tissue ablation technique where high voltage electric pulses of microsecond duration are applied to create irreversible nanoscale defects in the cell membrane, leading to apoptosis. We evaluated our initial IRE experience to assess feasibility, safety, effectiveness and radiographic outcomes of IRE renal tumor ablation.

**Materials and Methods:** A retrospective analysis of all IRE cases between April 2013 and March 2014 was performed. The NanoKnife 15 cm monopolar probe was used for all patients. All procedures were performed under general anesthesia and with cardiac synchronization. All patients underwent CT guided ablation and a post-procedure contrast-enhanced CT. 12 patients had a minimum of 6 week follow-up with a contrast enhanced CT.

**Results:** A total of 20 tumors(19pts) underwent IRE. Mean age was 65 years old. Median tumor size was 2.2 cm (1.2-3.6cm). Median R.E.N.A.L. score was 6. Nine patients had biopsy proven RCC (8 clear cell, 1 papillary) and 1 an oncocytic neoplasm. Five patients had a prior history of RCC. One patient had VHL syndrome. The remaining 2 patients had insufficient tissue or a lesion too small for biopsy. There was no significant difference between pre and post-procedure serum Cr (0.95 vs. 0.98 respectively). Procedure time from anesthesia start to finish ranged from 1 to 3.9 hours. The median number of probes placed was 4 (2-5). Median length of stay was 1 day (0-1). There were no complications. CT scan immediately post procedure typically showed decreased perfusion with an enhancing rim at the ablation site. CT scan at 6 weeks and 6 months was completed in 12 and 2 patients respectively. 12 patients (13 tumors) demonstrated no enhancement (< 10 HU) in the ablation site. At 6 weeks, two patients with tumors 3.6cm and 1.8cm failed IRE. These patients' CT scan demonstrated a persistent rim of enhancement. Both underwent successful salvage radiofrequency ablation. The remaining 5 patients have follow-up pending.

**Conclusions:** Percutaneous IRE of kidney tumors has shown to be feasible and safe in our retrospective review of 19 patients. Additional follow-up is needed to confirm the oncologic efficacy of IRE. Comparative studies with other ablative techniques are warranted.

### PILOT EVALUATION OF A NON-INVASIVE, ULTRASOUND-BASED LIQUID MOLECULAR BIOPSY: INDUCED RELEASE OF PROSTATE CANCER ASSOCIATED MIRNAS IN A RAT MODEL USING BOILING HISTOTRIPSY

John R Chevillet<sup>1,2</sup>, Tatiana Khokhlova<sup>2</sup>, George R Schade<sup>3</sup>, Maria D Giraldez<sup>4</sup>, Emily N Gallichotte<sup>4</sup>, Evan M Kroh<sup>4</sup>, Joo Ha Hwang<sup>2</sup>, Muneesh Tewari<sup>4,5</sup>

*Institute for Systems Biology, Seattle, WA<sup>1</sup>  
University of Washington, Departments of Gastroenterology<sup>2</sup> and Urology<sup>3</sup>, Seattle, WA  
University of Michigan, Departments of Internal Medicine<sup>4</sup> and Bioengineering<sup>5</sup>, Ann Arbor, MI*

**Introduction:** The ability of moderate intensity ultrasound to stimulate the release of cancer-specific extracellular protein biomarkers was recently reported suggesting a novel strategy for cancer detection. However, the release of potentially more useful intracellular biomarkers, such as cell-free tumor associated microRNA (miRNA) and other nucleic acids, may require exposures optimized for mechanical disruption of cells. Boiling histotripsy (BH), a pulsed focused ultrasound (PFUS) technique that results in mechanical cellular lysis, may be one approach. BH utilizes ms long pulses to induce boiling bubbles via rapid shockwave heating. Interaction between the ensuing vapor cavity and subsequent shocks lyses tissue with negligible thermal effect. The resulting tissue permeabilization may facilitate release of intracellular biomarkers into the circulation for detection. We evaluated the ability of two different PFUS strategies (hyperthermia and BH) to release PCa-derived miRNAs in a rat model.

**Methods:** Putative miRNA biomarkers were identified using reverse-transcription quantitative PCR (RT-qPCR) array profiling (Exiqon) of the syngeneic MatLyLu rat PCa cell line. Adult intact male Copenhagen rats with jugular-venous catheters were subcutaneously grafted with MatLyLu cells. When tumors were >1cm, subjects were divided into one of two PFUS treatment groups: PFUS optimized for sub-lethal gentle heating (120 W/cm<sup>2</sup>, 50% duty factor (DF), N=7), BH (~30KW/cm<sup>2</sup>, 1% DF, N=8) or a sham procedure (N=5) using a 1.5 MHz transducer under ultrasound guidance. Blood was collected immediately prior to treatment and serially over a 24-hour time course. Specimens were immediately processed into plasma, miRNA extracted, and concentrations of candidate tumor-derived miRNAs were measured via RT-qPCR. Relative plasma concentrations (RPC) of miRNAs were compared with ANOVA and the Mann-Whitney test.

**Results:** Following thermal PFUS treatment and sham procedures, no significant changes were observed in the RPC of any evaluated miRNA. Conversely, following BH treatment, the RPCs of the putative PCA-derived miRNAs miR-34c and miR-196a increased significantly, while the RPC of the broadly expressed, non-PCa specific miR-16 was not significantly altered by BH (1.24-fold peak increase). PCA-derived miRNA RPCs peaked at 0.25 hr (miR-34c: 23.4-fold, p= 0.0127 vs sham; miR-196a: 10.2-fold, p=0.0007 vs sham) from initiation of BH treatment, remained significantly elevated for 3 hrs (p= 0.008, p=0.0047, respectively vs sham), and then returned to baseline within 24 hrs. Histologically, BH treated tumors demonstrated extensive lysis, while minimal effect was observed in thermally treated tumors.

**Conclusion:** BH treatment efficiently increases the release of putative PCa-derived plasma miRNAs in a rat PCA model. Further studies will optimize exposures and kinetics, while determining the minimum lysed tumor volume needed for further development of BH “liquid molecular biopsy.”

**Funding:** ACS/Canary Foundation Postdoctoral Fellowship PFTED-09-249-01-SEID, SU2C-AACR-IRG1109, NIH 1K01EB015745, R01CA154451, R01DK085714

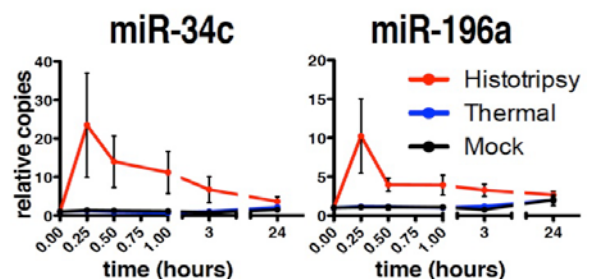


Figure: Relative plasma concentration of PCa derived miRNAs following PFUS treatment

### RE-DEFINING BLADDER INNERVATION WITH 3D IMAGE RECONSTRUCTION

Garen Abedi, Zhamshid Okhunov, Michael Del Junco, Renai Yoon,  
Jamie Wikenheiser, Jiaoti Huang AND Jaime Landman

<sup>1</sup>*Department of Urology, University of California, Irvine*

<sup>2</sup>*Department of Anatomy & Neurobiology, University of California, Irvine*

<sup>3</sup>*Department of Pathology, University of California, Los Angeles*

**Introduction:** There are a robust series of urologic pathologic conditions which have been associated with dysfunction of detrusor innervation. A precise understanding of the anatomical relationship of the autonomic nerves innervating the bladder to the bladder lumen could substantially improve treatment modalities. Currently, there is no comprehensive model that provides a detailed three-dimensional view of bladder innervation. As such, we utilized 3D computer assisted reconstruction of cadaver histopathology to re-define the relationship of bladder autonomic nervous tissue to the lumen of the bladder.

**Methods:** We harvested the bladder and surrounding tissues from a male cadaver. To create a 3D model of normal anatomy, the bladder lumen was filled with melted paraffin to semi-distended condition. Twenty three axial cross sections were created at 3mm intervals and stained with S100. We created a high resolution depiction of each cross section at magnifications of 0.3X to 20X optical zoom. We imported the images into ImageScope (Aperio; Vista, CA) software. Manual demarcation of the autonomic nerve supply of the bladder was performed. The distances between the autonomic nerves and the bladder lumen were measured and documented. Autonomic nerve tracings of each cross section were imported into SolidWorks (Waltham, MA, USA) and 3D reconstructions of the anatomy were created.

**Results:** The autonomic nervous tissue in the male bladder was successfully stained by S100 protein. The autonomic innervation was highly concentrated in the posterior aspects of the bladder lumen and was most pronounced at the level of the bladder neck and trigone region. The mean distance between the autonomic nerve branches and the bladder mucosa was 1.15mm posteriorly versus 4.0mm anteriorly (0.27-2.87 vs. 2.03-6.20,  $p < 0.001$ ).

**Conclusions:** Novel 3D reconstruction of the bladder is feasible and will help re-define our understanding of human bladder innervation. Autonomic bladder innervation is highly focused in the posterior aspect of the bladder and is most dense at the bladder neck. The most superficial fibers vary in distance from the urothelium from 1.15-4.0 mm.

### MORPHOMETRIC ANALYSIS OF PROSTATE ZONAL ANATOMY USING MRI IN 307 MEN BY COOPERATIVE STUDY IN JAPAN AND USA

Matsugasumi T<sup>1,2</sup>, Ukimura O<sup>1,2</sup>, Nakamoto M<sup>1</sup>, Ushijima S<sup>2</sup>, Kanazawa M<sup>2</sup>, Toiyama D<sup>2</sup>, Palmer S<sup>1</sup>, Gill IS<sup>1</sup>

<sup>1</sup>Institute of Urology, University of Southern California, Los Angeles, CA, USA

<sup>2</sup>Department of Urology, Kyoto Prefectural University of Medicine, Kyoto, Japan

**Introduction:** Magnetic resonance imaging (MRI) has been recognized as a reliable imaging to evaluate the prostate, and potentially enhance the morphometric analysis. Objectives of this study are to evaluate ability of MRI for the morphometric analysis of the prostate zonal anatomy in cooperative analysis between USA and Japan.

**Methods:** A total of 307 men, average age 68 years, including Japanese men (n=156) and non-Asian American men (n=151), who had elevated PSA and underwent MRI with slice thickness of 3-mm prior to prostate biopsy. Using Synapse Vincent version 2 (Fujifilm, Japan), the boundary of prostate zonal

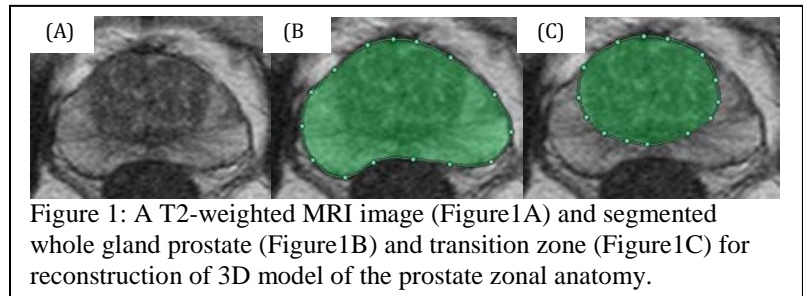


Figure 1: A T2-weighted MRI image (Figure1A) and segmented whole gland prostate (Figure1B) and transition zone (Figure1C) for reconstruction of 3D model of the prostate zonal anatomy.

anatomy was segmented in each step section of T2-weighted MRI [Figure 1], to reconstruct 3D-model of the prostate zonal anatomy to calculate following variables; (1) volume of whole gland prostate [Pr-vol.], (2) volume of transition zone [TZ-vol.], (3) volume of peripheral zone [PZ-vol.], which includes both the peripheral zone and central zone of McNeal's zonal anatomy, (4) **PCAR:** Presumed Circle Area Ratio, which is defined as the *ratio of the area* in the maximum axial section of the prostate *to the area* of a presumed circle with the equal circumference of the section. (PCAR evaluates how closely the shape of the section approaches a circle, and represents "increase of intra-prostatic pressure".), and (5) **PZ-thickness** (mm): defined as PZ-volume divided by the maximum coronal section-area of PZ, by computerized-calculation from the reconstructed 3D-prostate volume.

**Results:** In comparing between Japanese and American men, American men had greater volume in Pr-vol. (41.8 ml vs. 49.5 ml, p=0.001), and TZ-vol. (19.6 ml vs. 26.8 ml, p<0.001), but there were no statistical difference in PZ-vol. (19.9 ml vs. 20.0 ml, p=0.2), and PZ-thickness (16.1 mm vs. 15.9 mm, p=0.3), respectively. PZ-vol. and PZ-thickness had **no** age-related increase (p=0.3, and p=0.8) in each country and entire cohort.

PCAR had statistical positive correlation with TZ-vol. (r=0.280, p<0.001). PZ-thickness had statistical negative correlation with PCAR (r=-0.199, p<0.001) as well as TZ-vol. (r=-0.195, p=0.001). These suggested that the greater the PCAR (to represent increased intra-prostatic-pressure) due to the greater TZ-vol., the thinner the PZ-thickness [Figure 2].

**Conclusion:** MRI has ability to document morphometric analysis of the prostate zonal anatomy. PZ-volume and PZ-thickness had **no** age-related increase in both USA and Japan. *The greater the TZ-volume grows, the higher the intra-prostatic pressure and the thinner the PZ-thickness become.*

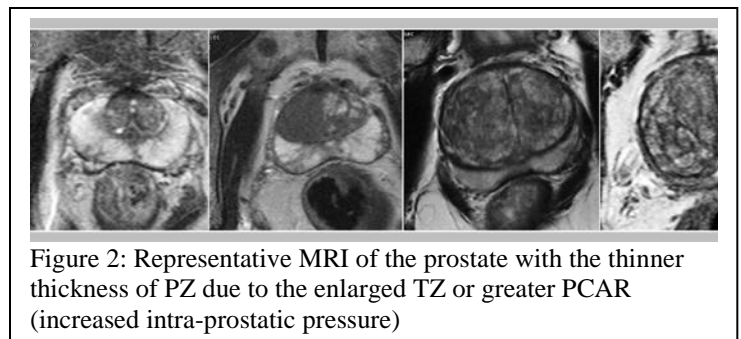


Figure 2: Representative MRI of the prostate with the thinner thickness of PZ due to the enlarged TZ or greater PCAR (increased intra-prostatic pressure)

## PILOT EVALUATION OF BOILING HISTOTRIPSY OF THE KIDNEY: ASSESSMENT IN HUMAN *EX VIVO* KIDNEYS AND VALIDATION OF THE PORCINE MODEL

George R. Schade<sup>1</sup>, Adam D. Maxwell<sup>1</sup>, Yak-Nam Wang<sup>2</sup>, Tatiana D. Khokhlova<sup>3</sup>, Daniel W. Lin<sup>1</sup>, Oleg A. Sapozhnikov<sup>2</sup>, Michael R. Bailey<sup>2</sup>, Vera A. Khokhlova<sup>2</sup>

*University of Washington School of Medicine, Departments of <sup>1</sup>Urology and <sup>3</sup>Gastroenterology*  
*<sup>2</sup>University of Washington Applied Physics Lab, Center for Industrial and Medical Ultrasound*

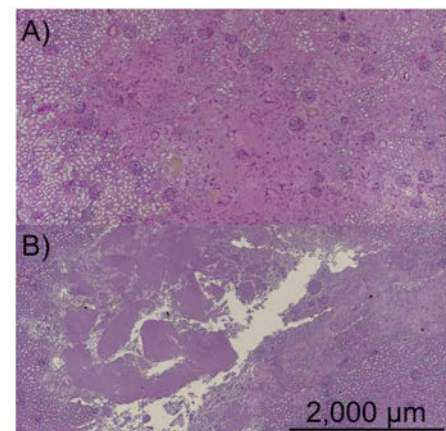
**Introduction:** Histotripsy is a non-thermal pulsed high intensity focused ultrasound (HIFU) technology that mechanically homogenizes targeted tissue. Our group has developed a new histotripsy technique, termed boiling histotripsy (BH), utilizing ms-long HIFU bursts containing shock fronts to create boiling bubbles at the focus. Interaction of shocks with the ensuing vapor cavity homogenizes tissue into sub-cellular debris with negligible thermal effects. As a noninvasive, non-thermal based approach; BH may have several advantages over existing clinically available thermal ablative technologies for renal masses. The aim of this study was to evaluate BH renal ablation in fresh porcine and human kidneys in order to demonstrate feasibility and to validate the porcine model for future preclinical studies.

**Methods:** Fresh porcine kidneys (n=20) were obtained from a local abattoir and fresh human kidneys/renal tissues (n=6) were obtained via an IRB approved institutional rapid autopsy/tissue procurement program. All specimens were acquired  $\leq 4$  hours from death/nephrectomy. Tissue was degassed for  $\geq 30$  min in phosphate buffered saline and then treated with BH using a 1-MHz 7-element HIFU transducer (duty factor 1%, 10 ms pulses, 98 MPa *in-situ* shock amplitude, 17 MPa peak negative) using ultrasound guidance. Single focal volumes within the cortex, medulla, or collecting system were treated at various doses (15-300 pulses). Treated tissue was evaluated grossly or formalin-fixed for histologic assessment.

**Results:** During treatment, BH produced localized hyperechoic bubbles at the focus that dissipated between pulses. Grossly, there was cortical evidence of BH treatment at 15 pulses, which evolved into liquid filled “mushroom” shaped lesions in a dose-dependent fashion with minimal observable thermal effects. Histologically, human kidneys generally appeared more resistant to BH than porcine, requiring greater pulse number to achieve complete homogenization, with relative sparing of the glomeruli compared to other cortical structures (see figure). The medulla was more resistant to BH than cortical tissue, requiring  $\geq 60$  pulses to produce apparent tissue effect. Histologically, lesions were found to be comet shaped at high doses with near complete homogenization of the head region and a fan-like tail of incompletely homogenized tissue. The collecting system was still more resistant, requiring  $\geq 120$  pulses in the “head” region to produce histologic effect and  $\geq 300$  pulses in the “stem” to produce significant effect. Intra-renal arterioles were spared at doses  $< 240$  pulses.

**Conclusion:** Renal BH appears feasible, yielding anticipated tissue disintegration in a dose dependent fashion. The increased resistance of the medulla and collecting system may provide a margin of safety when developing BH clinically for ablation of renal tumors. The observed similarities between porcine and human renal tissue in response to BH support the development of the porcine model for further preclinical studies.

**Funding:** NIH 2T32DK007779-11A1, R01EB007643, 2P01DK043881-15, 1R01DK092197-02, and NSBRI through NASA NCC 9-58.



*Cortical boiling histotripsy lesions (60 pulses) in human (A) and porcine (B) kidneys. 20X PAS*

### A NEW MULTI-DOF DEXTEROUS MANUAL INSTRUMENT FOR LAPAROSCOPIC SURGERY

Mitchell, C.<sup>2</sup>, Lathrop, R.<sup>1</sup>, and Webster, R.<sup>1,2</sup>, Herrell, S.D.<sup>1,2</sup>

<sup>1</sup>*Department of Mechanical Engineering, Vanderbilt*

<sup>2</sup>*Department of Urologic Surgery, Vanderbilt*

**Introduction:** The wristed instrumentation and design of the Intuitive Surgical daVinci robotic platform allows for “intuitive” or “natural” movements of the tools including coordinating multiple degrees of freedom (DOF) of motion in the wrist, thus easing complex surgical tasks such as suturing and curvilinear incision. While a variety of articulated manual laparoscopic tools have been developed, none have reached critical levels of acceptance and commercial success. Existing designs have failed to provide a natural hand-mechanical interface similar to the da Vinci. Thus while the manual tools previously designed provided the same range of motion as the EndoWrist™ tools, performing the compound movements has been difficult and no mechanical instrument design has been optimized. We hypothesized that with careful design, the critical user interface end (handle) of the device can be connected to a multiple DOF end effector to create a manual tool with truly usable dexterity.

**Methods:** Our research team iteratively created an initial multi-DOF wristed mechanical tool. During this process it became clear that the hand-mechanical control interface was the critical driver of the “natural” feel of the instrument and initial research was focused on creating the optimal design. We hypothesized that placing the handle pivot point within the surgeon’s grasp was a key to achieving a natural control interface, and developed a new handle design that achieve this goal. To experimentally evaluate this, we constructed a family of four prototype wristed dexterous tools that were identical in all respects except for handle design. Handles representing traditional laparoscopic hemostat and pistol grips were compared to a new unique handle design (*Patent Pending*). Nine surgeons and nine novice users were asked to perform a series of dexterous tasks including needle passage into tissue, placing sutures at acute and obtuse angles, and a challenging curvilinear ring / wire following task. Each handle design was scored based on time and number of errors made. The two prototypes with our new handle design differed as to whether end effector motion was parallel to handle motion or reversed with respect to handle movement.

**Results:** Users were shown to perform statistically better with the new handle design compared to handles based on more traditional laparoscopic surgical tools.

**Conclusion:** The results of the user study support the idea that placing the pivot point within the surgeon’s grasp contributes to the naturalness of the user interface of a manual dexterous laparoscopic tool. The direction of wrist coupling was a matter of user preference, with more surgeons better with a reversed mapping, but some surgeons favoring a forward mapping. Based on the results additional prototype tools have been constructed for use in further studies and pursuit of commercial development.



User Study Tools: Hemostat, Parallel Prototype, Pistol, Reversed Prototype.

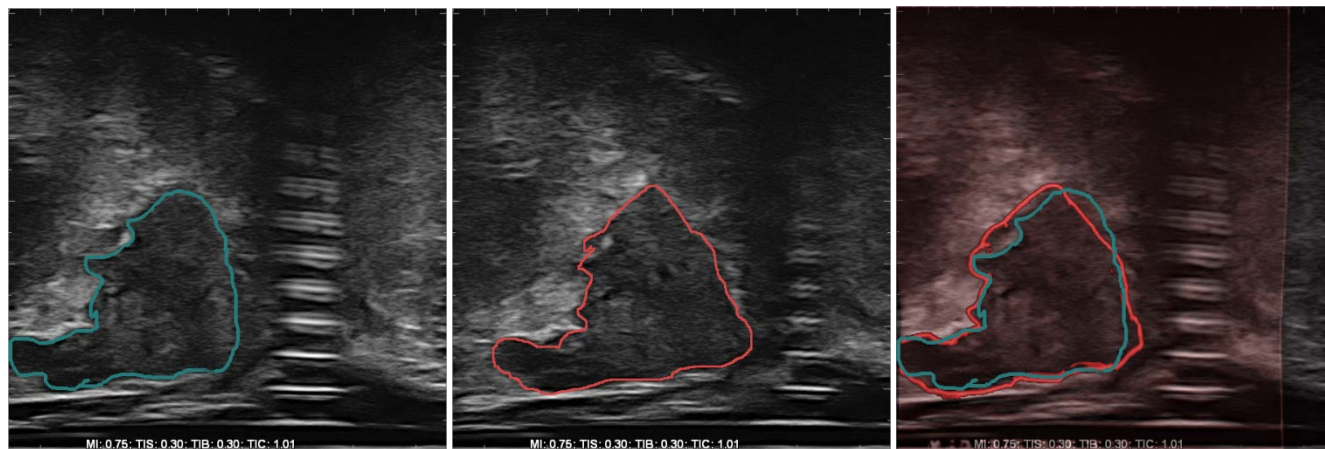
### ELASTIC REGISTRATION OF ULTRASOUND IMAGES

P. Zogal<sup>1</sup>, E. García-Corisco<sup>2</sup>, G. Sakas<sup>1,2</sup>  
<sup>1</sup>MedCom GmbH, <sup>2</sup>Technical University Darmstadt

**Introduction:** MRI-targeted, US-guided “fusion” prostate biopsy becomes increasingly popular as it provides significantly higher cancer detection rates (Hadaschik, *J Urol* Dec 2011) and enables precise treatment planning, especially for different types of focal therapy (Singh, *Eur Urol* Oct 2013). However, during treatment the initial fusion between the MR dataset and live ultrasound image becomes less accurate due to prostate deformation and movement during the procedure.

**Methods:** Our image processing algorithm to elastically register two ultrasound images (before and after deformation) consists of three steps: (a) preprocessing, (b) global rigid registration and (c) elasticity modeling by registering image sub-patches. Preprocessing involves image filtering, down-sampling and local parameter extraction of local features, here a Fisher-Tippet filter and a fast SUSAN corner detector. Areas with high corner density are regarded to contain significant information. Global registration is utilizing normalized mutual information (NMI). For the following elastic part, the globally registered images are sub-divided into dynamically sized patches; those showing a significant corner density are selected and matched between pre- and post-deformation images by normalized cross correlation (NCC). Elasticity is modeled as deformation field by smoothly interpolating between the corresponding partial patch registration outcomes.

**Results:** Phantom (CIRS 053) was initially used to test the rigid registration, whereas prostate scans of 5 patients were used to evaluate the elastic deformation. In all cases the algorithm showed a consistent behavior leading to a fast convergence, provided the displacement between images was within the range of ca. +/-10 mm shift and/or ca. 15° of rotation. In the current unoptimized implementation, a typical case (resolution 512<sup>2</sup>) requires 0.5 seconds on a Core2Duo 3GHz PC.



From left to right: reference organ, deformed organ, both images elastically registered

**Conclusion:** The proposed approach for elastic registration of 2D ultrasound images looks very promising and shall be integrated in the BiopSee<sup>®</sup> device. We aim to further optimize its performance to a frame rate around 5-10 fps on our standard PC, a GPU platform will increase the speed to real time.

### **IN VITRO FRAGMENTATION OF RENAL CALCULI BY BURST WAVE LITHOTRIPSY: EFFECT OF STONE COMPOSITION**

Adam D. Maxwell<sup>1</sup>, Franklin C. Lee<sup>1</sup>, Bryan W. Cunitz<sup>2</sup>, Barbrina Dunmire<sup>2</sup>, Wayne Kreider<sup>2</sup>, Mathew D. Sorensen<sup>1,3</sup>, Michael R. Bailey<sup>2</sup>, and Jonathan D. Harper<sup>1</sup>

<sup>1</sup>Department of Urology, University of Washington School of Medicine, Seattle, WA

<sup>2</sup>Center for Industrial and Medical Ultrasound, Applied Physics Laboratory, University of Washington, Seattle, WA

<sup>3</sup>Division of Urology, Department of Veteran Affairs Medical Center, Seattle, WA

**Introduction:** Burst wave lithotripsy (BWL) is a new experimental treatment for the extracorporeal delivery of pressure pulses to fragment renal calculi. Unlike shock wave lithotripsy, BWL uses broadly focused bursts of ultrasound to fracture stones. This modality may provide improved energy delivery to the stone at reduced pressure amplitudes, and thus, potentially reduced kidney injury compared to shock wave lithotripsy. The purpose of this study was to determine the effect of stone composition on stone fragmentation *in vitro*.

**Methods:** Calcium oxalate dihydrate (COD) and calcium oxalate monohydrate (COM) human stones were used for this study. Stones 5-9 mm were weighed and photographed in a dry state, then placed in deionized water for 1 week. For each experiment, a stone was transferred (underwater) into a transparent polyvinyl chloride tissue phantom intended to mimic a kidney calyx. A 170 kHz focused ultrasound transducer driven by a radiofrequency amplifier was used to deliver the BWL exposure. The transducer focus was aligned with the stone using inline B-Mode ultrasound imaging. The total exposure time for each stone was 10 minutes. Treatment parameters included a 10-cycle burst length with 6.5 MPa focal pressure amplitude and a delivery rate of 200 bursts per second. After exposure, the stone fragments were removed from the tissue phantom and allowed to dry. The fragments were passed through a series of sieves to determine the fragment size distribution by weight resulting from treatment.

**Results:** Exposure of both types of stones to BWL resulted in stone fracture and subsequent fragmentation. COD stones ( $n = 8$ ) appeared to separate into many small fragments around 1 mm while COM stones ( $n = 8$ ) fragmented into relatively fewer pieces near 3 mm during the 10 minute exposure. Fragmentation of stones into clinically passable pieces ( $< 4$  mm) was achieved in 7/8 COD stones and 6/8 COM stones. A mean of 60% of the fragment weight (COD) and 24% (COM) was  $< 2$  mm ( $p = 0.02$ ). The figure shows the distribution of fragment sizes by weight for both stone types.

**Conclusion:** Both COD and COM stones can be fragmented by BWL. COD stones were reduced to smaller fragments in comparison with COM stones. Selection of acoustic parameters for BWL should account for different stone compositions to ensure all types can be reduced to small, easily passable fragments.

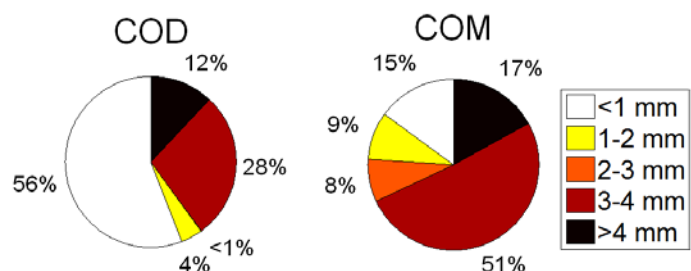


**Figure:** Size distribution by weight of fragments generated from treatment of COD and COM stones by BWL.

Work supported by NIH 2T32DK007779-11A1, R01 EB007643, 2P01 DK043881-15, and NSBRI through NASA NCC 9-58.

# ABSTRACTS

## ABSTRACT 30

### PCA SCORE: A SIMPLE MR IMAGING-BASED SYSTEM TO IDENTIFY MEN AT RISK FOR PROSTATE CANCER

Jason T. Rothwax<sup>1</sup>, Minhaj Siddiqui<sup>1</sup>, Baris Turkbey<sup>2</sup>, Arvin George<sup>1</sup>, Nabeel Shakir<sup>1</sup>, Soroush Rais-Bahrami<sup>1</sup>, Chinonyerem Okoro<sup>1</sup>, Dima Raskolnikov<sup>1</sup>, Annerleim Walton-Diaz<sup>1</sup>, Daniel Su<sup>1</sup>, Peter Choyke<sup>2</sup>, Peter A. Pinto<sup>1</sup>

<sup>1</sup> Urologic Oncology Branch, National Cancer Institute, National Institutes of Health, Bethesda, MD

<sup>2</sup> Molecular Imaging Program, National Cancer Institute, National Institutes of Health, Bethesda, MD

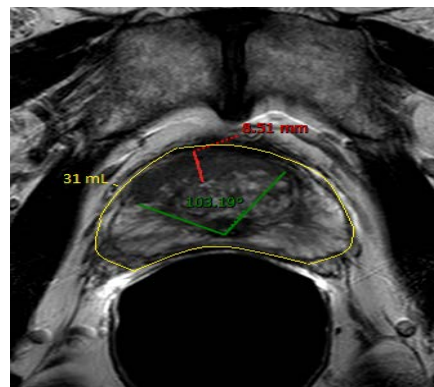
**Introduction:** Prostate MRI has emerged as a useful tool in prostate cancer assessment. While much progress has occurred in the risk stratification of lesion suspicion scoring, less is understood about how information can be combined from multiple lesions to give patient-specific risk assessment. We propose a practical, MRI-based scoring system to reliably and non-invasively risk stratify men for incidence of all and high-grade prostate cancer.

**Methods:** Patients underwent a multiparametric prostate MRI as part of a prospective study at our institution. We reviewed 101 lesions identified on MRI from a cohort of 37 patients. A “PCA” scoring system using three parameters was developed to characterize lesions based on geometric indices. One point was assigned for each of the following: Prostate volume  $\leq 70$ ml, total depth of identified lesions (Cross-measure)  $\geq 17$ mm, and the sum of all measures of the angle between two lines drawn through the midpoint of the urethra to the opposing edges of the identified lesions (Angle)  $\geq 140^\circ$ . Measurements were recorded using PACS and statistical analysis was conducted using the JMP software package (SAS, Cary, NC).

**Results:** Median age of the cohort was 64.5 (IQR 57.6 to 68.1). Median PSA was 6.3 (IQR 5.2 to 9.4). Mean cross-measure of lesions was 19.5mm (95%CI 15.8-23.2). Mean angle of tumors was  $101.4^\circ$  (95%CI 80.6-122.1). Mean prostate volume was 58.7 (95%CI 47.4-69.9). For patients with a PCA score of  $\geq 2$ , cancer was detected with a sensitivity of 77.8% and specificity of 89.5%. The positive predictive value was 87.5% and the negative predictive value was 81%. The accuracy of the test was 83.8%. Cancer was detected on all patients with a PCA score of 3 (n = 6/6), while 95% of patients with a PCA score of  $\leq 1$  had either no cancer or clinically insignificant (Gleason  $\leq 3+4$ ) prostate cancer (n = 20/21).

**Conclusion:** The PCA score is a novel, objective and simple MRI-based scoring system that reliably identifies men with prostate cancer and stratifies for high-grade disease. Further validation studies are needed to determine the utility of this standardized system for the assessment, treatment, and outcomes of prostate cancer.

Result	0-1	2-3
No cancer	17	2
Cancer	4	14
Gleason score $\geq 4+3$	1	8
Gleason score $\leq 3+4$	3	6



### IMPACT OF SPATIAL DISTRIBUTION OF SAMPLES ON TARGETING ACCURACY IN MR-US FUSION GUIDED BIOPSY

James Garritano<sup>1</sup>, Jesse Le<sup>2</sup>, Alan Priester<sup>1</sup>, Daniel Margolis<sup>4</sup>, Jiaoti Huang<sup>3</sup>, Warren Grundfest<sup>1</sup>, Leonard Marks<sup>2</sup>, Shyam Natarajan<sup>1,2</sup>

<sup>1</sup> University of California Los Angeles, Department of Bioengineering

<sup>2</sup> University of California Los Angeles, Urology

<sup>3</sup> University of California Los Angeles, Radiology

<sup>4</sup> University of California Los Angeles, Pathology

**Introduction:** Multiparametric MR-US fusion targeted biopsy has been shown to have an increased sensitivity over blind biopsy in the detection of prostate cancer. Previous studies characterized in vivo registration error to be 3.2 mm and targeting error to be 1.1 mm. However, the clinical impact of targeted biopsy accuracy *vis-a-vis* registration and targeting errors has not yet been systematically studied.

**Methods:** We performed a retrospective analysis on 99 patients who received an MR-US fusion guided biopsy and were positive for cancer. 39 cases had at least one positive systematic core, with zero positive targeted cores; these groups were labeled as “targeting failures.” The remaining 60 targeted procedures positive for cancer had at least one targeted core positive for cancer – these procedures were labeled as “targeting successes.”

The ROI and the biopsy needle positions for all of the procedures were imported into custom software written in MATLAB 2013a (MathWorks). For each core, the shortest distance of the recorded needle position to the ROI surface was computed (Figure 1), and the needle was checked for intersection.

**Results:** The number of targeted cores taken is determined by the longest axis of the ROI. For procedures with two targeted cores, the average distance of the targeted cores to the surface of the ROI was  $7.7 \pm 0.2$  mm for successful cases and  $14.4 \pm 0.3$  mm for failed cases ( $p = 0.0039$ , Welch’s t-test). For procedures with three targeted cores, the average distance of the targeted core to the surface ROI was not significantly different between successful procedures and failed procedures, with distances of  $10.0 \pm 0.4$  mm and  $12.9 \pm 0.8$  mm respectively ( $p = 0.38$ , Welch’s t-test). The proportion of procedures with at least one needle intersecting the ROI was not significantly different between the successes and failures for procedures with two cores (73% and 78%, respectively), or for cases with three cores (83% and 67%, respectively).

**Conclusion:** A similar rate of needle-ROI intersection was seen with successful and failed targeting. This strongly suggests that visually inspecting the 3D model of the core and ROI for targeting efficacy is insufficient for accurate targeting. However, the exact distance of the needles to the ROI surface is highly related to targeting success in cases with two targeted cores. This may be because this metric is less influenced by registration error than the 3D intersection of the needle and the ROI. Registration errors affecting targeting accuracy appear inversely related to the diameter of the ROI. In the future, MR-US fusion targeting platforms could provide near real-time quantitative feedback on the needle distances to the ROI with potentially better targeting outcomes.

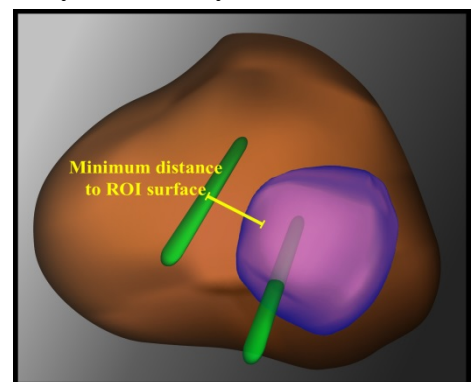


Figure 1 - 3D model of a prostate with an ROI and two needle volumes. Needle A intersected the ROI, while Needle B is outside the ROI. Shown is the minimum distance from needle B to the ROI's surface.

## ABSTRACT 32

### COMPARISON OF *IN VIVO* TEMPERATURE CHANGES INDUCED BY A 902-928 MHZ AND A 2450 MHZ MICROWAVE SYSTEM

Karli Pease<sup>1,2</sup>, Stacie Arechavala<sup>1,2</sup>, Raymond J. Leveillee<sup>1,2</sup>, Nelson Salas<sup>1,2</sup>

<sup>1</sup> *Joint Bioengineering and Endourology Developmental Surgical Laboratory, Division of Endourology, Laparoscopy, and Minimally-Invasive Surgery, Department of Urology, University of Miami Miller School of Medicine, Miami, FL,*

<sup>2</sup> *Department of Biomedical Engineering, University of Miami, Coral Gables, FL, USA*

**Introduction:** The microwave penetration depth achieved during microwave ablation (MWA) of solid tumors depends on the relative permittivity of the tissue, which can vary with the microwave frequency, temperature, and water content. It is theorized that 915MHz microwaves have a larger penetration depth than those at 2450MHz. A larger energy field may result in more controllable heating environment for larger sized ablations. Two currently available MWA systems were investigated: one system that offers frequency variability between 902-928MHz with output power of up to 32 W and ablation time up to 15 minutes and another system which operates at 2450 MHz for 2-8 minutes with a maximum power of 180 W. The objective of this study was to measure the temperature changes in-vivo at 5 mm and at 10 or 15 mm from the emitting region of the MW antenna when using both systems and compare the results.

**Methods:** Two ablations per kidney were performed in in-vivo porcine kidneys using either the Medwaves AveCure System (San Diego, CA) in power mode with a single 16 gauge needle or the Acculis MTA System (Denmead, Hampshire UK) with a single saline-cooled 1.8mm needle. The needle was inserted into the kidney at either the upper or lower pole, parallel to Brodel's line. Five ablations using the AveCure system were performed at an output power of 24 W, a set temperature of 106 °C, and irradiation time of 5 minutes. Using the Acculis system, five ablations at an output power of 180W were performed for 2 minute. Temperatures during treatment were measured with 8 fiber optic thermal sensors placed 5, 10, and/or 15 mm from the antenna axis, depending on the system. Maximum temperatures reached at 5 mm from the emitting region of the MW antenna were determined for both systems and then at 10 mm for the Acculis and 15 mm for the Avecure. Curve fitting was completed for the initial 10 seconds of ablation using Origin 8 (Northampton, MA).

**Results:** The curves for temperature change within the first 10 seconds for both systems were best fit to a power equation having the form  $T=a*t^b$ , where "T" is the change in temperature (°C) measured in the tissue, "t" is the time into ablation (s), and "a" and "b" are equation parameters. The average values of these parameters, the R-squared value of the curve fits, and the maximum temperatures reached during the entire ablation are provided in the table. The large standard deviations in temperatures and equation parameters may be attributed to the variability in placement of the thermal sensor of up to 5mm away from the targeted location.

**Conclusion:** The 2450 MHz system achieved more rapid increases in temperature over a shorter period of time when compared to the 902-928 MHz system. The heating is more controlled over a larger volume when using the 915 MHz, as shown in the reduced variation in the "a" values between the 5 mm and 15 mm distances from the probe axis. Further investigations using precise placement of temperature sensors are warranted to refine aequation parameters for both the 902-928 MHz and 2450 MHz systems.

Table. Average values of the maximum temperatures reached during ablations, fitted curve equation parameters, and the R-squared value of the curve fit for both an AveCure 902-928 MHz system and an Acculis 2450 MHz system.

System	Maximum Temp (°C)		Equation Parameters @ 5 mm			Equation Parameters @ 15 mm / 10 mm		
	5 mm	15mm/10mm	a	b	R-squared	a	b	R-squared
Avecure 902-915 MHz	98.12±4.82	94.97±13.42	0.0831±0.107	1.751±0.464	0.999±0.001	0.040±0.057	1.661±0.604	0.984±0.019
Acculis 2450 MHz	104.38±2.76	104.38±2.76	3.049±3.383	1.126±0.326	0.992±0.012	1.597±3.895	1.126±0.326	0.941±0.177

### **A LONG TERM SOLUTION IN SECONDARY BLADDER NECK SCLEROSIS CASES – BIPOLAR PLASMA VAPORIZATION OVERCOMING STANDARD TUR IN A PROSPECTIVE, RANDOMIZED COMPARISON**

Bogdan Geavlete, Razvan Multescu, Cristian Moldoveanu, Florin Stanescu, Marian Jecu, Leon Adou, Cosmin Ene, Catalin Bulai, Petrisor Geavlete

*“Saint John” Emergency Clinical Hospital, Department of Urology, Bucharest, Romania*

**Introduction:** A long term, prospective, randomized trial assessed the surgical efficiency and safety, perioperative morbidity, postoperative convalescence and follow-up parameters specific for the bipolar plasma vaporization (BPV) approach by comparison to monopolar transurethral resection (TUR) in cases of secondary bladder neck sclerosis (BNS).

**Methods:** A total of 70 patients with BNS subsequent to TURP (46 cases), open prostatectomy for benign prostatic hyperplasia (BPH – 18 cases) and radical prostatectomy for prostate cancer (6 cases) were equally randomized for BPV and standard TUR (35 cases each). The inclusion criteria consisted of maximum flow rate (Qmax) below 10 mL/s and International Prostate Symptom Score (IPSS) over 19. All patients were evaluated preoperatively and every 6 months after surgery for a 2½ year’ period by IPSS, quality of life score (QoL), Qmax and post-voiding residual urinary volume (PVR).

**Results:** The mean operation time (10.3 versus 14.9 minutes), catheterization period (0.75 versus 2.1 days) and hospital stay (1.1 versus 3.2 days) were significantly reduced in the BPV series. During the immediate postoperative evolution, the re-catheterization for acute urinary retention only occurred in the TUR group (5.7%). The long term re-treatment requirements due to BNS recurrence were significantly lower in the BPV study arm (4.2% versus 11.2%). During all the semiannual follow-up check-ups, statistically similar values were determined for the two therapeutic alternatives concerning the IPSS, QoL, Qmax and PVR features.

**Conclusion:** BPV represents a reliable treatment approach for secondary BNS patients, favorably comparable to standard TUR in terms of surgical efficiency, perioperative morbidity and postoperative recovery. The method emphasized similar long term follow-up symptom scores and voiding parameters when compared to monopolar resection as well as a significantly reduced BNS recurrence rate.

### WHEN IS AN OPERATION LEARNED? HOW TO MONITOR PATIENT SAFETY? PROSPECTIVE EVALUATION OF PERFORMANCE UTILIZING TECHNIQUES OF STATISTICAL PROCESS CONTROL DURING ADOPTION OF ROBOTIC KIDNEY TRANSPLANTATION

Akshay Sood<sup>1</sup> M.D., Khurshid R. Ghani<sup>1</sup> M.D., Wooju Jeong<sup>1</sup> M.D., Rajesh Ahlawat<sup>2</sup> M.Ch., Pranjali Modi<sup>3</sup> M.Ch., Ronney Abaza<sup>4</sup> M.D., Jesse D. Sammon<sup>1</sup> D.O., Mahendra Bhandari<sup>1</sup> M.D., Mani Menon<sup>1</sup> M.D.

<sup>1</sup>Vattikuti Urology Institute, Henry Ford Hospital, Detroit, MI, USA

<sup>2</sup>Kidney and Urology Institute, Medanta-The Medicity, Gurgaon, India

<sup>3</sup>Department of Urology, H.L. Trivedi Institute of Transplantation Sciences, Ahmedabad, India

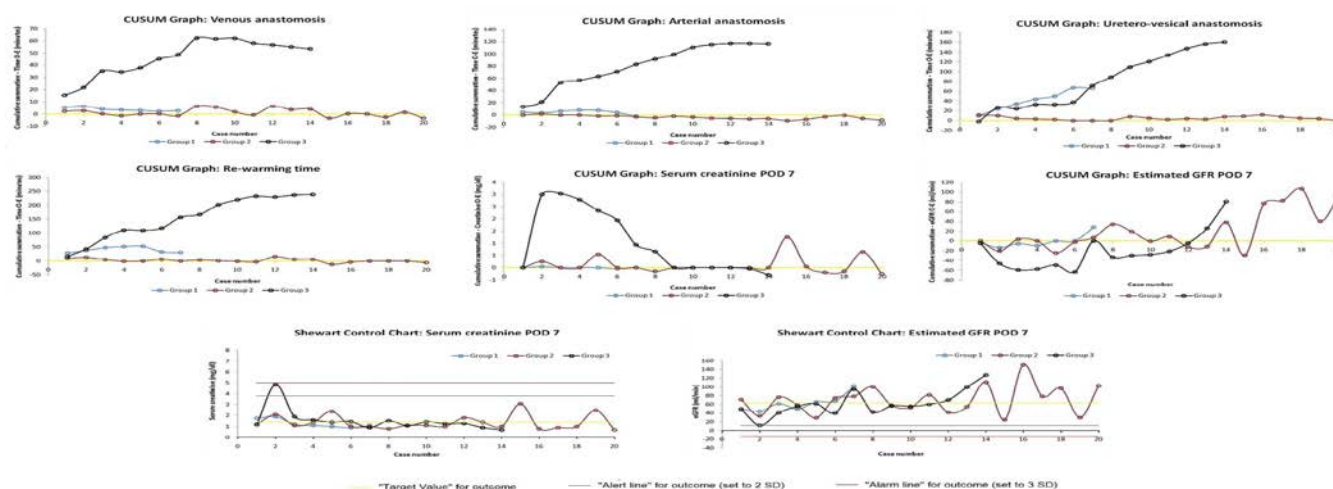
<sup>4</sup>Department of Urology, Ohio State University, Columbus, OH, USA

**Objective:** Traditional evaluations of the learning curve (LC) of an operation have been retrospective. Furthermore, LC analysis does not permit patient safety monitoring. We sought to examine LCs and monitor patient safety, in a prospective fashion, during development of robotic kidney transplantation (RKT) with regional hypothermia, utilizing the techniques of Statistical Process Control (SPC).

**Methods:** Between Jan-May 2013, 41 patients with end stage renal disease underwent RKT at two tertiary referral centers. Transplant recipients were classified into 3 groups based on robotic training and KT experience of the surgeons; Group 1: robotic trained with limited KT experience (n=7); Group 2: robotic trained and KT experienced (n=20); and Group 3: KT experienced with limited robotic training (n=14). Outcomes assessed were post transplant graft function and the measures of surgical process (anastomotic and ischemic times). We utilized the techniques of SPC; cumulative-summation (CUSUM) and Shewart-control charts to perform LC analysis and patient safety monitoring, respectively. CUSUM and Shewart-control charts are time-trend analysis techniques which allow comparison between outcomes achieved with an already established technique (open KT in our case; “target-value”) to those achieved with a novel intervention (RKT), in real time.

**Results:** CUSUM analysis revealed an initial learning phase for group 3 whereas groups 1 and 2 had none. The LC for group 3 varied depending on the parameter assessed (Figure 1a). Shewart-control charts analysis showed that functional outcomes were never compromised in group 1 and 2 patients. Graft function was compromised in one patient in group 3 (p<0.05) (Figure 1b), secondary to reasons unrelated to RKT.

**Conclusions:** By utilizing a set of predetermined outcomes, based upon the outcomes achieved with established techniques of KT, CUSUM and Shewart-control charts allowed prospective assessment of LCs and patient safety during establishment of RKT, aiding in determining the duration of mentorship, if and when needed; and identification of adverse patients events in a timely manner. Further, functional rather than technical outcomes should be examined when evaluating new techniques.



## ABSTRACT 35

### INNOVATION, CONSTRUCTION AND ASSESSMENT OF A NOVEL SEAMLESS LAPAROSCOPIC PORT PLACEMENT SYSTEM

Ashish Rawandale-Patil, Lokesh Patni, Preeti Patil  
*Institute of Urology, Dhule*

**Introduction:** Transperitoneal laparoscopy has a significant learning curve. First port placement is a mandatory and crucial initial step which contributes to complications, *e.g.*, intraoperative gas leak, visceral injuries, *etc.* Newer ports have distinct advantages but considerable fiscal constraints, *e.g.*, optical port, cuffed disposable ports, *etc.* Hence, today the need for a safe, reliable and cheap, reusable laparoscopic port placement system. Our innovative Laparoscopic port placement system is an attempt towards the same.

**Methods:** A survey of expectations of the type of initial port, was carried out. CAD design; patent and prototype creation was done. Our system consists of a 2 mm diameter initial puncture needle with a safety mechanism; attached to a barometer. The needle is inserted through a 2 mm skin incision. Successful peritoneal entry is indicated by the Boyle's principal causing fluid level changes in the barometer. Wire is then introduced through the needle into the peritoneal cavity. The needle is dissembled leaving behind a rod guided system for insertion of screw dilator, dilator, and port. An airlock valve allows for continuous peritoneal insufflation during the safe port placement. The water well design, markings on the components and endoscopic compatibility, helps confirmation of peritoneal entry of each component at various stages. The special tip design of part 3 facilitates blunt port placement by tissue separation through the "same site" of the initial puncture. Smooth peritoneal entry; eliminates the possibility of sharp injuries

**Results:** Port placement system was evaluated in 5 cases. Time to port placement was measured. Problems and disadvantages of the system were analyzed. Subjective assessment of the surgeon, assisting surgeon, anaesthetist and trolley nurse for ease of port placement was accessed with GRS scale. Post operative port site pain assessment was performed using the VAS. The port placement system demonstrated significantly lower port placement time and anxiety related to the initial port placement. Subjective port placement GRS score indicated a high degree of satisfaction on the effectiveness and safety.

**Conclusion:** Our port placement system is an efficient means of safe, seamless port placement. It provides peritoneal entry confirmation using barometrics and utilizes the same entry point for port placement (as the initial needle). It allows a low force, guided entry into the peritoneum. Allows visual confirmation before port placement. Maintains continuous pneumosufflation during the procedure. It is reusable and can be autoclaved. Developing such systems would reduce the healthcare costs for laparoscopic urology.

Fig 1: Prototype: Laparoscopic port placement system

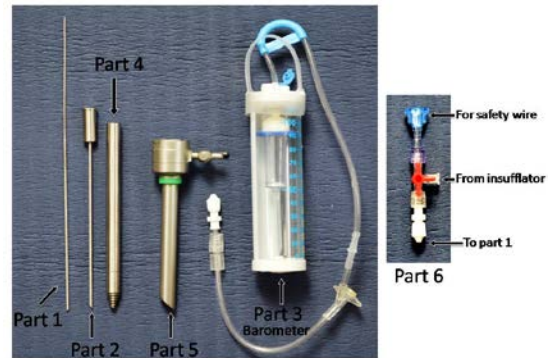


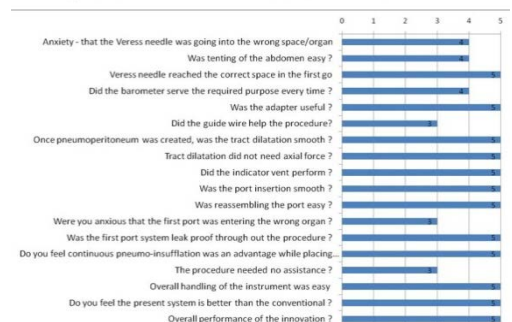
Fig 2a: PORT PLACEMENT SURVEY ANALYSIS

Question	Options	No.
1. Do you perform transperitoneal laparoscopy?	Yes No	98 2
2. What technique do you prefer for port placement?	Open Veress needle Others	8 90 2
3. What type of port do you use as the first port	Reusable metal Disposable	88 10
4. Would you prefer to have a disposable port (like the sealing port) for the open technique?	Yes No	94 4
5. Your preferred size for the first port is?	5mm 10mm Others	2 96 2
6. While using veress needle: Do you have the anxiety that you may be in the wrong space/organ	Yes No	96 2
7. Does the Veress needle always reach the correct space in the first go?	Yes No	90 8
8. Once pneumoperitoneum is created: Are you always sure that your camera port will go in smoothly (without force and jerks)? Without any anxiety?	Yes No	18 80

Fig 2b: PORT PLACEMENT SURVEY ANALYSIS

Question	Options	No.
9. For first port placement you prefer	Well inflated abdomen Inflated abdomen Deflated abdomen	96 2 2
10. Do you think that after pneumoperitoneum is created the first port (10mm) placement needs a lot of force	Yes No	90 8
11. Do you dread your first port entering the wrong organ?	Yes No	97 1
12. Are you sure that your port uses the same peritoneal rent created by the veress needle for entry?	Yes No	0 98
13. Would you like the first port placement system to be leak proof, more safe, and easy?	Yes No I am not sure	97 1 2
14. Would you prefer a cost effective, reusable and safer first port system that confirms peritoneal entry at each stage	Yes No Cost not my domain	96 1 1
15. Would you prefer the continuous pneumo-insufflation while placing the first port?	Yes No Does not make a difference	80 10 8

Fig 3: GRS score for FIRST PORT PLACEMENT



### COMPARISON OF RADIATION DOSE MEASUREMENTS FROM CONVENTIONAL AND TRIPLE BOLUS CT UROGRAPHY PROTOCOLS IN THE DIAGNOSIS AND MANAGEMENT OF RENAL CORTICAL NEOPLASMS

Garen Abedi B.S.<sup>1</sup>, Zhamshid Okhunov M.D.<sup>1</sup>, Chandana Lall M.D.<sup>2</sup>, Michael del Junco B.S.<sup>1</sup>, Kara Babaian M.D.<sup>1</sup> and Jaime Landman M.D.<sup>1</sup>  
<sup>1</sup>*Department of Urology, University of California, Irvine*  
<sup>2</sup>*Department of Radiology, University of California, Irvine*

**Introduction:** Increased utilization of computed tomography (CT) imaging has increased concerns about radiation exposure in patients with renal cortical neoplasms (RCN). As part of the treatment plan, patients with RCN often undergo routine imaging to evaluate the progress of their disease and the outcomes of their surgical treatment. In this retrospective study, we compared the radiation dose of a recently introduced CT protocol, triple bolus, and conventional CT urography for radiation exposure as well as quality of imaging.

**Methods:** We used standard volumetric computed tomography index (CTDIvol) and dose length product (DLP) to estimate radiation exposure while undergoing a CT scan of the abdomen and pelvis with and without intravenous contrast. CT Urography scans performed over the past 3 years at the UC Irvine Medical Center Douglas Hospital were included. The two CT imaging techniques reviewed, included conventional triple phase and recently introduced triple bolus CT urography protocols. The triple bolus CT protocol utilized during the study included a pre-contrast scan followed by 3 equal aliquots of 40-50ml of Isovue 370 intravenous contrast injections separated by 12-16 minute, 35 seconds and 40 seconds wait times, respectively. Following the final wait time, a post contrast scan was obtained for each triple bolus protocol. CTDIvol and DLP were obtained from our radiology department PACS imaging system for a total of 136 patients who either underwent CT imaging because of active surveillance of RCN, pre-operative planning for RCN, post-surgical follow-up for RCN or for hematuria. Additionally, two experienced urologists rated the subjective image quality of 20 randomly selected renal mass CT images from each protocol group using a non-validated survey using a 1-5 scale. The survey consisted of ten questions relating to the ability of the scan to identify relevant renal anatomy important for a urologist's evaluation of a RCN.

**Results:** After adjusting for BMI, CTDIvol and DLP were 27.4% and 36.5% lower in the triple bolus CT urography protocol respectively ( $p=0.015$  and  $p<0.001$ ). BMI increase was not correlated with an increase in CTDIvol in the triple bolus CT urography group ( $r^2<0.001$ ,  $p=0.986$ ), but had a positive correlation with CTDIvol in the conventional CT urography group ( $r^2=0.111$ ,  $p=0.009$ ). Similarly, DLP had a lower correlation with BMI in the triple bolus group than in the conventional group ( $r^2=0.168$  and  $r^2=0.500$  respectively). Subjective assessment of CT imaging quality did not show any difference between the two imaging protocols regardless of reviewer except for the question of ability to identify segmental renal vessels and their relationship to the renal mass; which received a lower mean rating in the triple bolus protocol for reviewer 2 ( $p=0.01$ ).

**Conclusions:** Triple bolus CT urography provides a lower radiation alternative for imaging of patients with RCN with a similar quality to conventional CT protocols. The lower radiation dose is most likely related to the single post-contrast scan in the triple bolus protocol versus three post contrast scans during a conventional CT urography protocol. Obese patients may benefit more from triple bolus CT protocol CT scans.

### EFFECT OF OUTPUT POWER ON THERMAL LESION ZONE DURING RADIOFREQUENCY ABLATION

Matthew Ishahak<sup>1,2</sup>, Stacie Arechavala<sup>1,2</sup>, Karli Pease BS<sup>1,2</sup>, Nelson Salas PhD<sup>1,2</sup>,  
Raymond Leveillee MD<sup>1-3</sup>

<sup>1</sup> Biomedical Engineering, University of Miami, Coral Gables, FL

<sup>2</sup> JBEDS Laboratory, University of Miami Miller School of Medicine, Miami, FL

<sup>3</sup> Department of Urology, University of Miami Miller School of Medicine, Miami, FL

**Introduction:** Thermal lesions produced by radiofrequency ablation (RFA) depend on many factors, including the power applied, the temperature achieved, and the duration of the ablation. The CoolTip™ RF Ablation System (ValleyLab, Covidien, Boulder, CO) employs an impedance feedback algorithm, which, depending on tissue impedance during ablation, controls power output in an on/off fashion in order to maximize energy delivery. Desired thermal lesions may be achieved with lower output power, thus controlling the heating environment to minimize the risk of damage to healthy renal tissue. The purpose of this experiment is to investigate the effect of varying output power on the thermal lesion zone in ex-vivo porcine kidney following RFA with the CoolTip™ RF Ablation System in impedance mode.

**Methods:** RFA was performed in the upper and lower pole of ex-vivo porcine kidneys with a 2cm tip for 12 minutes in impedance mode using the CoolTip™ RF Ablation System. Five ablations were performed at quarter, half, three-quarter, and full output power for a total of twenty ablations. Temperature was measured throughout the ablation at 0.5 and 1.5 cm from the probe axis using fiber optic thermal sensors. Power, current, voltage, and impedance were recorded during ablations using the Radionics Real-Time Graphics Software. After RFA, the kidneys were sectioned and the length, width, and depth of the ablation zone were measured. Average maximum temperatures at 0.5 and 1.5 cm were calculated for each output power. Ablation volume was calculated assuming an ellipsoidal ablation zone. Thermal damage was calculated based on the temperature data using the Arrhenius equation.

**Results:** At every output power level except quarter power, a decrease in output power was observed over the course of the ablation. Complete thermal damage at 0.5cm was achieved fastest at full and three-quarter powers, but only quarter and half powers achieved 100% thermal damage at 1.5cm consistently. Average ablation volume at quarter, half, three-quarter, and full power was  $3.18 \pm 0.06 \text{cm}^3$ ,  $2.32 \pm 1.00 \text{cm}^3$ ,  $2.66 \pm 1.42 \text{cm}^3$ ,  $2.17 \pm 1.24 \text{cm}^3$ , respectively. The maximum temperature at 0.5cm and 1.5 cm from either side of the RFA probe was  $91.98 \pm 10.66^\circ\text{C}$ ,  $81.27 \pm 11.47^\circ\text{C}$ ,  $86.66 \pm 11.42^\circ\text{C}$ ,  $81.58 \pm 11.42^\circ\text{C}$  and  $81.76 \pm 7.94^\circ\text{C}$ ,  $68.11 \pm 8.11^\circ\text{C}$ ,  $68.13 \pm 10.07^\circ\text{C}$ , and  $70.09 \pm 12.40^\circ\text{C}$  at quarter, half, three-quarter, and full power, respectively.

**Conclusion:** Varying output power during RFA has a clear effect on the thermal lesion zone volumes. At full power, thermal damage is achieved rapidly, resulting in charring and an increase in the impedance (Figure). The increased impedance results in a feedback to the CoolTip™ RF Ablation System, which leads to a decrease in output power. Further studies should be performed *in vivo* to determine if blood flow impacts this phenomenon.

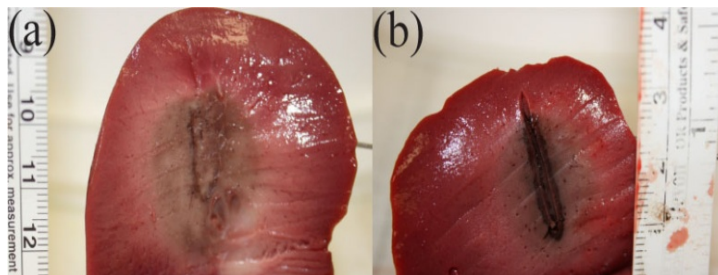


Figure: Comparison of ablation zone at (a) quarter and (b) full power

### PROSTATE CANCER LOCALIZATION BY MAGNETIC RESONANCE DISPERSION IMAGING

M. Mischi<sup>1</sup>, S. Turco<sup>1</sup>, C. Lavini<sup>2</sup>, J.J. de la Rosette<sup>3</sup>, M. Engelbrecht<sup>2</sup>, H. Wijkstra<sup>1,3</sup>

<sup>1</sup>Eindhoven University of Technology, Electrical Engineering Department, the Netherlands

<sup>2</sup>Academic Medical Center, University of Amsterdam, Radiology Department, the Netherlands

<sup>3</sup>Academic Medical Center, University of Amsterdam, Urology Department, the Netherlands

**Introduction:** Multiparametric magnetic resonance imaging (mpMRI) is a promising option for prostate cancer (PCa) localization. Nevertheless, large multicenter studies are still lacking and recent studies evidence room for improvement [Isebaert *et al.*, *JMRI* 2013]; as a result, mpMRI has not yet proven sufficient reliability to guide focal therapy and replace systematic biopsies. Additional parameters might improve mpMRI performance. In particular, due to gadolinium extravascular leakage, current mpMRI methods investigate functional rather than structural features of the microvasculature, overlooking changes in the microvascular architecture. Here we propose and evaluate a method to characterize the microvascular structure by dynamic contrast enhanced (DCE) MRI, providing a new parameter that is sensitive to those changes in the microvascular architecture that result from cancer angiogenesis.

**Methods:** Following an intravenous injection of a Gadobutrol bolus, concentration-time curves (CTCs) are measured at each voxel in the prostate. A convective-dispersion model, proposed for intravascular agents in the context of DCE ultrasound imaging, is adopted to describe the intravascular dispersion kinetics of the agent, characterizing the microvascular architecture [Kuenen *et al.*, *IEEE TMI* 2011]. This model is combined with the Tofts model for leakage, resulting in a new model for CTC fitting and estimation of an intravascular-dispersion parameter,  $\kappa$ , characterizing the microvascular architecture. Separate estimation of an arterial input function is no longer necessary. An initial validation was carried out including 90 MRI slices in 15 patients referred for radical prostatectomy. As shown in the Figure 1, voxel classification performance was evaluated by comparison of DCE MRI and histology results.

**Results:** Voxel classification by  $\kappa$  maps yielded sensitivity, specificity, and ROC curve area equal to 85.0%, 90.2%, and 0.94, respectively. These results outperformed those obtained by the standard (Tofts) leakage parameter,  $K^{trans}$ .

**Conclusions:** PCa localization by the dispersion parameter  $\kappa$  was accurate and superior to the standard leakage parameter  $K^{trans}$ , encouraging further research to establish the additional value of dispersion imaging in the context of mpMRI for PCa diagnosis.

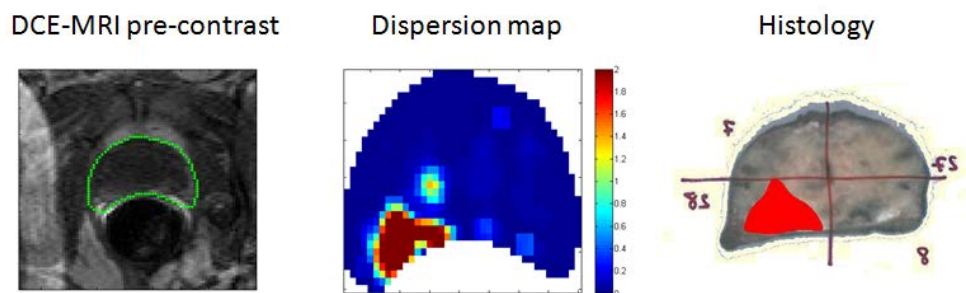


Figure 1: DCE-MRI slice with corresponding dispersion map and histology result.

### EVALUATION OF A DISPOSABLE FLEXIBLE DIVERTING 17FR CYSTOSCOPE IN EVERYDAY UROLOGICAL PRACTICE

Joseph V. DiTrollo M.D., Samuel Aly B.S., Michael D. LaSalle M.D.

*St. Barnabas Medical Center, Livingston, NJ  
Department of Urology, Rutgers New Jersey Medical School, Newark, NJ*

**Introduction:** Endoscopic urological procedures are a vital part of the urological practice. Cost of using and maintaining a flexible cystoscope is approaching \$100 per case. Adding to that is a more complex and destructive sterilization process. There is an increasing need for a disposable flexible diverting cystoscope at an affordable price.

**Methods:** We had the opportunity to evaluate and employ an FDA approved 17Fr chip-on-the-tip disposable (CMOS) flexible diverting cystoscope, with a 5Fr working channel for irrigation and instrumentation from ProSurg. Using a standard laptop (HP DV4), we were able to power the integrated 6 LED light source and the chip-on-the-tip 400x400 pixel camera as well as the ability to store and transmit images to the laptop hard drive. At the time of utilization, all that was required was the following:

1. Disposable 17Fr flexible diverting cystoscope (ProSurg)
2. Bag of irrigation fluid with tubing
3. Laptop/tablet computer (Windows 7/Windows8)
4. 6 foot USB 2.0 Connecting Cable

**Results:** Using the 17Fr ProSurg flexible diverting cystoscope, we were able to insert into the male urethra and under direct vision, evaluate and document the urological landmarks. The laptop was able to record an AVI video and take JPEG and BMP images. Complete endoscopic evaluation of the bladder was possible. The CMOS viewing endoscope with 6 LEDs allowed for visualization. A 5Fr working channel allowed for irrigation and instrumentation.

**Conclusion:** Cost to maintain and sterilize endoscopic equipment is approaching \$100/case. The more demanding sterilization requirements make this a challenging proposition. Along with the high risk destruction to cystoscope components, one can make a case for disposable cystoscope. Additionally, the power light source, video monitor, and documentation device are all being replaced by an everyday laptop/tablet computer only adds to the benefits. The portability, disposability, and improving quality demands for a functional, low-cost endoscopic system and warrants further evaluation.

## **IN VITRO RESULTS OF ROBOTIC CYSTOSCOPE AND 3D PANORAMA FOR AUTOMATED BLADDER SURVEILLANCE SYSTEM (ABSS)**

Xianming Ye<sup>1</sup>, Yuanzheng Gong<sup>2</sup>, and W. Jong Yoon<sup>1</sup>

<sup>1</sup>*Department of Mechanical and Industrial Engineering, Qatar University, Doha, Qatar*

<sup>2</sup>*Mechanical Engineering Department, University of Washington, Seattle, USA*

**Introduction:** This abstract presents the latest results in the development of an automated cystoscope in order to provide better efficiency and unique 3D user interface (UI) for bladder cancer surveillance. Using a thin ( $\varnothing 1.2$  mm) Scanning Fiber Endoscope (SFE) and highly customized image stitching software, the 3D panoramic view of the bladder's inner surface can be reconstructed from the cystoscopic video frames obtained in computer-controlled scans.

**Methods:** The automated bladder surveillance system (Figure 1) consists of a 60 mm-long wire-driven steering section which has serially connected six sub-segments that alternately rotate in the  $x$ - and  $y$ - directions. With the advantages of the multiple degrees-of-freedom of the structure, the flexible endoscopic camera can be steered to follow optimized scanning trajectories satisfying safety and design requirements. Video outputs of the SFE are recorded for subsequent 2D image stitching and 3D panorama reconstruction.

**Results and Future work:** About 60% of the bladder's inner surface could be covered and 3D reconstructed from the *in vitro* phantom bladder experiment by warping the 2D stitching image to the 3D geometric model (Figure 2). This 3D model allows 3D axes rotation and zoom in and out by regular MATLAB graphics interface. The proposed cystoscope can be further improved by increasing the maximum bending angle of sub-segments in the steering section, from the current  $\pm 45^\circ$  up to preferably  $\pm 60^\circ$ , to cover the areas near the internal urethral orifice.

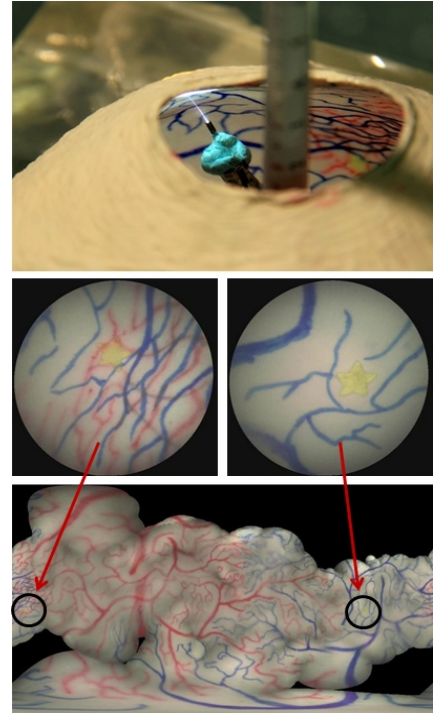


*Fig. 2: The result of 2D image stitching. Upper: Scanning the inner surface of a bladder phantom using a SFE. Middle and lower: Image stitching using cystoscopic v*

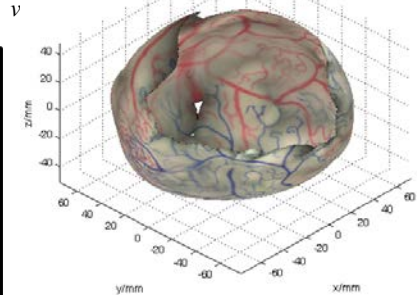


*Fig. 3: Reconstruction of the actual-sized 3D panorama of bladder's inner surface.*

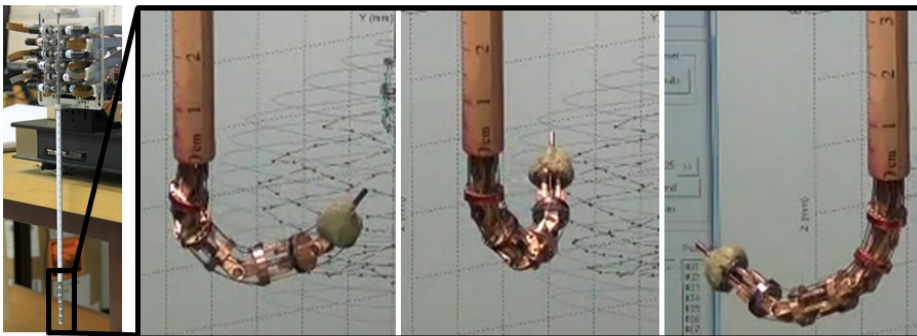


*Fig. 5: Design of automated cystoscope. Left: Structure of the robotic steering mechanism with a motor module, an insertion tube, and a steering section. Right: Exemplary versatile configurations of the 7 DOF steering section.*

## MRI-GUIDED PROSTATE CANCER FOCAL LASER ABLATION THERAPY USING A MECHATRONIC NEEDLE GUIDANCE SYSTEM: INITIAL EXPERIENCE AND FUTURE DIRECTIONS

Jeremy Cepek<sup>a,b</sup>, Uri Lindner<sup>c</sup>, Sangeet Ghai<sup>d</sup>, John Trachtenberg<sup>c</sup>, Aaron Fenster<sup>a,b</sup>

<sup>a</sup>Robarts Research Institute, London; <sup>b</sup>Biomedical Engineering, The University of Western Ontario, London; <sup>c</sup>Department of Surgical Oncology, Division of Urology, University Health Network, Toronto; <sup>d</sup>Department of Medical Imaging, University Health Network, Toronto, Canada

**Introduction:** It has been widely recognized that prostate cancer is currently over-treated, and that conventional, whole-gland therapies may be excessive for a considerable proportion of men with the disease, exposing them to potential genitourinary, gastrointestinal and sexual side effects. As a potential solution to this problem, the concept of focal therapy for prostate cancer is being evaluated in the urologic community. Among several emerging techniques, MRI-guided focal laser ablation (FLA) therapy is particularly attractive, as it offers intra-treatment tumor localization, needle guidance, real-time thermometry, and immediate post-treatment imaging of the ablated region. Despite these attractive features, however, performing a needle-based procedure within an MRI environment presents many technical challenges due to the high magnetic field strength, presence of fast-switching magnetic field gradients and RF fields, and a limited workspace. These challenges are important to overcome, since the placement of needles for FLA therapy must be done with high accuracy to ensure complete ablation of the target volume and to avoid damage to surrounding tissue. In an attempt to overcome these challenges and take full advantage of the utility of intra-treatment MRI, we developed an MRI-compatible mechatronic needle guidance system for accurate delivery of needles to the prostate for FLA therapy, and treatment planning and patient selection guidelines in order to utilize this system most effectively.

**Methods:** A custom MRI-compatible mechatronic needle guidance device was developed and integrated with custom 3D visualization software. The resulting system features the ability to specify desired angulated needle trajectories using a 3D imaging interface, precisely align the device's needle guides to these trajectories, and manually insert needles into the prostate under MRI guidance. The system was used to guide 29 needles in eight cases of MRI-guided prostate FLA therapy, and the error in needle placement was quantified for each insertion. Monte Carlo simulations of needle placement error were then performed to determine the relationships between target size and shape, the level of uncertainty in needle placement error, and the probability of achieving complete focal target ablation. The goal of the simulations was to determine the maximum target size that can be confidently ablated with this system, and to quantify the clinical benefit that could be gained by increasing needle guidance accuracy.

**Results:** The median error in needle placement was 3.4 mm, and device alignment and needle insertions were performed with the patient and device remaining inside of the MRI bore. This feature contributed to a significant decrease in the time required to guide each needle to its target, compared to a fixed grid template approach (median 8 vs. 18 minutes,  $p < 0.0001$ , Mann-Whitney U test). The device's ability to target arbitrary points in the prostate through angulated trajectories was found to be extremely valuable, and ensured that each focal target was reachable. For a given level of needle placement uncertainty, our model predicts the maximum length of targets that can be completely ablated with at least 90% certainty. Currently, the achievable diameter of each individual ablation region is ~15 mm, limiting the treatable target length to 10 – 14 mm, depending on its width.

**Conclusion:** The MRI-guided FLA therapy procedure was improved with the use of a mechatronic needle guidance system. However, the maximum size of target that can be confidently ablated using the current technique is ~14 mm, which limits its applicability to approximately 1/3 of the patients who were otherwise deemed potentially good candidates for focal therapy. Improved methods of reducing needle deflection are being developed to enable larger targets to be confidently ablated using MRI-guided FLA therapy.

### **IN VITRO EVALUATION OF LithAssist: A NOVEL COMBINED HOLMIUM LASER AND SUCTION DEVICE**

Zhamshid Okhunov<sup>1</sup>, Michael del Junco<sup>1</sup>, Renai Yoon<sup>1</sup>,  
Kevin Labadie<sup>1</sup>, and Michael Ordon<sup>2</sup>

<sup>1</sup>Department of Urology, University of California, Irvine, Orange, USA

<sup>2</sup>Division of Urology, Department of Surgery, University of Toronto, Toronto, Canada

**Introduction:** The aim of this *in vitro* study was to evaluate and compare a novel intracorporeal lithotripter, LithAssist (LA), (Cook Medical, Bloomington, IN), with the Swiss LithoClast Ultra (SLU), (Boston Scientific, Boston, MA) for the efficacy of fragmentation and removal of artificial stones made of gypsum-based cement.

**Methods:** Five soft and 10 hard U-30 stones were subjected to fragmentation using the SLU and LA, respectively. We recorded the stone weight (grams) prior to placing them into a 60-mL syringe for fragmentation. We inserted a 30Fr percutaneous access sheath into the syringe and positioned the stone within its lumen. Next, we inserted the lithotripter into a right-angled nephroscope. We recorded mean times for first disintegration, disintegration to 2-mm, complete stone disintegration, and complete stone removal for each device. In addition, we recorded the stone mass following each minute of stone fragmentation.

**Results:** All soft stones were completely disintegrated and removed with both the SLU and LA device. For soft stones, first disintegration was not significantly different for the SLU compared to the LA (1.30 ±0.64 vs. 2.15 ±0.61 min, p=0.11). Disintegration to 2-mm (2.83 ±0.41 vs. 4.15 ±0.70 min, p=0.049), complete disintegration (3.18 ±0.20 vs. 6.40 ±1.95 min, p=0.038), and complete removal (3.30 ±0.22 vs. 8.82 ±1.05 min, p=0.001) were faster for the SLU compared to the LA. For hard stones, fragmentation was not accomplished with the SLU, whereas with the LA, mean time for first disintegration, disintegration to 2-mm, complete disintegration, and complete removal were 3.60 ±1.36 min, 7.25 ±3.33 min, 7.54 ±2.94 min and 8.64 ±2.78 min, respectively.

**Conclusions:** The SLU demonstrated faster times for disintegration to 2-mm, complete disintegration, and complete stone removal when compared to the LA, however, the LA was superior at fragmenting and completely removing harder artificial stones in the model tested. The next step, which is currently underway, is to conduct a prospective randomized clinical trial to confirm these findings in a clinical setting and assess the impact on operative time and outcomes.

### FAT EMULSIFICATION BENEFIT OF SURFACTANT COMPARED TO WATER FOR LAPAROSCOPIC DEFOGGING AND CLEANING

Peter Stuhldreher MD<sup>1</sup>, Xiao Gu MD PhD<sup>2</sup>, Carson Wong MD<sup>3</sup>

<sup>1</sup>University Hospitals Case Medical Center, Cleveland, OH

<sup>2</sup>First Clinical Medical College at Yangzhou University, Yangzhou, China

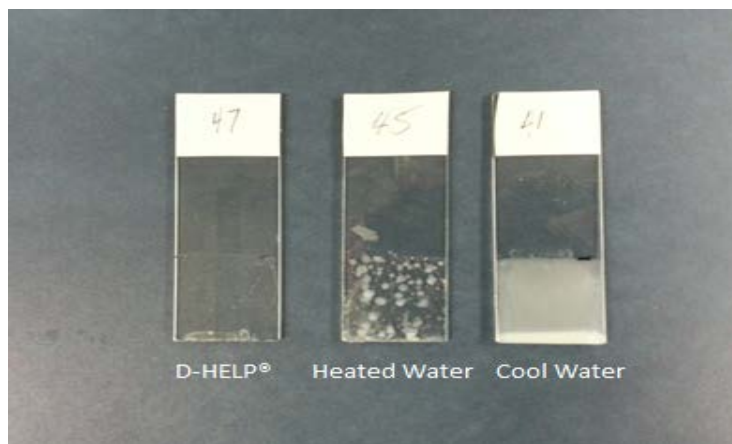
<sup>3</sup>University Hospitals Parma Medical Center

**Introduction:** Optimal visualization during laparoscopic and robot-assisted surgery is integral to being able to perform safe and effective surgery. Various methods have been developed to keep the laparoscope fog free and clean the laparoscope of bodily fluid and other debris. The D-HELP<sup>®</sup> (New Wave Surgical, Coral Springs, FL) system has been developed to defog and clean the laparoscope with one system. To compare the D-HELP<sup>®</sup> surfactant versus standard cleaning media, we evaluate each of their ability to emulsify fat.

**Methods:** Glass slides were used to simulate the lens of a laparoscope. Each slide was cleaned from the manufacturer with alcohol and then weighed with a tared scale. They were submerged into 1 inch of heated animal fat solution (134F) to one inch and immediately removed. The slide was then cooled to solidify the fat, and re-weighed. Slides were then placed 1 inch into one of three separate solutions: D-HELP<sup>®</sup> surfactant (122F), heated sterile water (122F), cool sterile water (65F). Slides were placed in solution for 5 seconds and removed for 10 second: this process was repeated 5 times. After air drying the slides for 12 hours, they were re-weighed and reduction in mass was calculated. Groups were analyzed using the Student's t-test for statistical significance defined as  $p < 0.05$ .

**Results:** After calculating the percentage of the material removed, it was found to be 1.6% with cool water, 72.7% with heated water and 94.7% with D-HELP<sup>®</sup>. Removal of fat material was significant for both D-HELP<sup>®</sup> when compared to heated ( $p < 0.01$ ) and cool water ( $p < 0.01$ ), and heated water compared to cool water ( $p < 0.01$ ). Figure 1 illustrates the treated slides.

**Conclusions:** D-HELP<sup>®</sup> surfactant offers superior cleaning to heated and cool water for fat removal from glass, even without wiping with gauze. The surfactant facilitates fat emulsification, allowing for efficient cleaning of the laparoscope lens during laparoscopic and robot-assisted surgery.



### COMPARISON OF TWO HIGH FIDELITY WITH ONE LOW FIDELITY ENDOUROLOGICAL SIMULATOR

Ann Kathrin Orywal, Sophie Knipper, Andreas J. Gross, Christopher Netsch

*Department of Urology, Asklepios Hospital Barmbek, Hamburg, Germany.*

**Introduction:** A lot of low fidelity and high fidelity surgical simulators for training the ureteroscopy (URS) procedure are available on the market. Only few studies performed standardized comparisons of these different devices. Aim of this study was to compare two high fidelity URS simulators with a low fidelity simulator with regard to realistic appearance, usability, and training effect.

**Methods:** The following three endourology simulators were tested: the Endouro trainer LS 50<sup>®</sup> by Samed<sup>®</sup> (high-fidelity), the Adam Endo Trainer<sup>®</sup> by Prodelphus<sup>®</sup> (high fidelity) and the Endouro Trainer<sup>®</sup> by Cook Medical<sup>®</sup> (low fidelity). Nine experienced endourologists (>30 URS procedures/year) and nine inexperienced residents (0 URS procedures) performed a semi-rigid ureteroscopy with endoscopic stone extraction via a tipped Dormia-basket in every trainer. The order of the use of the different trainers was randomized. The performance was rated, using the global rating scale (GRS). After the use of the simulators the participants answered seven questions concerning realistic appearance, usability and training effect of the simulator.

**Results:** GRS scores differed significantly between experienced and unexperienced urologists (mean values of 33.26 vs. 19.15,  $p < 0.001$ ). All participants were in agreement concerning usability, appearance and use for training of all simulators. Only, the question of suitability for training was evaluated differently since experienced endourologists would rather not use the Endouro Trainer<sup>®</sup> whereas the inexperienced residents would use it for training. Comparing all simulators, the Adam Endo Trainer<sup>®</sup> and Endouro trainer LS 50<sup>®</sup> were seen to be most realistic, whereas the participants agreed to only use the Endouro Trainer<sup>®</sup> and the Endouro trainer LS 50<sup>®</sup> for regular training.

**Conclusions:** The high-fidelity Endouro trainer LS 50<sup>®</sup> showed the best realistic appearance and suitability and was recommended for training, both, by experienced and inexperienced urologists, although inexperienced residents would also consider the low-fidelity trainer to be a good training option. Proper endourologic skills for URS might also be achieved with a low-fidelity simulator.

### COMPARISON OF NITINOL STONE RETRIEVAL BASKETS IN AN URETEROSCOPY SIMULATOR

Christopher Netsch, Sophie Knipper, Andreas J. Gross

*Department of Urology, Asklepios Hospital Barmbek, Hamburg, Germany*

**Introduction:** Nitinol stone retrieval baskets facilitate extraction of caliceal calculi during flexible ureteroscopy. However, stone retrieval baskets may compromise ureteroscope deflection and irrigation flow. We evaluated the stone capture rates of 5 commercially available nitinol stone retrieval baskets in an ureteroscopy simulator using a flexible ureteroscope. The impact of nitinol baskets on ureteroscope's deflection and irrigation flow was also tested.

**Methods:** Six-mm metal beads were placed in the upper, mid, and lower kidney pole of a commercially available ureteroscopy simulator of the human kidney. An 11.5 F ureteral access sheath was placed at the ureteropelvic junction. A 6/8.8F flexible ureteroscope (Viper<sup>®</sup>, Richard Wolf) of the latest generation was used for access and visualisation of the metal beads. Four board certified urologists, two endourologists and two laparoscopic surgeons, tested each device. The Cook N-Gage<sup>®</sup> 1.7F, Cook N-Circle<sup>®</sup> 2.2F, Boston Optiflex<sup>®</sup> 1.3F, Boston Zerotip<sup>®</sup> 1.9F, and Coloplast No-tip<sup>®</sup> 2.2F stone retrieval basket were tested. The time to extract the 6-mm metal beads was recorded in seconds. Each basket was tested by each surgeon in each location three times. Deflection angles and flow rates of the empty and loaded (with stone retrieval baskets) flexible ureteroscope were measured three times each.

**Results:** There were no significant differences in the mean stone capture times between endourologists and laparoscopic surgeons (27.74 vs. 33.06 sec,  $p>0.05$ ). The Cook N-Gage<sup>®</sup> 1.7F resulted in the most rapid extraction of the metal beads for the upper, mid, and lower pole ( $p\leq 0.008$ ). However, the time to extract the metal beads differed not significantly between the stone locations for each basket. The mean loss of ureteroscope irrigation ranged between 60.3 (Boston Optiflex<sup>®</sup> 1.3F) and 85.51% (Coloplast No-tip<sup>®</sup> 2.2F). The mean loss of deflection ranged from 0 (Cook N-Circle<sup>®</sup> 2.2F, Boston Optiflex<sup>®</sup> 1.3F) to 8.9% (Cook N-Gage<sup>®</sup> 1.7F) when the loaded basket was open, and increased to a range from 8.9% (Cook N-Circle<sup>®</sup> 2.2F) to 18.5% (Coloplast No-tip<sup>®</sup> 2.2F) with occlusion of the devices, respectively.

**Conclusions:** The Cook N-Gage<sup>®</sup> 1.7 F basket resulted in the most expeditious extraction of 6 mm beads in the ureteroscopy simulator. However, loss of irrigation flow and deflection of the loaded ureteroscope seems not to be simply related to basket diameter.

### TRANS-PERITONEAL ROBOT-ASSISTED LAPAROSCOPIC HIGH INTENSITY FOCUSED ULTRASOUND FOR TARGETED THERAPY OF THE PROSTATE AND BLADDER: NOVEL APPROACH

Matsugasumi T., Abreu A.L.C., Leslie S., Shoji S., Marien A., Chopra S., Gill I., Ukimura O.

*Institute of Urology, University of Southern California, Los Angeles, CA, USA*

**Introduction:** A novel laparoscopic probe of High Intensity Focused Ultrasound (HIFU) has been developed (SonaCare Medical, 11 mm in diameter), and FDA-approved. This device delivers HIFU energy continuously in tissue to ablate 1cc of tissue in 1 minute. We first developed a new approach with trans-peritoneal robot-assisted HIFU for targeted therapy of the human prostate and bladder in fresh male cadaver.

**Methods:** In the prostate (n=3), gold fiducials (0.9mm in diameter x 3mm in length, CIVCO Medical), which served as a center of virtual target tumor, were implanted by TRUS guidance in left-posterior peripheral zone (PZ) (n=3) and right-anterior transition zone (TZ) (n=3). Standard robotic and 12 mm ports (total n=5) were placed with use of a 12 mm trocar for the HIFU probe. Posterior approach in the Denonvillier space was applied for targeting of the posterior PZ tumor [Figure 1(A)], and anterior approach in the Retzius space for targeting of the anterior TZ tumor [Figure 1(B)]. Bladder wall was longitudinally opened and mimic bladder tumor (2 tumors per case; total 6), which was prior dissected from the striated muscle (25 mm in diameter), were implanted intra-vesically in bilateral side walls. The bladder was closed as water-tight and filled by 250ml water. The HIFU probe was directly contacted with surface of the targeted zone to visualize the virtual tumor and to ablate it under real-time US guidance which is built-in function of the device. Pelvic lymph node dissection was performed for staging and therapeutic purpose. For assess the precision, efficacy and safety, gross inspection and microscopic evaluations of the pelvic organs were performed.

**Results:** In targeting prostate tumor, both posterior approach (to PZ tumor) and anterior approach (to TZ tumor) were feasible in all cases. In targeting bladder tumor, extra-vesical approach was feasible in all cases. Real-time US could clearly visualize the tumor in all cases. Simultaneous display of both initial planning and real-time monitoring US images provided confirmation of targeting precision and, if necessary, alignment of the targeting. Entire surgical time of robotic-assisted HIFU per a tumor required approximately one hour. The microscopic margins between the treated and untreated zones were clear [Figure 2][Figure 3], with no thermal damages and no mechanical injury in the untreated areas.

**Conclusion:** We first developed novel techniques with newly developed laparoscopic HIFU probe in fresh cadaver. Robotic assisted trans-peritoneal approach of laparoscopic HIFU for targeted therapy of the human prostate and bladder is feasible.

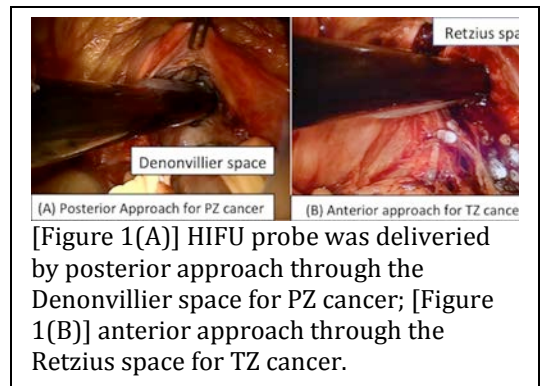


[Figure 1(A)] HIFU probe was delivered by posterior approach through the Denonvillier space for PZ cancer; [Figure 1(B)] anterior approach through the Retzius space for TZ cancer.

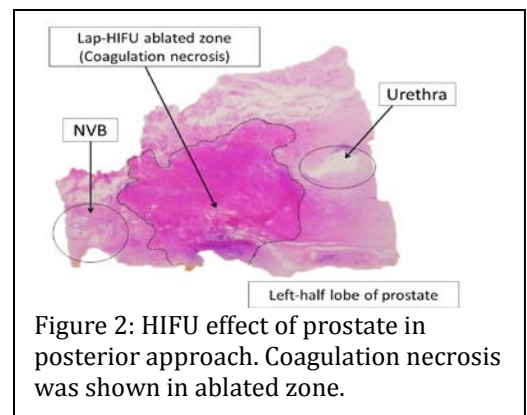


Figure 2: HIFU effect of prostate in posterior approach. Coagulation necrosis was shown in ablated zone.

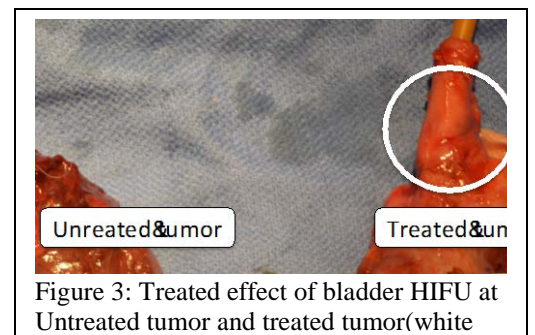


Figure 3: Treated effect of bladder HIFU at Untreated tumor and treated tumor(white)

## BODY WALL FORCES AT PORT SITES IN LAPAROSCOPIC AND ROBOTIC SURGERY

Smita De M.D., Ph.D.<sup>1</sup>, Paul Loschak Ph.C.<sup>2</sup>, Brett Page B.S.<sup>3</sup>, Amy Kerdok Ph.D.<sup>3</sup>

<sup>1</sup>Department of Urology, Stanford University Hospital, Stanford, CA, USA

<sup>2</sup>Harvard School of Engineering and Applied Sciences, Cambridge, MA, USA

<sup>3</sup>Intuitive Surgical Operations, Inc., Sunnyvale, CA, USA

**Introduction:** Minimally invasive surgical (MIS) techniques have been shown to provide numerous patient benefits. One of the limitations, especially in robotic surgery, is the lack of touch sensation. A common perception is that this could potentially lead to excessive force application on tissues, including the port site. There is little data comparing forces applied in robotic surgery versus laparoscopic surgery to evaluate this question. Our objective was to measure and compare forces applied to the abdominal wall at port sites during robotic and laparoscopic tasks in a live animal model.

**Methods:** We first developed a novel device for measuring *in vivo* body wall forces during MIS. Off the shelf force sensors were fixed to a standard long length robotic cannula. The sensors were then modified to achieve an appropriate force range (0-50 N based on earlier tests) and housed in a waterproof covering. The cannula was calibrated using standard force gauges and validated *in vivo* with a laparoscopic instrument outfitted with a commercially available force-torque sensor (ATI Nano25, NC, USA). The cannula was then used in *in vivo* porcine experiments to perform simple standard surgical tasks using robotic (*da Vinci*<sup>®</sup> Si<sup>™</sup>, Intuitive Surgical, Inc., Sunnyvale, CA) and laparoscopic platforms through the same port site. Tasks performed by multiple users included bowel manipulation, dissection of the ureter, instrument collisions, suturing, and retraction of the uterus, bladder, and rectum. The change in resultant force magnitude (delta force) at the body wall was measured for each task.

**Results:** Our preliminary results demonstrate that the *da Vinci*<sup>®</sup> Surgical System applies similar, if not lower, forces to the body wall compared to laparoscopy during simple surgical tasks. The mean delta forces during bowel manipulation, rectal retraction, ureteral dissection, and instrument collisions were respectively 1.2 N (6%), 2.1N (16 %), 1.7 N (20%), and 0.4 N (6%) lower with the robot as compared to laparoscopy.

**Conclusion:** The absence of force feedback in robotic surgery is often viewed as a risk factor for inadvertent tissue injury. Results of this preliminary study indicate that the *da Vinci*<sup>®</sup> Surgical System does not apply higher forces to the body wall as compared to laparoscopy during common surgical tasks. In fact, lower forces were observed with the robotic platform in several cases. Future studies in this area may help understand potential relationships between body wall forces and port site complications, such as hernias and infections.

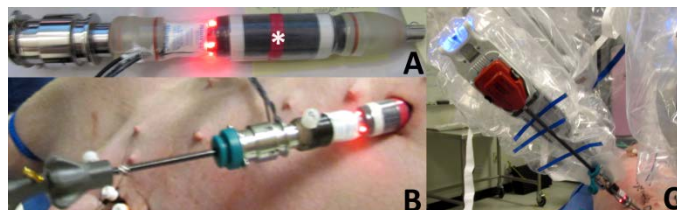


Figure. A) Sensorized cannula. \*Remote center within body wall. B) Cannula during laparoscopic tasks. C). Cannula during *da Vinci*<sup>®</sup> tasks.

## ABSTRACT 49

### DESIGN AND EVALUATION OF 3D PRINTED MOLDS AND SLICING DEVICE FOR WHOLE MOUNT PROSTATE SECTIONING

Alan Priestler<sup>1</sup>, James Garritano<sup>1</sup>, Jesse Le<sup>2</sup>, Bryan Radosavcev<sup>3</sup>, Daniel Margolis<sup>4</sup>, Jiaoti Huang<sup>3</sup>, Warren Grundfest<sup>1</sup>, Leonard Marks<sup>2</sup>, Shyam Natarajan<sup>2</sup>

<sup>1</sup> University of California Los Angeles, Department of Bioengineering

<sup>2</sup> University of California Los Angeles, Urology

<sup>3</sup> University of California Los Angeles, Pathology

<sup>4</sup> University of California Los Angeles, Radiology

**Introduction:** To improve the accuracy of MRI-histological correlations in prostate cancer (CaP), a 3D-printed mold and slicing device have been developed. The system is designed to regulate sectioning depth and orientation such that each tissue slice corresponds precisely with an MR imaging plane. Furthermore, an agarose prostate phantom with embedded fiducials has been developed to characterize the accuracy of this technique.

**Methods:** Each mold is generated from the *in vivo* MR segmentation of a prostate prior to surgery. The mold is designed to conform precisely to the prostate surface, with parallel slits at 4.5 mm intervals along its length. Each slit corresponds to a specific MR imaging plane, which facilitates 3D reconstruction and MR/histology comparisons. In order to prevent specimen displacement, a multi-bladed slicing device has also been developed (Figure A).

To characterize the system's accuracy, an agarose phantom with embedded fiducials was designed with 12 inked needle tracks of known location (Figure B). Using Matlab, a digital library of possible phantom slices was generated for views  $\pm 10$  degrees off-axis, in 0.1 mm depth increments. After sectioning the phantom both manually and via the mold, needle track locations were recorded and cross-referenced to the digital library. Manual and mold-based sectioning were then compared with reference to slice position, slice orientation, and reconstruction accuracy.

**Results:** Substantial benefits in slice thickness ( $4.60 \pm 0.35$  vs.  $5.26 \pm 0.44$  mm), orientation error ( $3.09^\circ \pm 1.16^\circ$  vs.  $4.5^\circ \pm 4.6^\circ$ ), and reconstruction accuracy ( $0.63 \pm 0.34$  vs.  $2.44 \pm 1.22$  mm) were observed relative to manual sectioning techniques. Prostate and region-of-interest surfaces were also reconstructed with higher fidelity using the mold technique (Figure C).

**Conclusion:** The 3D printed mold and slicing device facilitate reconstruction with sub-millimeter accuracy, and appear helpful in improving MR-histological correlations of CaP. Characterizing the true extent of cancer relative to MR predictions may aide in future surgical planning, targeted biopsies, and perhaps focal therapy. Furthermore, the parameters associated with missed lesions can be incorporated into future analyses, improving MR sensitivity overall. This method may also be appropriate for analysis of other solid tumors, including breast and pancreas.

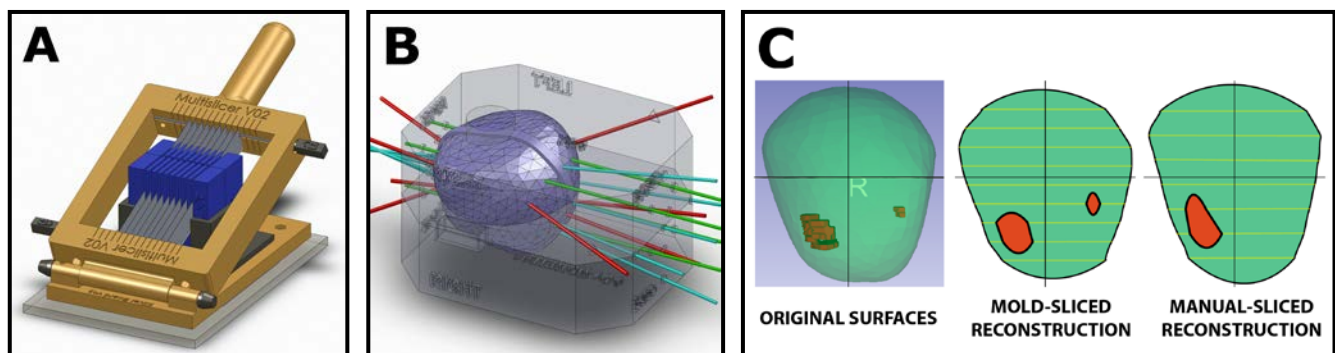


Figure: A) CAD of mold and slicer, B) CAD of phantom with fiducials, C) Mold-sliced vs. manual surface reconstruction

## ABSTRACT 50

### EXPLORATION OF AN AMPLITUDE-MODULATED PULSE SEQUENCE USING THE VORTX R<sub>X</sub><sup>®</sup> SYSTEM FOR PROSTATE HISTOTRIPSY IN A CANINE MODEL

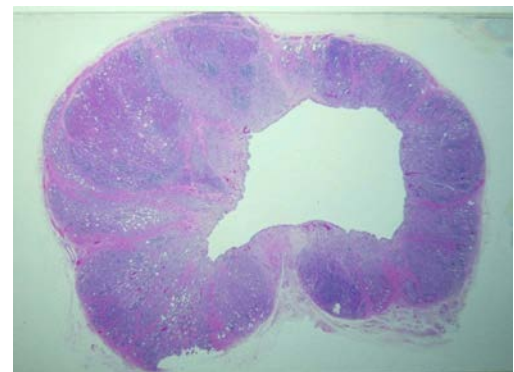
Jonathan M. Cannata, PhD<sup>1</sup>, James A. Bertolina, PhD.<sup>1</sup>, William W. Roberts, MD<sup>2</sup>  
*HistoSonics, Inc.<sup>1</sup> and University of Michigan Department of Urology<sup>2</sup>*

**Introduction:** Histotripsy is a noninvasive pulsed focused ultrasound technology that uses controlled acoustic cavitation to homogenize targeted tissue. Feasibility of prostate tissue debulking in the canine model with the VORTX R<sub>X</sub><sup>®</sup> system has previously been demonstrated [1]. However, subclinical fibrosis in the abdominal rectus muscle of two subjects was found to be the result of prefocal heating. The objective of this canine study was to assess whether an amplitude-modulated pulse sequence would eliminate pathologic prefocal heating while maintaining effective debulking of prostate tissue.

**Methods:** Following animal care and use committee approval, transabdominal histotripsy was applied to the prostates of eight canine subjects using an amplitude-modulated sequencing scheme (high amplitude 3 cycle initiation pulses followed by lower amplitude 2 cycle maintenance pulses). This sequence modification reduced time-averaged intensity by 50% compared to the 500 Hz 3 cycle sequence used previously [1]. The resultant cavitation cloud was manually translated throughout the targeted volume for 60 minutes in each subject followed by TRUS and cystoscopic assessment. Laboratory tests (CBC, comp, UA) were collected pretreatment, POD 2, 7 and weekly. Prostates were harvested on POD 28 following repeat TRUS and cystoscopic evaluation.

**Results:** A treatment cavity was apparent within each prostate on TRUS. Seven of eight treatment volumes were in communication with the urethra and appeared well-healed by time of harvest. A mean of 19.9% (range: 0 - 40.2%) of prostate volume was homogenized. Expected changes in urinalysis (hematuria, pyuria, and proteinuria) and transient elevation in WBC were observed following treatment. In two cases, due to small prostate size, the cavitation bubble cloud was identified anterior to the prostate at initiation of treatment. In both of these subjects, histology revealed a small zone of fibrosis within the rectus muscle. No evidence of thermal injury was present.

**Conclusions:** An amplitude-modulated acoustic pulse sequence for canine prostate histotripsy produced effective tissue homogenization and debulking without evidence of prefocal thermal effect in the rectus muscle or other tissues. Small areas of fibrosis within the rectus muscle in two subjects were attributed to direct tissue cavitation at initiation of treatment. Applying histotripsy acoustic pulses in an amplitude modulated fashion improves the safety profile for the VORTX R<sub>X</sub><sup>®</sup> system and will be the pulse sequence used in human trials.



Resultant tissue cavity 28 days after histotripsy treatment using an amplitude-modulated acoustic pulse sequence.

[1] Roberts WW, Teofilovic D, Jahnke RC, Patri J, Risdahl JM, Bertolina JA: Histotripsy of the prostate using a commercial system in a canine model. *J Urol* 191: 860-5, 2014.

Funding: HistoSonics, Inc.

Disclosure: WWR has royalty, equity, and consulting interests in HistoSonics, Inc.

### THE INTRODUCTION OF ADVANCED BIOMATERIALS FOR USE IN UROLOGIC PROCEDURES

Robert Grubb III<sup>1</sup>, Hiram Gay<sup>2</sup> and Gerald L. Andriole<sup>1</sup>

<sup>1</sup>Washington University School of Medicine, 1. Department of Surgery (Urology),

<sup>2</sup>Department of Radiation Oncology, St. Louis, MO

**Introduction:** The utilization of absorbable polyethylene glycol (PEG) hydrogels has become commonplace in neurosurgery (DuraSeal<sup>®</sup> Dural Sealant, DuraSeal<sup>®</sup> Spine Sealant, Covidien) and in Interventional Cardiology (MynxGrip<sup>®</sup>, AccessClosure). The development of two new hydrogels (SpaceOAR<sup>®</sup> Spacer, TraceIT<sup>®</sup> Tissue Marker, Augmenix) with Urologic applications may impact the treatment patterns of certain common urologic conditions.

**Materials and Methods:** The main limitation of prostate irradiation in PCa patients is concern about injury to the Organ at Risk (OAR), the rectum. Under transrectal ultrasound guidance SpaceOAR liquid is injected via a transperineal 18G needle into the perirectal fat posterior to Denonvilliers' fascia where it expands the space and then polymerizes, forming an absorbable spacer. The ability to safely create space, and the resulting reduction in rectal irradiation was evaluated in 52 T1-T2 men in a multicenter European clinical trial.

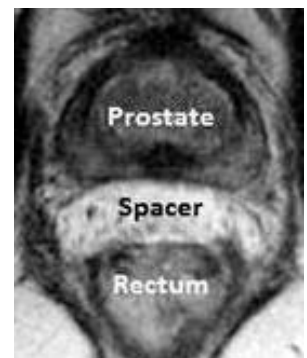
Bladder preservation in non-surgical bladder cancer (BCa) patients would be more likely if the tumor was visible during radiation delivery, allowing for reduced irradiation of healthy bladder. TraceIT hydrogel is a particulated iodinated PEG hydrogel designed for cystoscopic injection into bladder wall, effectively marking the tumor bed to facilitate targeted radiotherapy. A series of three patients were implanted to evaluate marker visibility, the ability to delineate in RT plans, and resistance to migration.

**Results:** In a procedure that took minutes, sterile saline (18±10ml) was injected to create a potential perirectal space prior to 10ml SpaceOAR injection. Greater than 7.5mm of space was obtained in 96% of patients (mean 10±6 mm), resulting in a 61% rV70 reduction. Proctoscopy at 15mo had a VRS score of 0 in 71% of patients. Hydrogel spacer was well tolerated and absorbed at 6 mo.

Via a flexible cystoscopic 22G needle, five-seven 0.3ml (avg) TraceIT hydrogel injections were performed around the periphery of the resected tumors. Subsequent imaging showed marker stability, and CT visibility allowed for tumor localization during RT planning and delivery.

**Conclusions:** In-situ forming hydrogels for use as perirectal spacers appear to be well tolerated and significantly reduce radiation dose to the rectum. Reduction of rectal radiation and the resulting toxicity may provide opportunities for dose escalation, hypofractionation, and additional treatment options for cancer recurrence patients. Additionally, the introduction of an easy to use bladder marker that resists migration may allow for improved radiation targeting, potentially increasing bladder preservation in non-surgical patients, or those who refuse surgery.

Reference: G. Hatiboglu, et al. Multicenter phase II trial of perirectal hydrogel spacer application in men scheduled for dose escalation prostate radiotherapy. AUA2014, Orlando, FL



### THEORETICAL AND *EX VIVO* THERMAL MAPPING FOR RENAL TUMOR RADIOFREQUENCY ABLATION WITH PYELOPERFUSION

Glamore M<sup>1</sup>, Masterson T<sup>2</sup>, Pease K<sup>2</sup>, Lorber G<sup>2</sup>, Salas N<sup>2</sup>, Leveillee R<sup>2</sup>

<sup>1</sup> Florida International University, Herbert Wertheim College of Medicine, Miami, FL  
<sup>2</sup> JBEDS Laboratory, Dept. of Urology, University of Miami Miller School of Medicine, Miami, FL

**Introduction:** Radiofrequency ablation (RFA) is an effective technique for the treatment of small renal tumors. The modality is often limited to tumors at least 2 cm from the renal pelvis or ureter, as excessive heat can cause scarring and obstruction without temperature monitoring. Retrograde pyeloperfusion (PPF) of the pelvis during RFA may keep renal pelvis temperatures low but little has been written to support this claim. We sought to design a mathematical and ex vivo model for RFA with PPF.

**Methods:** Our theoretical model uses a cylindrical, heat-emitting RFA probe adjacent to an infinite, fluid boundary. In the ex vivo model, a 20mm RFA probe was placed in an *ex vivo* porcine kidney 18mm from the pelvis. Thermal sensors were placed at 5 mm distances on either side of the RFA probe (Cool-Tip, Covidien) (Figure 1A). Control trials with no PPF were compared to either cold saline (2°C), warm saline (38°C), or antifreeze (-20°C) perfused into the renal calyx at a rate of 60ml/min for 3 minutes before RFA, 12 minutes of RFA set at 75V under manual mode, and 5 minutes after RFA. Ablated volumes were measured and confirmed histologically.

**Results:** The average steady state temperatures at each probe were highest with no PPF, followed by warm saline, cold saline then antifreeze (Figure 1B). Compared to no PPF all temperatures were significantly ( $p < 0.05$ ) colder with warm saline (-8.4°C temperature drop), cold saline (-18°C) and significantly colder at the calyx (warm -14 °C, cold -27°C). While RFA output a constant voltage, significantly lower resistances in warm (171Ω) and cold (124Ω) PPF vs. no PPF (363Ω) translated to significantly greater power outputs in warm (40W) and cold (42W) vs. no PPF (14W). The ablated volumes were significantly higher in warm saline (2.3cm<sup>3</sup>) vs. cold saline (0.84cm<sup>3</sup>) and no PPF (1.1cm<sup>3</sup>). Histological analysis revealed sparing of the calyx only with cold saline PPF. *Ex vivo* trials were used to obtain constants for tissue conduction and fluid convection for mathematical modeling which produced a predictive temperature model with an  $R^2 = 0.44$ .

**Conclusion:** Pyeloperfusion lowers temperatures throughout the entire kidney during RFA, most notably near the collecting system and is dependent on the temperature of the liquid used. Additionally, PPF may cause less charring of the tissue around the probe resulting in lower resistance and higher power outputs.

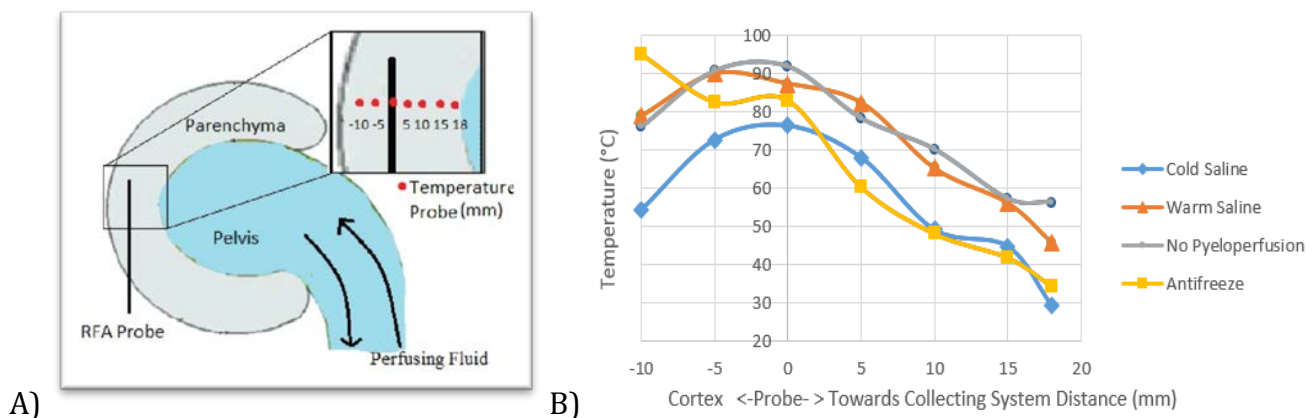


Figure 1: A) *Ex vivo* RFA with PPF model showing temperature probe location B) Steady state temperatures at varying distances from the RFA probe for no PPF, of PPF with cold saline (2°C), warm saline (38°C) or antifreeze (-20°C).

## HUMAN URETHRA ENGINEERED WITH HUMAN MESENCHYMAL STEM CELL BY NEWLY DEVELOPED SCAFFOLD-FREE THREE-DIMENSIONAL CELL PRINTER

Tokunori Yamamoto<sup>1</sup>, Yasuto Funahashi<sup>1</sup>, Morihisa Mastukawa<sup>1</sup>,

Koichi Nakayama<sup>2</sup> and Momokazu Gotoh<sup>1</sup>

<sup>1</sup> University of Nagoya, Department of Urology

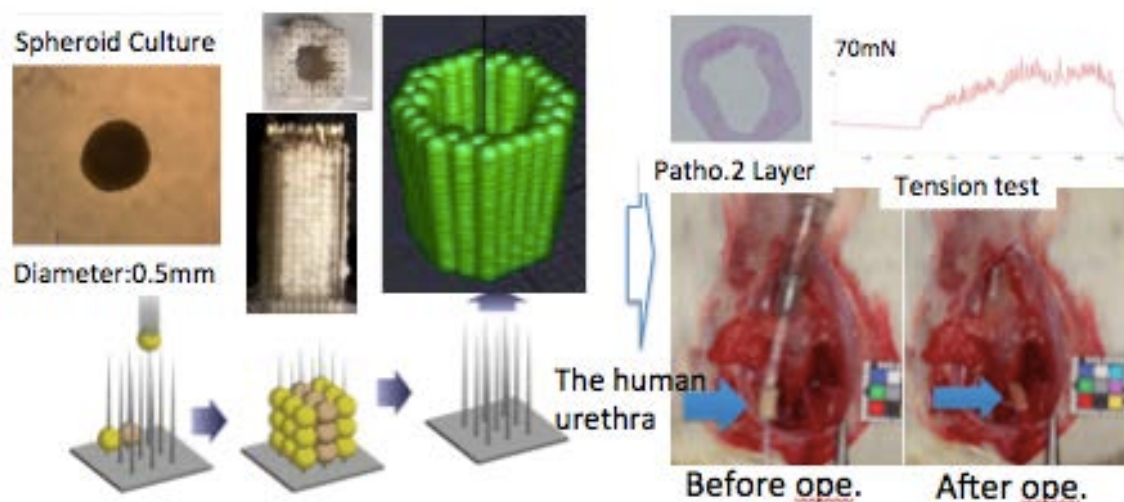
<sup>2</sup> University of Saga, Department of Engineering

**Introduction:** The current tissue engineering approaches typically use matrices such as animal collagen or hydro gel as scaffold material. However, as these materials are foreign for human bodies, the use of scaffold raises a concern about safety such as toxicity, rejection response, and unknown infection. In addition, these materials sometimes reduce effectiveness of tissue regeneration by limiting cellular interactions and oxygen/nutrient diffusion.

**Methods:** Using our proprietary technologies, cell aggregates(diameter:0.5mm) by human mesenchymal stem called “spheroids” are conditioned into three-dimensional macroscopic structures without the need for any scaffold. This scaffold-free approach will have superior safety as it eliminates risks linked to the material. It could also provide more effective tissue regeneration due to a high concentration of naturally interacting cells in the constructs. In order to reproduce the 3D shape of urethral tissue, we adds numerous 10 mm long, 0.1 mm diameter metal needles on the 3D printer. By adjusting needles' length and quantity researchers could change the thickness of urethra.

**Results:** The histologic staining showed that two layers of cells developed in the human urethra(Internal diameter:0.7X0.7X4mm) with tention force(68.1mN)for the X-SCID rat(132.4mN).The retrograde insertion of dye revealed no sign of stricture. The human urethra were transplanted to X-SCID rat(n=3) .

**Conclusion:** We has successfully printed human urethra by cell the aggregates of human mesenchymal stem in 10 days time using this needle array system and transplanted to X-SCID rat(n=3) by newly developed scaffold-free 3D bio fabrication system. (Fig) This technology will enable researchers to develop a wide range of cell-products for restoring tissues and urological organs from living cells safely and efficiently.



### DEVELOPMENT OF A SYNTHETIC HUMAN MODEL FOR TRAINING IN UROLOGY OF PERCUTANEOUS NEPHROLITHOTRIPSY SURGERY

Enrico Andrade, Raphael Pedroso, Raphael Freitas, Carlo Passerotti, Gustavo Alarcon

*Santa Virginia Urology Institute, Sao Paulo, Brazil*

**INTRODUCTION:** The equipment in urology evolved with great speed in recent years, so there is a need to develop models for training in urological surgery, and this needs models that simulate the human body, with very similar characteristics and details of the reality of the human body, so that the training is realistic and facilitates the learning of the urologist.

**METHOD:** A model of the human body was built with two kidneys, urinary stones, and ribs using glycerin, collagen, water and calcium carbonate. The model's components simulated the dimensions of the human body. Model tissue was very close in consistency to reality. The model was tested for training of percutaneous surgery and nephrolithotripsy of a fellow in urology training at this urologic institution of education.

**RESULTS:** The model was built in 8 hours at a cost of USD \$200 and provided a simulation model for training of percutaneous nephrolithotripsy surgery, where he performed renal puncture, directed by fluoroscopy, percutaneous dilatation, introduction of a nephroscope via an Amplatz sheath, and fragmentation of kidney stones.

**CONCLUSION:** There was an easiness of construction of this low-cost model, with close to reality simulation in surgical percutaneous nephrolithotripsy, which provided training for all steps of the surgical technique. This model can be developed and adapted to other urological conditions such as training in prostate biopsy, brachytherapy, renal biopsy, and extracorporeal lithotripsy.

### INITIAL EVALUATION OF A THIRD GENERATION HIGH INTENSITY FOCUSED ULTRASOUND CLAMP FOR LAPOROSCOPIC PARTIAL NEPHRECTOMY

George R. Schade<sup>1</sup>, Stuart B. Mitchell<sup>2</sup>, Franklin Lee<sup>1</sup>, Yak-Nam Wang<sup>2</sup>, Jonathan D. Harper<sup>1</sup>, Lawrence A. Crum<sup>2</sup>

<sup>1</sup>University of Washington, <sup>1</sup>Department of Urology and  
<sup>2</sup>Applied Physics Lab, Center for Industrial and Medical Ultrasound, Seattle, WA

**Introduction:** Partial nephrectomy (PN) remains underutilized for the management of small renal masses, despite nephron sparing surgery being considered the standard of care when feasible. A major contributor to the underutilization of PN is the technical demands of PN, in particular minimally invasive PN. Consequently, a facile laparoscopic device capable of creating a reproducible hemostatic plane of resection in order to decrease the technical difficulty of PN is desirable. Towards this goal, we have previously described a third generation prototype high-intensity focused ultrasound (HIFU) clamp, wherein acoustic energy is delivered from the jaws of a laparoscopic device to induce thermal coagulative necrosis and hemostasis in the planned plane of resection. Here-in we describe *ex vivo* characterization and initial *in vivo* evaluation of a next generation clamp.

**Methods:** A custom-designed 36 element 3.5 MHz therapy clamp transducer with a focal depth of 1.5 cm for each element pair was constructed for use through a 20 mm laparoscopic trocar. The clamp was designed with a gentle concavity to facilitate coupling to the kidney and to produce a 6 mm wide ablation plane with maximal surface area of 12.94 cm<sup>2</sup>. Initial ablation parameters were determined on *ex vivo* porcine kidneys placed in a custom made tank filled with degassed water with clamp deployed 2-2.5 cm from tip of the renal pole. A total of 3 ablations in 3 porcine kidneys were then performed *in vivo* via midline laparotomy with the clamp placed 2-2.5 cm from the renal pole and the kidney submerged in degassed PBS. Three HIFU activation strategies were evaluated: 12 W/cm<sup>2</sup> for 10 min, 15 W/cm<sup>2</sup> for 10 min, or 15 W/cm<sup>2</sup> until a change in impedance was seen, all with 100% duty factor. Hemostasis was assessed from the cut edge of the kidney distal to the ablation site. Following HIFU treatment, the degree of ablation was assessed both grossly and histologically.

**Results:** *Ex vivo* characterization demonstrated rapid heating at all acoustic powers  $\geq 39$ W achieving  $\geq 59$ C in  $\leq 3$  min application. Additionally, a linear relationship between 10 min max temperature ( $T_{max}$ ) and intensity ( $R^2=0.98$ ) was observed, achieving a  $T_{max}$  of 100 C at 60 W acoustic power and 15W/cm<sup>2</sup> intensity. An inflexion point in the impedance of the transducer was observed at a mean of 56.1 C (range 49.6-70.5 C), before which ablation appeared incomplete and after which ablation appeared complete. *In vivo* ablations were then performed at 12W/cm<sup>2</sup> and 15W/cm<sup>2</sup> for 10 min total demonstrating extensively ablated tissue which when incised appeared desiccated and over-treated with only ~50% hemostasis. Based on the observation of impedance inflexion point correlating with adequate ablation *ex vivo*, we then performed a final ablation until the inflexion point was observed in 225s. Sectioning of the plane of ablation revealed complete ablation with very minimal oozing from large-caliber sinus vessels.

**Conclusion:** Preliminary data on a next generation laparoscopic HIFU PN clamp demonstrates the ability to generate a plane of ablation *in vivo*. Further studies will determine optimal treatment duration and if the impedance inflexion point is a reliable marker of treatment success.

**Funding:** NIH (EB013365)

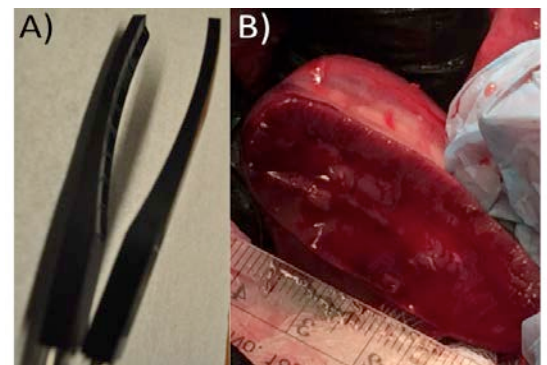


Figure: Next generation HIFU clamp (A) and gross appearance of kidney treated *in vivo* (B).

### WRINKLE CELLOMICS: SCREENING BLADDER CANCER CELLS WITH ULTRA-THIN SILICONE MEMBRANE WRINKLE PATTERNS

Jennie H. Appel<sup>1</sup>, Mandy L.Y. Sin<sup>2</sup>, Joseph C. Liao<sup>2</sup>, Junseok Chae<sup>1</sup>

<sup>1</sup>*School of Electrical, Computer and Energy Engineering, Arizona State University, USA*

<sup>2</sup>*School of Medicine, Department of Urology, Stanford University, USA*

**Introduction:** There is a significant clinical need for non-invasive urine-based diagnostics for bladder cancer that improve upon the well-recognized shortcomings of urine cytology. We report a platform to visualize alterations in biomechanical properties of cancerous cells in urine samples. Using an ultra-thin silicone membrane, cancerous cells were found to induce membrane deformation and distinct wrinkling patterns, which were absent in non-cancerous cells. Quantitative wrinkle measurement may represent a powerful non-invasive diagnostic tool for bladder cancer.

**Methods:** The ultra-thin membrane, approximately 28 nm in thickness, is fabricated by selectively cross-linking the surface of a small droplet of high viscosity liquid silicone. Cancerous (RT4), non-cancerous (HEK293f), and buffy coat (WBCs, RBCs and platelets) are incubated on the membrane and the ultra-thin membrane cell interactions are observed at 2 hour time intervals.

**Results:** The wrinkling responses of RT4, HEK293f, and buffy coat were compared by separately incubating  $5 \times 10^5$  of each cell type on the membrane. One hour post membrane adhesion, RT4 cells induced distinct wrinkles formed under these cells (Figure 1a). Wrinkle pattern, defined as the number, length, direction of wrinkles, was visualized by a standard microscope. In contrast, 24 hours post membrane adhesion, HEK293f and buffy coat cells failed to induce wrinkles (Figure 1b-c). Furthermore, a heterogeneous cell population comprised of RT4, HEK293f, and buffy coat cells, failed to suppress, enhance, or otherwise alter RT4 cell-generated wrinkles (Figure 1d).

The onset and persistence of membrane wrinkling induced by RT4 cells were determined by a time-lapse experiment at 0, 4, 6, and 8 hours post membrane adhesion (Figure 2). The number and length of RT4 cell-generated wrinkles increased from 4 to 6 hours and persisted past 8 hours. We further tested the ability of cancerous cells to induce membrane wrinkles in the simultaneous presence of a high concentration of HEK293f and white blood cells. To better simulate clinical urine samples, mixed ratios of RT4:HEK293f:buffy coat cells 1:1:1, 1:2:2 and 1:5:5 were tested. After 20 hours of incubation, the RT4 cells in each of the mixed ratios produced a similar number and length of wrinkles.

**Conclusion:** We present preliminary study for the detection of cell-line derived cancerous bladder cells from a mixed cell-type sample. Cancerous cells exclusively induce deformation of our ultra-thin silicone membrane, generating wrinkles. Wrinkle formation, and thus detection of cancerous cells, is observed as early as 4 hours post sample preparation with standard microscopy. Further development of this technology will produce a simple, yet effective, tool to discern the presence of cancerous cells in urine samples as an aid in the diagnosis of bladder cancer.

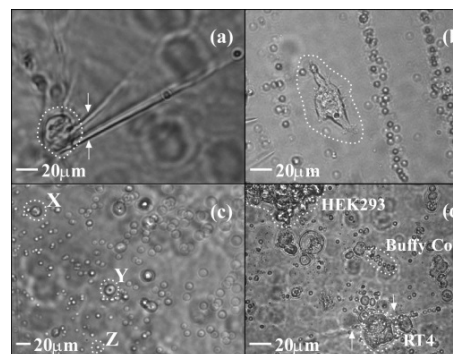


Figure 1: (a) RT4 cells generating wrinkles 5 hours after incubation; (b) HEK293f cells (c) and buffy coat cells (X=WBC, Y=RBC, and Z=platelet) fail to generate wrinkles 24 hours post incubation; (d) Wrinkle generation was specific to RT4 cells in a mixed sample.

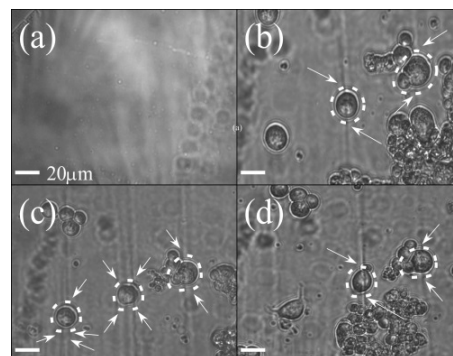


Figure 2: (a) Membrane with 1 mL of media. The fabrication and addition of media intermittently induces non-specific wrinkles. Time-lapse of RT4 cells on membrane after (b) 4, (c) 6, and (d) 8 hours of incubation.

### CONSTANT COAGULATION DEPTH WITH NANOSECOND GREEN LASER-BASED PHOTOSELECTIVE WARM VAPORIZATION (PWV)

Hui Wang, David Jenbens, Ray Aditi, Ray Chia  
*American Medical Systems, Endo International PLC*

**Introduction:** Green light photoselective vaporization of the prostate (PVP) relies on the strong absorption of hemoglobin at 532nm. The tissue temperature around blood vessels could rise very fast with high power green light illumination and leads to two important processes, vaporization and coagulation, simultaneously. Vaporization is the removal of tissue and coagulation is related to hemostasis. Both of processes are related to laser parameters, such as pulse width. In this study, we quantified the vaporization and coagulation processes with a nanosecond pulsed green laser through “photoselective warm vaporization” (PWV).

**Methods:** The system used in the experiment included a nanosecond pulsed green laser (AMSAMS™ GreenLight XPS™ laser) and a fiber for laser delivery (AMSAMS™ MoXy™ fiber). Fresh porcine kidney tissues were used as the tissue samples. We vaporized the tissues at different energy densities by controlling scanning speed between tissue and laser beam. The vaporized grooves were cut at three different locations and processed with TCC for stain to enhance the contrast of the coagulation layer. The vaporization volume and coagulation depth were quantified using Image J and correlated with the corresponding energy densities.

**Results:** We demonstrated that PVP can generate a constant coagulation depth at different energy density levels that could be related to the operation, such as scanning the fiber at different speeds. The vaporization volume was also fitted to the blow-off model (1). The result suggested that PVP with nanosecond green laser is a thermal confinement process.

**Conclusion:** This observation helps provide objective evidence to support that PVP has excellent hemostasis. We believe that thermal confinement vaporization, PWV, is responsible for the effective vaporization and constant coagulation depth when nanosecond green laser is used for PVP.

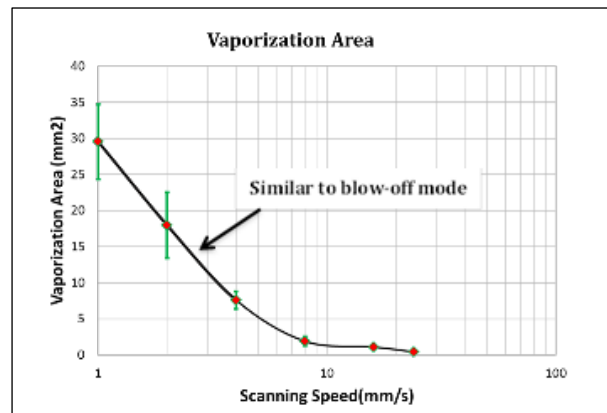
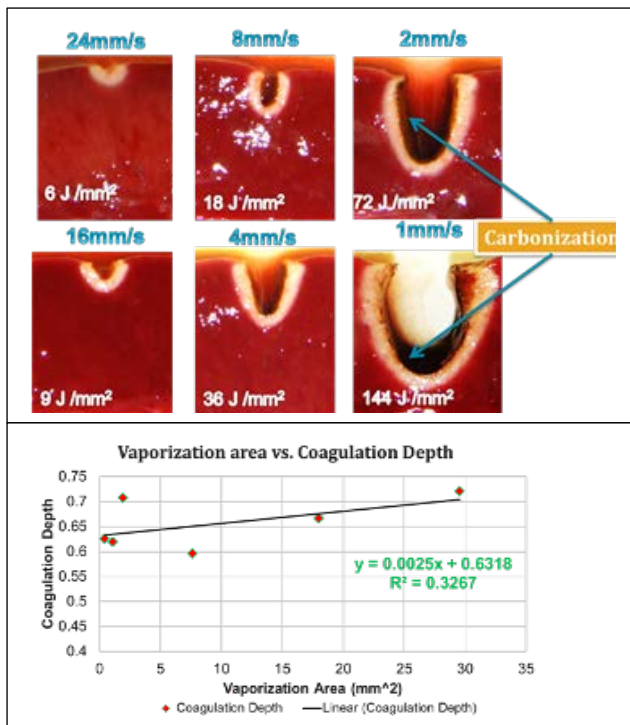


Figure (a): Vaporized tissue appearances at different energy densities

Figure (b): Vaporization volume fitted to blow-off model at different scanning speeds (energy density levels)

Figure (c): Low correlation between vaporization and coagulation depth

(1) Srinivasan, R, Mayne-Banton, V: *Applied Physics Letters* 1982 41: 576-578

### INTEGRATED IMAGING AND HISTOTRIPSY THERAPY RAT MODEL PLATFORM FOR UROLOGIC APPLICATIONS

Timothy L Hall<sup>1</sup>, Xu Chen<sup>2</sup>, William W Roberts<sup>1,2</sup>

*Departments of <sup>1</sup>Biomedical Engineering and <sup>2</sup>Urology, University of Michigan, Ann Arbor, MI*

**Introduction:** Histotripsy is a method of ultrasound ablation using intense bursts of sound to disrupt and liquefy targeted tissue. In our previous work, we have devised a non-invasive debulking treatment for BPH using histotripsy. In order to develop additional urologic and oncologic applications, we created a new histotripsy ablation system suitable for rat models.

**Methods:** The complete system is comprised of five integrated modules constructed using a mix of standard machining techniques and stereolithography rapid prototyping:

1. Histotripsy ultrasound transducer composed of 8 replaceable modules arranged in a ring configuration constructed in-house.
2. Coaxial ultrasound imaging with a small footprint 20 MHz linear probe (L40 – Ultrasonix).
3. Three-axis motorized positioning system controlled through MATLAB software on PC.
4. Water conditioning system using a dual tank configuration to filter, heat, and degas a water bath through which ultrasound is coupled to the subject.
5. Set of swappable treatment beds with cutout apertures for targeting various organs.

In an initial feasibility trial, the system was used to target and homogenize targeted volumes of kidney, prostate, testicle, and liver tissue in 10 anesthetized depilated subjects. The focal zone was an elliptical volume approximately 1 x 2 mm representing the minimal ablation volume. The focal zone was scanned over 3 mm-10 mm square grid patterns with up to 400 focal locations to build up a larger ablation volume. Following ablations, subjects were euthanized and targeted organs were harvested, fixed, and processed for H&E staining and histological analysis.

**Results:** A cavitation bubble cloud was identified and observed in real-time during the ablation process in each case. The targeted tissue became progressively hypoechoic during treatment. Zones of subcellular debris consistent with homogenized tissue were identified in kidney, liver, prostate, and testicle. The shape of the homogenized zone was consistent with the treatment pattern for liver in kidney. In prostate and testicle the homogenate appeared to have migrated from the targeted volume, and occupied spaces between normal appearing glandular tissue and tubules. Sample ablations in the prostate and liver are shown in Figure 1.

**Conclusion:** A new therapeutic platform for studying histotripsy ablation in the rat model has been developed. This system should prove useful in researching new urologic applications for histotripsy.

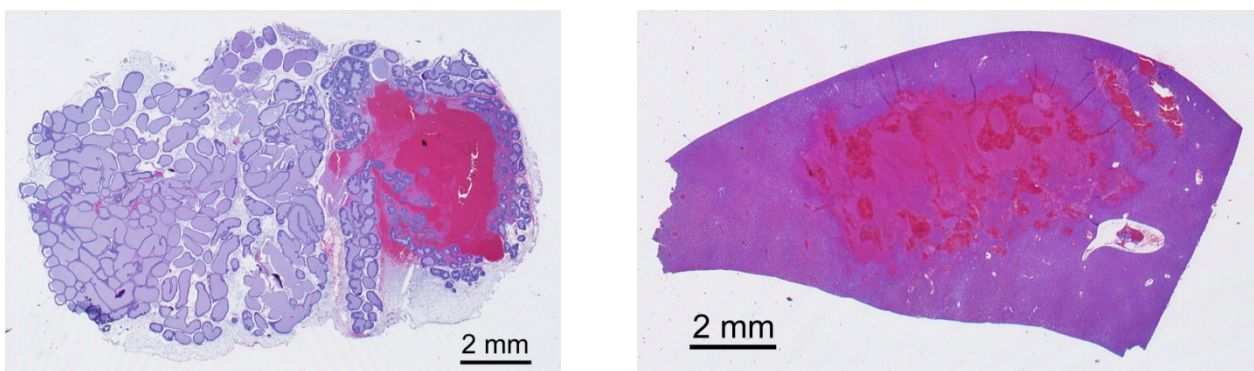


*Figure 1: Focal ablation in the rat prostate (left) and liver (right).*

Funding: R01 DK087871

Disclosures: TLH and WWR have equity, royalty, and consulting interests in HistoSonics, Inc.

# ABSTRACTS

## ABSTRACT 59

### ULTRASONIC PROPULSION OF KIDNEY STONES: PRELIMINARY RESULTS OF THE INITIAL CLINICAL TRIAL

Jonathan Harper MD<sup>1</sup>, Franklin Lee MD<sup>1</sup>, Bryan Cunitz MS<sup>2</sup>, Barbrina Dunmire MS<sup>2</sup>, Marla Paun BS<sup>2</sup>, Susan Ross RN<sup>1</sup>, Michael Bailey PhD<sup>2</sup>, Ryan Hsi MD<sup>1</sup>, James E Lingeman MD<sup>3</sup>, Michael Coburn MD<sup>4</sup>, Hunter Wessells MD<sup>1</sup>, Mathew Sorensen MD<sup>1</sup>,  
*University of Washington, <sup>1</sup>Department of Urology and <sup>2</sup>Applied Physics Lab; <sup>3</sup>Indiana University, Department of Urology; <sup>4</sup>Baylor University Department of Urology.*

**Introduction:** Safety and effectiveness of using focused ultrasound to reposition kidney stones in a porcine model has been demonstrated. We are now reporting preliminary findings from the first use of this technology in humans.

**Methods:** There are three arms of the study: de novo stones, post-lithotripsy fragments, and the preoperative setting. A pain questionnaire is completed immediately prior to and following the study. A maximum of 40 push attempts are administered on either low (50 V) or high (90 V) power settings. Movement is classified as 1, 2, 3, or U (Table 1).

**Results:** Six subjects have been enrolled and undergone ultrasonic propulsion to date. None of the subjects reported pain associated with the treatment. Subjects did report a mild warming of the skin with a high (90 V) power push; no sensation was reported with a low power (50 V) push. A summary of push movement results is provided in Table 1. One subject in the post-lithotripsy arm passed two small stones immediately following treatment corresponding to the two stones displaced from the interpolar region. Two subjects reported passage of multiple small fragments on days 1 and 2 post treatment. In three subjects, ultrasonic propulsion identified a collection of stones previously characterized as a single stone on KUB and ultrasound. There have been no treatment related adverse events reported with mean follow-up of 3 weeks.

**Conclusions:** This is the first report on the successful repositioning of kidney stones in humans using ultrasound. Treatment was therapeutic in two subjects and provided diagnostic information in three. Subjects who did not have significant movement were in the *de-novo* arm. To date, there have been no reports of pain or adverse events associated with this treatment.

Table 1: Ultrasonic Propulsion of Kidney Stones – Preliminary Results

Study Arm	Patient #	Number of stones	Stone size (mm)	Motion Grading*				Total Push Bursts
				1	2	3	U	
De- Novo Stones	1	3	2-3	20 (75%)	5 (19%)	0	2 (7%)	27
	2	5	2-3	17 (44%)	16 (41%)	0	2 (5%)	39
	3	2	3	21 (91%)	1 (4%)	0	1 (4%)	23
Post-Lithotripsy	4	2	2	9 (24%)	23 (62%)	5 (13%)	0	37
	5	5	2-3	17 (42%)	21 (53%)	2 (5%)	0	40
	6	Multiple	< 2	24 (60%)	12 (30%)	4 (10%)	0	40

\*1: no motion; 2: movement with rollback or stone jiggle; 3: movement to new location; U: unintentional push. All subjects treated with a combination of 50 V and 90 V output.

**Source of Funding:** Trial supported by NSBRI through NASA NCC 9-58. Research and development supported by NIH DK043881 and DK092197.

## ABSTRACT 60

### SETUP USING UNIVERSAL SMARTPHONE ADAPTERS TO TELESCOPES DURING VIDEO CYSTOURETHROSCOPY WITH SCREEN MIRRORING

Ernesto V. Arada III, MD\*, Angelica Versoza, MD  
*De la Salle University Medical Center, Dasmariñas, Cavite, Philippines*

**Introduction:** Equipment for Video Cystourethroscopy is expensive. Sohn *et. al* in 2013 developed Endoscope coupling iPhone 4S with flexible endoscopes. We present an economical setup to connect any Android, Apple or Windows smartphone to a telescope using commercially available universal “digiscoping” adapters during video cystourethroscopy with wired or wireless screen mirroring.

**Methods:** In the wired setup of screen mirroring, an MHL (mini-usb to HDMI) cable was connected to LCD monitor via HDMI port (Figure 1). In the wireless setup, smartphones compatible with LCD monitors mirror image from cystoscope (Figure 2). Two different commercially available universal “digiscoping” adapters that can fit any Android, Apple or Windows smartphone: vertical screw-in type (Figures 3 & 4) and round clip-on type (Figures 5 & 6) were fitted with shims to three different Android smartphone models and one Coolpix digicam coupled with telescopes during video cystourethroscopy.

**Results:** In the two screen mirroring setups presented, the current models of smartphones were connected and fitted to two types of universal adapters to telescopes. Images viewed in the screens of smartphones as well as in the LCD monitors were acceptable for diagnostic purposes. In the setup for wireless screen mirroring, there appears to be some delay in viewing the image in the LCD monitor.

**Conclusion:** Our setup using universal digiscoping adapters to fit smartphones to telescopes gives acceptable images during cystoscopy. It is also possible to share online these images from smartphones.



Figure 1: Setup of wired “screen mirroring” connecting Smartphone with LCD monitor using red MHL cable during simulated cystoscopy using bladder-urethra model.



Figure 2: Setup of wireless “screen mirroring” with compatible LCD monitor and Android Smartphone during simulated video cystoscopy using bladder-urethra model.



Figure 3: Screw-in universal digiscoping adapter to phone after MHL cable connection.



Figure 4: Screw-in universal digicam adapter to cystoscope to view and capture images.



Figure 5: Round clip-on universal smartphone adapter to cystoscope.



Figure 6: Round clip-on smartphone adapter during video cystourethroscopy.

## LAPAROSCOPIC WIRELESS PALPATION PROBE: FEASIBILITY OF SIMULATED TUMOR DETECTION IN A HUMAN PROSTATE

Christopher Mitchell<sup>1</sup>, Marco Beccani<sup>2</sup>, Christian Di Natali<sup>2</sup>, Aaron Benson<sup>1</sup>, S. Duke Herrell<sup>1</sup>, Pietro Valdastrì<sup>2</sup>

<sup>1</sup> Vanderbilt University, Department of Urologic Surgery,  
<sup>2</sup> Vanderbilt University, Department of Mechanical Engineering

**Introduction:** With the recent widespread adoption of robotic assisted laparoscopic prostatectomy (RALP), this minimally invasive procedure has effectively supplanted open radical retropubic prostatectomy for surgical treatment of prostate cancer. Many proposed advantages of RALP include smaller incisions, improved visualization, less blood loss, and faster recovery. However, these gains come at the expense of tactile feedback from palpation of the prostate, which is lost during RALP. Considering this, we developed a laparoscopic wireless palpation probe (WPP) to measure differences in sub-surface tissue densities (similar to digital palpation) and provide a 3-D map for localization.

**Methods:** The WPP, which utilizes an external static magnetic field source, can be used to palpate the target with a laparoscopic grasper as in Figure 1. The WPP is cylindrical with a 12.7 mm diameter and a 60 mm length, (compatible with a 12 mm laparoscopic port). Indentation pressure is obtained by a tactile sensor embedded in the tip. WPP relative position is obtained in real-time by magnetic field sensors. Tissue indentation depth is obtained by integrating the WPP position as indentation pressure is detected. A wireless microcontroller transmits the measurements acquired by the magnetic field sensors and the tactile element. The WPP was used to palpate a human cadaver prostate where three distinct tumor simulators were created by injecting Agar gel at the locations represented in Figure 2A. Lump  $\alpha$  was superficial and  $5 \times 9 \times 4 \text{ mm}^3$ , lump  $\beta$  was at a median depth and  $18 \times 15 \times 10 \text{ mm}^3$ , while lump  $\gamma$  was the deepest and  $6 \times 3 \times 5 \text{ mm}^3$  (dimensions were measured at the end of the procedure by dissecting the prostate). Using a real-time mapping interface, the tumors and relative locations were assessed on the map.

**Results:** Palpating the prostate to create the map represented in Figure 2B required one minute. All three tumors were correctly visualized on the stiffness map with a spatial resolution of 3 mm. The planar dimensions for each tumor measured by the proposed method were  $9 \times 6 \text{ mm}^2$  for  $\alpha$ ,  $18 \times 15 \text{ mm}^2$  for  $\beta$ , and  $6 \times 6 \text{ mm}^2$  for  $\gamma$ . If compared to the planar dimensions of each tumor, the localization error was  $9 \pm 9 \text{ mm}^2$ . The measured stiffness range was  $0.9 \pm 0.2 \text{ kPa}$  for lump  $\alpha$ ,  $0.85 \pm 0.27 \text{ kPa}$  for lump  $\beta$ , and  $0.79 \pm 0.21 \text{ kPa}$  for lump  $\gamma$ . Surrounding tissue stiffness was  $0.07 \pm 0.04 \text{ kPa}$  for regions without features, increasing to  $0.35 \pm 0.2 \text{ kPa}$  in case of buried structures such as the urethra.

**Conclusion:** In the human cadaveric prostate, the WPP accurately measured sub-surface tissue densities and relative positions, which can be represented on 3-dimensional mapping. This has the potential to provide important, real-time information of tumor location during RALP, which may allow for more precise surgical dissection of the prostate to ensure negative surgical margins and improved outcomes.

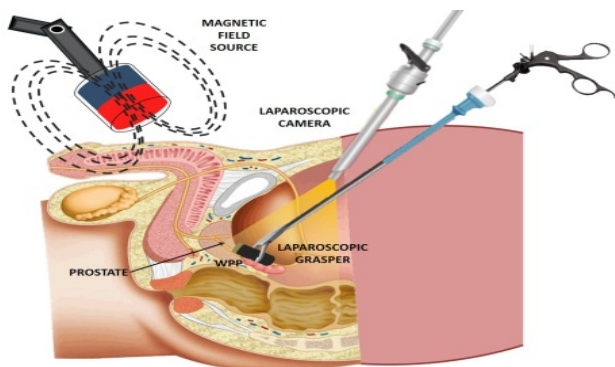


Figure 1. Incorporation of wireless palpation device during robotic/laparoscopic prostatectomy

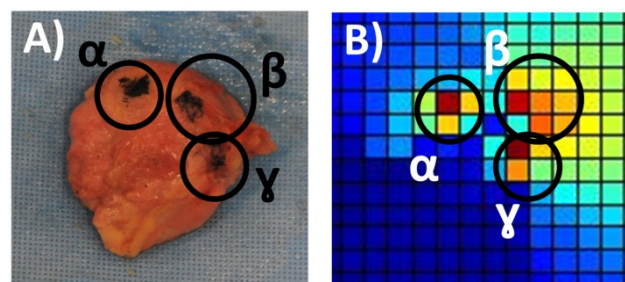


Figure 2. A) Cadaveric prostate with identified target lesions. B) Simulated map of corresponding lesions

### USING CROWD-ASSESSMENT TO SUPPORT SURGICAL TRAINING IN THE DEVELOPING WORLD

Lee W. White, Andrew Wright, Abebe Bekele, Berhanu Kottisso, Amezene Tadesse, Brant Oelschlager, Daniel Holst, Yves Borbely, Thomas S. Lendvay  
*University of Washington and Stanford University*

**Introduction:** Performance feedback to novice surgical trainees in developing countries remains difficult due to sparse expertise. The gold standard of doing structured assessments in-person or by video review with expert graders is costly, time-intensive, and logistically difficult. We hypothesize that crowd sourcing surgical skills assessment using the Amazon.com Mechanical Turk Project could be as effective as scoring surgical performances by expert surgeon graders.

**Methods:** After IRB approval, ten surgeons (three R1, two R2, two R4, two faculty) from a surgical training center in Ethiopia performed blinded video-recorded dry lab suture tasks for scoring using the Global Assessment of Basic Surgical Skills (GABSS) - three Likert scales on instrument handling, knot-tying and wound closure, and a seven-item checklist. Three expert surgeon graders and 1,000 remunerated (\$0.50/video) Turkers (100 Turkers/video) evaluated the performances within 11 hours of posting the surveys.

**Results:** Agreement was found to be ‘excellent’ (IRR=0.90) among the surgeon graders for the Likert score sum, ‘very good’ for the checklist score (IRR=0.85) and global(sum) score (IRR=0.89). Global score agreement was found to be ‘acceptable’ to ‘good’ between the crowds and experts with Cronbach’s alpha (CA)=0.77 and correlation coefficient (CC)=0.85. A subset of the crowd (first 50 respondents) yielded a CA=0.84 and CC=0.91 (Figure 1).

**Conclusions:** Crowd-Sourced Assessment of Technical Skills (CSATS) is time- and cost-efficient, and demonstrated good correlation with expert graders. CSATS requires video capture and uploading which could be performed over cell phones. With further optimization of crowds, CSATS may be a viable solution to providing ‘expert’ skills assessment for developing regions of the world to enhance global surgical education.

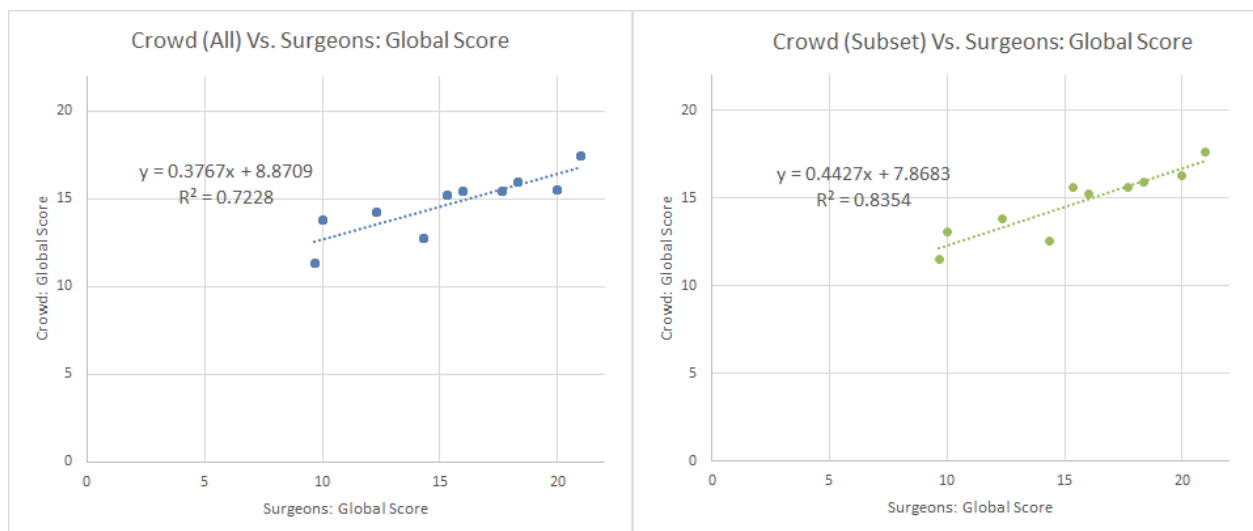


Figure 1 – Agreement between a lay crowd on the Amazon Mechanical Turk crowd-sourcing site was found to agree well with assessment by expert surgeons. A subset of the respondents (the first 50) demonstrated even better agreement with the surgeons. Both the crowd and surgeons used the GABSS assessment tool.

# ABSTRACTS

## ABSTRACT 63

### CYSTOSCOPIC TELECONFERENCING OF IMAGES FROM INTRAOPERATIVE REFERRALS SHARED ONLINE USING SMARTPHONES

Ernesto V. Arada III, MD\*, Luis Florencio MD, Michael Macalalag MD, Frederick Mendiola MD, Jun Dy MD, Ceasar Ballesteros MD, Jeremiah Mangahas MD  
*Quirino Memorial Medical Center, Quezon City, Philippines*

**Introduction:** Currently, referrals to urology consultants for surgical management of urological cases are done during pre-operative conferences. During intraoperative referrals, images can be taken by any Android, Apple, or Windows smartphone indirectly from video monitors or directly by universal “digiscoping” phone adapters; and then shared online. In 2013 Sohn *et al.* showed “Endockscope” coupling endoscopes to iPhone 4S. We aim to find feasibility of “cystoscopic teleconferencing” of intraoperative referrals using any smartphone by sharing images online images to help the urologist in his planned management.

**Methods:** Images of intraoperative referrals were taken indirectly from video monitors (Figure 1) or directly with Android smartphones fitted with universal adapters to cystoscopes (Figure 2). Cystoscopic images with brief text of history, physical exam and imaging studies were shared online using email or the WhatsApp Messenger cross-platform app. Consultants were texted to see if they agreed or disagreed to the planned management (Figures 3-8). Urologists made management decisions based upon agreed consensus.

**Results:** 172 responses by 6 urology consultants for 43 images were shared online using email or the WhatsApp Messenger program. Consultants texted AGREE in 146 (85%) and DISAGREE in 26 (15%). Using test of proportions, there was significant agreement of the consultants with the planned management ( $p = 0.0001$ ).

**Conclusion:** It is feasible to share online with urology consultants using email or the WhatsApp Messenger app the images of intraoperative referrals for cystoscopic teleconferencing of planned management.

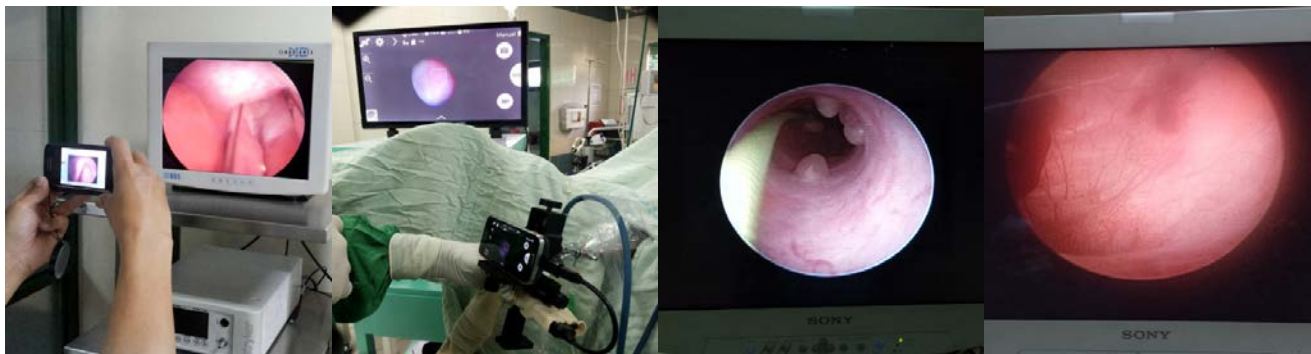


Fig 1: Smartphone taking image from video monitor

Fig 2: Universal digiscoping phone adapter to cystoscope

Fig 3: Plan- Biopsy polyp AGREE or DISAGREE?

Fig 4: Plan- Biopsy Mass AGREE or DISAGREE?



Fig 5: Plan- I. C. Lithotripsy AGREE or DISAGREE?

Fig 6: Plan- Ureterolithotomy AGREE or DISAGREE?

Fig 7: Plan- End lithotripsy AGREE or DISAGREE?

Fig 8: D.J. stenting stricture AGREE or DISAGREE?

### DIFFERENTIATING SURGICAL SKILL THROUGH THE WISDOM OF CROWDS

Thomas Lendvay, MD<sup>1</sup>, Daniel Holst<sup>1</sup>, Lee White, PhD.<sup>2</sup>, Timothy Kowalewski, PhD.<sup>3</sup>, Timothy Brand, MD.<sup>4</sup>, Matthew Sorensen, MD<sup>1</sup>, Jonathan Harper, MD<sup>1</sup>, Mireille Truong, MD<sup>5</sup>, Khara Simpson, MD<sup>6</sup>, Roger Smith, PhD.<sup>3</sup>

<sup>1</sup>University of Washington, Department of Urology, <sup>2</sup>Stanford University School of Medicine, <sup>3</sup>University of Minnesota, Department of Mechanical Engineering, <sup>4</sup>Madigan Army Medical Center, Department of Urology, <sup>5</sup>Columbia University School of Medicine, <sup>6</sup>Nicholson Center for Simulation, Florida Hospital

**Introduction:** Objective quantification of surgical skill is imperative as we enter a healthcare environment of quality improvement and performance-based reimbursement. The gold standard, Objective Structured Assessment of Technical Skills (OSATS)-like tools are infrequently used due to time-intensiveness, cost-inefficiency, and lack of standard practices. Crowd sourcing is a means of accomplishing tasks through the work of decentralized, independent, groups of people who may or may not have knowledge specifically dealing with the task at hand. We hypothesized that random crowds obtained through the crowd sourcing platform – Amazon.com Mechanical Turk – could discriminate surgical skill as effectively as a panel of expert surgeon graders.

**Methods:** After IRB approval, twelve surgeons of varying robotic surgical experience performed live porcine robotic-assisted urinary bladder closures. Blinded video-recorded performances were scored by expert surgeon graders and the Amazon crowd graders using the Global Evaluative Assessment of Robotic Surgery (GEARS) tool assessing five technical domains – Bimanual Dexterity/Depth Perception/Tissue Handling/Efficiency/Robotic Control. Seven expert graders and 50 unique Mechanical Turkers (each paid \$0.75/survey) evaluated each video. Global assessment scores were analyzed for correlation and agreement.

**Results:** Six-hundred Mechanical Turkers completed the surveys in under 5 hours, while 7 surgeon graders took 14 days. The duration of video clips ranged from 2-11 minutes. The correlation coefficient between the Turkers and expert graders' scores was 0.95, the best fit line was 0.91, and Cronbach's alpha was 0.93 (Figure 1). Inter-rater reliability among the surgeon graders was 0.89.

**Conclusion:** Crowd sourcing surgical skills assessment yielded rapid, inexpensive agreement with global performance scores given by expert surgeon graders. The crowd sourcing method may provide surgical educators and medical institutions with a boundless number of procedural skills assessors to efficiently quantify technical skills for use in trainee advancement and hospital quality improvement.

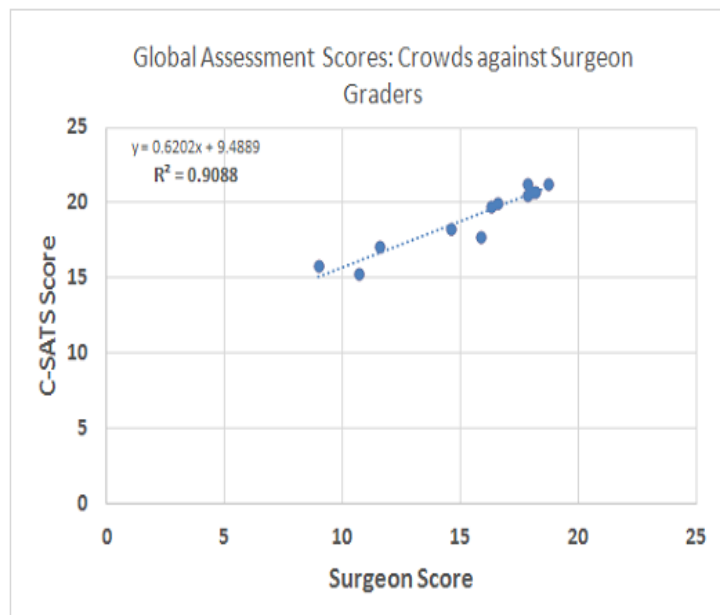


Figure 1. Crowd Sourced Assessment of Technical Skills (C-SATS): Global performance scores provided by the crowd against the global performance scores provided by the expert surgeon graders.

# **SOCIETY OFFICERS:**

## **Presidents**

Jeffrey Cadeddu  
Koon Ho Rha

## **Vice-Presidents**

Raymond Leveillee  
Arieh Shalhav

## **Secretary**

Jack Vitenson

## **Treasurer**

John Denstedt

## **Councilor**

Louis Kavoussi

## **Executive Director**

Dan Stoianovici

## **ADVISORY BOARD**

Jeffrey Cadeddu

Ralph Clayman

Jean de la Rosette

Misop Han

Pilar Laguna

Thomas Lawson

Manoj Monga

Pierre Mozer

Stephen Nakada

Jens Rassweiler

Koon Ho Rha

William Roberts

Arthur Smith

Li-Ming Su

Gerald Timm

Hessel Wijkstra

Kevin Zorn

# AWARDS:

## Best Paper Awards:

**DIRECT MRI-GUIDED TRANSPERINEAL PROSTATE BIOPSY WITH MR-SAFE ROBOT. FIRST FDA-APPROVED ROBOT FOR THE MR ENVIRONMENT.** Dan Stoianovici<sup>1</sup>, Chunwoo Kim<sup>1</sup>, Changan Jun<sup>1</sup>, Doru Petrisor<sup>1</sup>, Katarzyna J. Macura<sup>2</sup>, Ashley Ross<sup>1</sup>, Mohamad Allaf<sup>1</sup>; Robotics Laboratory, Urology<sup>1</sup> and Radiology<sup>2</sup> Departments, Johns Hopkins University, Baltimore, MD

**HUMAN URETHRA ENGINEERED WITH HUMAN MESENCHYMAL STEM CELL BY NEWLY DEVELOPED SCAFFOLD-FREE THREE-DIMENSIONAL CELL PRINTER.** Tokunori Yamamoto<sup>1</sup>, Yasuto Funahashi<sup>1</sup>, Morihisa Mastukawa<sup>1</sup>, Koichi Nakayama<sup>2</sup>, and Momokazu Gotoh<sup>1</sup>; <sup>1</sup> University of Nagoya, Department of Urology, <sup>2</sup> University of Saga, Department of Engineering

## Top 10 Abstracts:

**IN VITRO RESULTS OF ROBOTIC CYSTOSCOPE AND 3D PANORAMA FOR AUTOMATED BLADDER SURVEILLANCE SYSTEM (ABSS).** Xianming Ye<sup>1</sup>, Yuanzheng Gong<sup>2</sup>, and W. Jong Yoon<sup>1</sup>; <sup>1</sup>Department of Mechanical and Industrial Engineering, Qatar University, Doha, Qatar <sup>2</sup>Mechanical Engineering Department, University of Washington, Seattle, USA

**COGNITIVE-AUGMENTED ROBOTIC SYSTEM FOR ENDOSCOPIC NAVIGATION (CARSEN): A PROOF OF CONCEPT FOR MIND-CONTROL ENDOSURGERY USING LEGO®.** Neal Patel<sup>1</sup>, Philip T. Zhao<sup>1</sup>, Manoj B. Patel<sup>2</sup>; <sup>1</sup> Rutgers–Robert Wood Johnson Medical School, New Brunswick, NJ, <sup>2</sup> Cooper Medical School of Rowan University, Camden, NJ

**THE NUMBER OF SYSTEMATIC BIOPSY CORES RAISES PREDOMINANTLY THE DETECTION OF INSIGNIFICANT CANCER.** Doyoung Chang, Chong Xue, Chunwoo Kim, Changan Jun, Doru Petrisor, Misop Han, Dan Stoianovici; Robotics Laboratory, Department of Urology, Johns Hopkins University

**BODY WALL FORCES AT PORT SITES IN LAPAROSCOPIC AND ROBOTIC SURGERY.** Smita De M.D., Ph.D.<sup>1</sup>, Paul Loschak Ph.C.<sup>2</sup>, Brett Page B.S.<sup>3</sup>, Amy Kerdok Ph.D.<sup>3</sup>; <sup>1</sup> Department of Urology, Stanford University Hospital, Stanford, CA, USA, <sup>2</sup>Harvard School of Engineering and Applied Sciences, Cambridge, MA, USA, <sup>3</sup>Intuitive Surgical Operations, Inc., Sunnyvale, CA, USA

**COMPARISON OF CATHETER-DIRECTED WST11-VASCULAR TARGETED PHOTOTHERAPY (WST11-VTP) AND IRREVERSIBLE ELECTROPORATION (IRE) FOR INTRALUMINAL ABLATION IN THE PORCINE URETER.** Govindarajan Srimathveeravalli<sup>1</sup>, Ashley Winter<sup>2</sup>, Haruyuki Takaki<sup>1</sup>, Simon Kimm<sup>2</sup>, Tatum V Tarin<sup>3</sup>, Sebastien Monette<sup>3</sup>, Stephen B Solomon<sup>1</sup>, Jeremy C Durack<sup>1</sup> and Jonathan Coleman<sup>2</sup>; <sup>1</sup> Dept. of Radiology, <sup>2</sup>Dept. of Surgery, <sup>3</sup>Laboratory of Comparative Pathology, Memorial Sloan Kettering Cancer Center, New York, NY. <sup>3</sup>Dept. of Urology, Univ. of Pittsburg Medical Center, PA.

**LAPAROSCOPIC WIRELESS PALPATION PROBE: FEASIBILITY OF SIMULATED TUMOR DETECTION IN A HUMAN PROSTATE.** Christopher Mitchell<sup>1</sup>, Marco Beccani<sup>2</sup>, Christian Di Natali<sup>2</sup>, Aaron Benson<sup>1</sup>, S. Duke Herrell<sup>1</sup>, Pietro Valdastrì<sup>2</sup>; <sup>1</sup> Vanderbilt University, Department of Urologic Surgery, <sup>2</sup> Vanderbilt University, Department of Mechanical Engineering

**PILOT EVALUATION OF BOILING HISTOTRIPSY OF THE KIDNEY: ASSESSMENT IN HUMAN EX VIVO KIDNEYS AND VALIDATION OF THE PORCINE MODEL.** George R. Schade<sup>1</sup>, Adam D. Maxwell<sup>1</sup>, Yak-Nam Wang<sup>2</sup>, Tatiana D. Khokhlova<sup>3</sup>, Daniel W. Lin<sup>1</sup>, Oleg A. Sapozhnikov<sup>2</sup>, Michael R. Bailey<sup>2</sup>, Vera A. Khokhlova<sup>2</sup>; University of Washington School of Medicine, Departments of <sup>1</sup>Urology and <sup>3</sup>Gastroenterology <sup>2</sup>University of Washington Applied Physics Lab, Center for Industrial and Medical Ultrasound

**MRI-GUIDED PROSTATE CANCER FOCAL LASER ABLATION THERAPY USING A MECHATRONIC NEEDLE GUIDANCE SYSTEM: INITIAL EXPERIENCE AND FUTURE DIRECTIONS.** Jeremy Cepek<sup>a,b</sup>, Uri Lindner<sup>c</sup>, Sangeet Ghai<sup>d</sup>, John Trachtenberg<sup>c</sup>, Aaron Fenster<sup>a,b</sup>; <sup>a</sup>Robarts Research Institute, London; <sup>b</sup>Biomedical Engineering, The University of Western Ontario, London; <sup>c</sup>Department of Surgical Oncology, Division of Urology, University Health Network, Toronto; <sup>d</sup>Department of Medical Imaging, University Health Network, Toronto, Canada

# AWARDS:

## Best Reviewer Awards (5 Years):

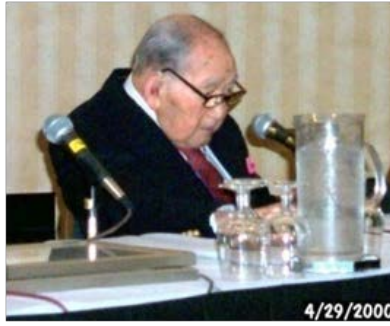
		2010	2011	2012	2013	2014
Ernesto III	Arada				☼	
Riccardo	Autorino	☼		☼		
Thorsten	Bach	☼	☼	☼		
Jeffrey	Cadeddu					☼
Haixin	Chen				☼	
Jean	de la Rosette	☼				
Mahesh	Desai			☼	☼	
Brian	Eisner		☼			
Mohamed	Elkoushy		☼	☼	☼	☼
Oscar	Fugita				☼	
Arvind	Ganpule			☼		
Petrisor	Geavlete			☼		☼
Wareef	Kabbani	☼				
Avinash	Kambadakone		☼			
Watid	Karnjanawanichkul		☼			
Louis	Kavoussi				☼	
Bodo	Knudsen		☼	☼		
Thomas	Lawson		☼	☼		
Salvatore	Micali	☼				
Kamol	Panumatrassamee			☼		☼
Sutchin	Patel	☼	☼	☼	☼	
Koon Ho	Rha	☼			☼	
Mathew	Sorensen				☼	
Govindarajan	Srimathveeravalli					☼
Cristian	Surcel		☼			
Kazuo	Suzuki	☼				
Chong	Xue					☼
Hessel	Wijkstra		☼		☼	☼
Kevin	Zorn	☼	☼			

## REVIEW COMMITTEE:

The active review committee comprises eighty-seven reviewers from around the world. We gratefully acknowledge their contribution to the success of the meeting and thank them for taking the time to promote the best science.

Gustavo Alarcon	Hyung-Joo Kim	Preeti Patil
Ernesto III Arada	HongWook Kim	Doru Petrisor
Motoo Araki	Chunwoo Kim	Thomas Polascik
Naeem Bhojani	Jayram Krishnan	Alan Priester
Timothy Brand	Jaime Landman	Soroush Rais-Bahrami
Jeffrey Cadeddu	Thomas Lawson	Ashish Rawandale
Jeremy Cepek	Jesse Le	KoonHo RHA
Doyoung Chang	Benjamin Lee	Gideon Richards
Haixin Chen	Hak Lee	William Roberts
Peter Choyke	Andrew Leone	Georgios Sakas
Sarah Darnell	Sey Kiat Lim	Fatma Saleh
Smita De	Paul Loschak	Bradley Schwartz
Mahesh R. Desai	Michael Macalalag	Yaniv Shilo
Mohamed Elkoushy	Steve Majerus	Minhaj Siddiqui
Cosmin Ene	Jeremiah Mangahas	Mathew Sorensen
Mohamed Etafy	Salvatore Micali	Govindarajan Srimathveeravalli
Aaron Fenster	George Mitroi	Dan Stoianovici
Luis Florencio	Razvan Multescu	Nithin Theckumpampil
Nathaly François	Yasutomo Nasu	Angelica Versoza
Raguram Ganesamoni	Shyam Natarajan	Hui Wang
James Garritano	Christopher Netsch	Hessel Wijkstra
Petrisor Geavlete	Gheorghe Nita	Henry Woo
Bogdan Geavlete	Yasser Noureldin	Chong Xue
Arvin George	Zhamshid Okhunov	Jennifer Yates
Yuanzheng Gong	Michael Ordon	Xianming Ye
Andreas J Gross	Cervando Ortiz-Vanderdys	W. Jong Yoon
Matthew Ishahak	Kamol Panumatrassamee	Homayoun Zargar
Changhan Jun	Sutchin Patel	Philip Zhao
Louis Kavoussi	Manoj Patel	Timothy Ziemlewicz

# THANKS:



Dr. George Nagamatsu, Engineering and Urology Society Founder



Special thanks to **Dr. Thomas Lawson** for his help formatting this program.

We thank **Michelle Paoli** and **Debra Caridi** for organizing the Annual Meeting.